Abstract

REESE, JILL PAULA. Examining the Significance of Advective Acceleration to Single-Phase Flow Through Heterogeneous Porous Media. (Under the direction of Dr. C. T. Kelley.)

Practically every groundwater flow simulator in use today implements Darcy's law to model saturated flow [1, 4, 64, 65]. Darcy's law is a linear relation derived experimentally in the mid 1800's by Henry Darcy. Since that time it has been used as an approximation to momentum conservation, thus simplifying the model of saturated flow through porous media.

In spite of its widespread appeal, Darcy's law does have limitations. Particularly in the case of higher velocities (i.e. Reynolds numbers much larger than one), Darcy's law is no longer a sufficient model for saturated flow through porous media. In this document, we propose a model for momentum balance which includes two terms that are nonlinear in velocity. One term, based upon the early 1900s work of Forchheimer, incorporates the magnitude of the fluid velocity. The other, known as the advective acceleration term in this document, models how the momentum is advected by the pore velocity and includes velocity gradients.

While the advective acceleration term is a core component of the exact momentum conservation equation, it is neglected in the groundwater flow literature due to the assumption that groundwater flow is generally slow. However, to our knowledge no one has performed numerical studies to examine the magnitude of the error introduced by this simplifying assumption. In this document, we focus on two-dimensional regional flow through heterogeneous porous media and examine the significance of advective acceleration in both the Darcy and Forchheimer flow regimes.

The non-Darcy flow simulator was written using the finite element simulation framework, Sundance 2.0. While the Raviart-Thomas finite elements are the appropriate element combination for solving the non-Darcy flow system, they were not available in Sundance 2.0. Therefore, a multiscale residual-based stabilization approach was implemented [50, 73, 78, 89]. We have proven that the modified equation set is stable. Moreover, we have shown that the discrete equations conserve mass both locally and globally and conserve momentum globally.

EXAMINING THE SIGNIFICANCE OF ADVECTIVE ACCELERATION TO SINGLE-PHASE FLOW THROUGH HETEROGENEOUS POROUS MEDIA

BY

Jill P. Reese

A DISSERTATION SUBMITTED TO THE GRADUATE FACULTY OF

NORTH CAROLINA STATE UNIVERSITY

IN PARTIAL FULFILLMENT OF THE

REQUIREMENTS FOR THE DEGREE OF

DOCTOR OF PHILOSOPHY

COMPUTATIONAL MATHEMATICS

RALEIGH, NORTH CAROLINA

November 2006

APPROVED BY:

C. T. Kelley CHAIR OF ADVISORY COMMITTEE	W. G. Gray
C. T. Miller	M. Shearer

Dedication

This body of work is dedicated to my incredible grandparents, Agnes Martha McFarland Leach, Mary Joanne Hargett Reese, and Paul Smith Reese. While you may not understand my work, you never stop believing in me and supporting every one of my decisions. Some people may think that this is just your job as grandparents, but I think it's a testament to what great individuals you are. Thank you for keeping my feet on the ground and reminding me each and every day about what is truly important in this world.

Biography

Jill Paula Reese was born on August 21, 1979 in Meadville, Pennsylvania to Jon B. and Margaret A. Reese. The youngest of four children, she grew up on a dairy farm in Guys Mills, Pennsylvania. After attending elementary, junior high, and high school in nearby Cochranton, Pennsylvania, Jill decided to become "the next Mrs. Hank" by majoring in Secondary Education - Mathematics at Clarion University of Pennsylvania.

Through her Clarion experiences Jill realized that she loved studying mathematics more than teaching it. Her goals (and major/minor) changed over the course of four years, culminating in a Bachelor of Science degree in Applied Mathematics with a minor in Computer Science. This was not the end of her academic journey, however. Thanks to the advice of Dr. Jon Beal, a recruitment talk by Katie (Kavanagh) Fowler on the infamous "Astrid Problem", and the combined dance moves of Katie, Vicki (Williams) Klima, and Karen Yokley, Jill decided to pursue her Ph.D. in Applied Mathematics at North Carolina State University.

During her time at NC State, Jill earned her Master of Science degree in Applied

Mathematics and her Doctor of Philosophy degree in Computational Mathematics with a concentration in Interdisciplinary Mathematics. She also completed three summer internships at Sandia National Laboratories in Livermore, CA.

Upon completion of her dissertation, Jill will begin a postdoctoral research position in the School of Computational Science at Florida State University.

Acknowledgments

Over the course of my graduate school career I have accumulated a varied list of people, places, and things I wish to recognize for contributing to the enjoyable years I have spent at NC State. My acknowledgments follow in no particular order.

- I want to recognize the financial support of a Department of Education GAANN Fellowship, as well as grants from the National Science Foundation and the Army Research Office.

- I would like to thank my committee members, Dr. Bill Gray, Dr. Casey Miller, and Dr. Michael Shearer, for all of the time and effort they have invested in me during my graduate school career, both in and out of class. Your helpful comments and suggestions regarding my dissertation have been greatly appreciated.

- I am grateful to Genetha Gray, Tammy Kolda, Kevin Long, Pamela Williams, and the entire Computational Sciences and Mathematics Research department of Sandia National Labs (Livermore). What I learned from all of you during

my summer internships is immeasurable.

- Kevin certainly deserves a second thank-you all his own for developing Sundance. Without that software framework, my dissertation would have developed into a very different beast. Thank you for answering every question, no matter how trivial, with your characteristic patience and thoughtfulness.

- Tammy, I'll never forget how much you've helped me professionally over the past three years. Thank you for all of your efforts as an advocate and mentor.

- Genetha, your generosity astounds me. I am indebted to you for saving me from student intern housing and for showing me the joys of French pastries.

- I want to thank the graduate school representative on my committee, Dr. Laura Clarke, for her active participation during my oral exams. I greatly appreciate all of your comments, suggestions, and advice.

- I must recognize Dr. Ipsen's course on communicating Applied Mathematics, as well as the faculty and student members of the Numerical Analysis Graduate Student Seminar. Your constructive criticism and suggestions continue to improve my work.

- I'm grateful for the timely hardware and software support provided by Eric Sills and Gary Howell through the NC State High Performance Computing Center. I will also miss my constant companion, henry2, but surely not for very long.

- I want to acknowledge past and present members of the math support staff for all they do each day to make my life less complicated. In particular I want to recognize Di Bucklad, Joel Cason, Brenda Currin, Carolyn Gunton, Denise Seabrooks, Frankie Stephenson, and Charlene Wallace.

- Thanks go out to the original members of the now defunct HA208 office - Katie (Kavanagh) Fowler, Brian Adams, Jordan Massad, Rachel Levy, Nick Luke, and Kristy Coffey. I may never find a better office or officemates. Thank you for all the great conversations and zwrites. And also for putting up with my tendency to put CDs on repeat... for hours.

- I'll never forget the "family" dinners and meetings, parties, cookouts, and yard sales with my housemates, Brian Adams, Brandy Benedict, Nick Luke, and Jason Osborne. I always looked forward to coming home to Glengarry, and for that I can't thank you enough. That, and for putting up with hours of back-to-back Law & Order.

- Cassie, thanks for keeping me on track those first couple of years while still taking time to play hookie at the $1.50 theater and join me for rejuvenating post-exam trips to Sadlack's.

- I would like to recognize the mathematics faculty at Clarion University of Pennsylvania for guiding me through my undergraduate education. I particularly want to acknowledge Dr. Jon Beal and Dr. James Reynolds for helping me find

the right path.

- Rachel, without you I never would have made it through qualifiers. Thanks for always being behind me.

- Shuttleworth, I'll never forget all the time spent in The Cube. Without you commiserating with me over various software issues, I would probably have gone insane.

- BA, my computer guru on call 24/7, there are too many things to enumerate with you. Your thoughtful, generous friendship has enriched my time in NC... even the part spent hurtling down an embankment in a shopping cart.

- Matthew, talking with you (about mathematics and every other topic under the sun) has helped me on more occasions than I can count. The spaceship has been pretty lonely without you.

- Dan and Matthew, thanks for never letting me go it alone at Speaker Fest... or at Copper... or at Sadlack's ... or ...

- Kelly Dickson and Karen Dillard (a.k.a. the "Angels"), this last year has been much more pleasant and sane thanks to your company. Thank you for listening to me ramble on about whatever was on my mind and for being right there beside me having all sorts of childish fun.

- Boo, I'm forever in your debt for teaching me that I can, indeed, run seven

miles. Thank you for being my travel companion, for always challenging me, and for making me laugh every day, especially when I don't want to. I would be lost without your support.

- Last, but far from least, I thank my advisor, Tim Kelley, for his patience and unswerving confidence in me. Tim, I am so grateful for all of the travel and networking opportunities you've provided over the years. Now stop reading this and get to work!

Table of Contents

List of Tables

List of Figures

Notation

mi	microscale (subscript)	3
ma	macroscale (superscript)	3
$\mathcal{P}_i(\ell)$	microscale property (i subscript)	3
$\mathcal{P}^i(\ell)$	macroscale property (i superscript)	3
ℓ	length scale	3
$\delta\ell$	perturbation of length scale ℓ	3
ϵ	specified precision required to estimate the property, $\mathcal{P}$	3
α	phase index	5
s	solid phase	5
w	liquid phase	5
ϕ	porosity	5
V_v	void volume	5
V_T	total volume	5
ι	species index	6
$\omega^{\alpha\iota}$	mass fraction of species ι in phase α	6

Chapter 1

Introduction

1.1 Contributions

This dissertation presents my research on simulating non-Darcy flow using the finite element method via the Sundance partial differential equation (PDE) simulation and optimization framework and the Trilinos solver framework. My contributions to this effort include

- contributing code to Sundance that extended its capabilities for solving nonlinear PDEs;
- contributing code to the Trilinos nonlinear solver, NOX, which enabled NOX to access Sandia's TSF linear algebra interface;
- deriving the nonlinear stabilization terms required to solve the non-Darcy flow model using Sundance;

- proving that the modified equations are stable, conserve mass globally and locally, and conserve momentum;
- implementing the first numerical simulations of this non-Darcy model for saturated flow through porous media; and
- providing numerical evidence that advective acceleration effects are negligible in the two-dimensional flow cases examined in this document.

1.2 Hydrology Overview

Modeling fluid flow through porous media is difficult for a number of reasons, including the complexity and heterogeneity of the subsurface domain [16, pages 18 and 19]. Properties of the porous medium can vary extensively over a short length scale, and it is nearly impossible to map the pore structure and void spaces through which the fluid flows. It is at this pore scale, or microscale ($10^{-9}\text{m} - 10^{-8}\text{m}$), where biological, chemical, physical, and thermodynamical models are valid for resolving the dynamics which occur between individual grains of the porous medium [59].

However, as most natural systems of interest occupy regions which are orders of magnitude larger than the micron level, much research is invested in other spatial scales of interest. We follow the spatial scale hierarchy developed by Gray and Miller in [61, pages 185-186] where they acknowledge five separate scales — the molecular scale, microscale, resolution scale, macroscale, and megascale. In this document we

focus on three of the five scales; thus, definitions of the microscale, the macroscale, and the megascale from [61] follow.

Definition 1.1. *The* **microscale**, ℓ_{mi}, *is the smallest length scale at which laws of continuum mechanics can be developed with*

$$|\mathcal{P}_i(\ell_{mi} + \delta\ell_{mi}) - \mathcal{P}_i(\ell_{mi})| \leq \epsilon_{mi} \ \forall i$$

where $\mathcal{P}_i(\ell)$ *is a microscale property estimated by a well-defined average over over length scale* ℓ, $\delta\ell_{mi}$ *is a change in the length scale, and* ϵ_{mi} *is a specified precision of the estimate of* $\mathcal{P}_i$.

Definition 1.2. *The* **macroscale**, ℓ^{ma}, *is the length scale at which the set of averaged properties of concern for the system can be rigorously defined and*

$$|\mathcal{P}^i(\ell^{ma} + \delta\ell^{ma}) - \mathcal{P}^i(\ell^{ma})| \leq \epsilon^{ma} \ \forall i$$

where $\mathcal{P}^i(\ell)$ *is a macroscale property estimated by a well-defined average over length scale* ℓ, $\delta\ell^{ma}$ *is a change in the length scale, and* ϵ^{ma} *is a specified precision of the estimate of* $\mathcal{P}^i$.

Definition 1.3. *The* **megascale** *is the length scale corresponding to the domain of interest,* Ω.

The definitions of the microscale and macroscale both rely on identifying a length

scale in which averaged properties take on "stable" values. That is, slight perturbations in the length scale should only affect the value of averaged properties to within a specified tolerance. By carefully averaging microscale properties over some representative elementary volume (REV), one can describe systems of interest using macroscale system properties and governing equations [57], while still retaining the connection to the "true" microscale quantities.

Figure 1.1 provides a schematic of the requirements for a representative elementary volume. A REV should be large enough so that averaging microscopic deviations in a property over the entire REV will yield a corresponding macroscopic property value that is independent of slight changes in REV size. This requirement provides a lower bound on the size of the REV. An upper bound on REV size also exists, above which deviations due to macroscale heterogeneity in the property are apparent.

From this description, one can see that the size of the REV is dependent upon the grain size of the porous medium system of interest. For example, a REV of coarse gravel would be much larger than a REV of fine sand. As a rule of thumb, a sample containing approximately twenty grains of the porous medium of interest would provide a reasonable REV. Gray and Miller provide another example in [61, page 186] where they estimate the macroscale for a sample of well-sorted grains with a diameter of approximately 100 microns to be approximately 10^{-2}m. In any case, the REV scale is the smallest scale required to resolve continuum models.

The intricacies of the subsurface domain are due not only to the porous medium,

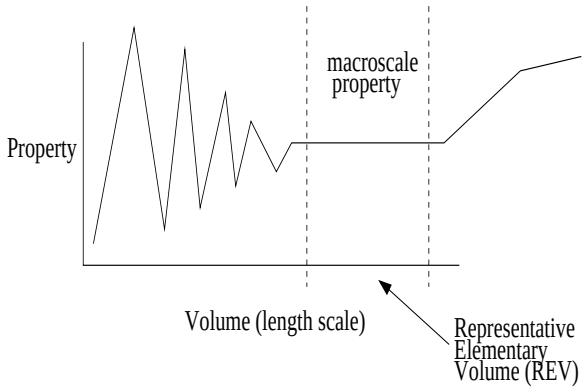

Figure 1.1: Importance of REV to determining macroscale properties

or solid phase, but also to the fluids that flow through the pore space of the medium. Examples of what may be considered a fluid include water, air, oil, or pollutants foreign to the subsurface; each fluid will be considered as a separate phase. In this document we consider only single-phase flow; thus, at most two phase categories are considered, indexed by α. The solid phase is denoted by $\alpha = s$, while the liquid phase is denoted by $\alpha = w$.

Only one phase exists at a point at the microscale, while a "point" at the macroscale actually refers to the REV discussed previously. Within the REV all phases are represented, with each taking up some percentage of that volume. This percentage, called the porosity and denoted by ϕ, is the ratio of the void (pore space) volume, V_v, to the total volume, V_T [38, page 13].

1.3 Single Phase Flow: Traditional Modeling Approach

When modeling fluid flow through porous media, the partial differential equation (PDE) model should conserve both mass and momentum at the macroscopic level. We first focus on mass conservation over a REV, where we wish to satisfy the statement that

$$\begin{bmatrix}\text{rate of accumulation of}\\ \text{mass within the REV}\end{bmatrix} = \begin{bmatrix}\text{net influx of mass into}\\ \text{the REV across its boundary}\end{bmatrix} + \begin{bmatrix}\text{net rate of mass}\\ \text{production in the REV}\end{bmatrix}.$$

In deriving the statement of mass conservation for phase α, we follow the notation from [91]. It is necessary first to define some averaged quantities of interest. First of all, within the α phase there may exist different species, ι. For example, when $\alpha = w$ one is interested in the liquid phase which fills the pore space of the solid. There may be several different liquids within the pore space, and these different liquids are indexed by the ι variable. The mass fraction of species ι in phase α is denoted by $\omega^{\alpha\iota}\left(\frac{\mathrm{M}^{\iota}}{\mathrm{M}^{\alpha}}\right)$ where M^{ι} denotes the mass of the ι species and M^{α} denotes the mass of the α phase. The volume fraction of the α phase is denoted by $\theta^{\alpha}\left(\frac{V_{\alpha}}{V_T}\right)$. The variable $\rho^{\alpha}\left(\frac{\mathrm{M}^{\alpha}}{V_{\alpha}}\right)$ represents the density of the α phase, and $\mathbf{v}^{\alpha}\left(\frac{\mathrm{L}}{\mathrm{T}}\right)$ is the mean pore velocity of the α phase. Note that V_{α} represents the volume of the α phase.

Now we can examine in more detail the contributions to the net influx of mass

and the net rate of mass production in the REV.

$$\begin{bmatrix}\text{rate of mass}\\ \text{accumulation}\end{bmatrix} = \begin{bmatrix}\text{bulk advective}\\ \text{transport}\end{bmatrix} + \begin{bmatrix}\text{nonadvective transport}\\ \text{(ex: diffusion)}\end{bmatrix} + \begin{bmatrix}\text{mass transfer}\\ \text{(ex: evaporation)}\end{bmatrix} + \begin{bmatrix}\text{chemical/biological}\\ \text{reactions}\end{bmatrix} + \begin{bmatrix}\text{mass sources/sinks}\\ \text{(ex: wells)}\end{bmatrix}$$

This text statement is expressed mathematically via the species mass conservation equation

$$\frac{\partial\left(\theta^{\alpha}\rho^{\alpha}\omega^{\alpha\iota}\right)}{\partial t} = -\nabla\cdot\left(\theta^{\alpha}\rho^{\alpha}\mathbf{v}^{\alpha}\omega^{\alpha\iota}\right) - \nabla\cdot\mathbf{j}^{\alpha\iota} + \mathcal{I}^{\alpha\iota} + \mathcal{R}^{\alpha\iota} + \mathcal{S}^{\alpha\iota}, \tag{1.1}$$

where t is time, $\mathbf{j}^{\alpha\iota}$ is the nonadvective flux term for species ι in phase α, $\mathcal{I}^{\alpha\iota}$ represents mass transfer from species ι to the α phase, $\mathcal{R}^{\alpha\iota}$ represents reactions of species ι in the α phase, and $\mathcal{S}^{\alpha\iota}$ represents external sources of species ι in the α phase. The bulk advective flux term is represented by $\theta^{\alpha}\rho^{\alpha}\mathbf{v}^{\alpha}\omega^{\alpha\iota}$. The conserved quantity is the mass of the ι species over the total volume.

To develop the conservation of mass equation for the entire α phase one can sum

equation (1.1) over all species ι and apply the following identities.

$$\sum_{\iota} \omega^{\alpha\iota} = 1; \quad \sum_{\iota} \mathbf{j}^{\alpha\iota} = 0; \quad \sum_{\iota} \mathcal{R}^{\alpha\iota} = 0; \quad \sum_{\iota} \mathcal{I}^{\alpha\iota} = \mathcal{I}^{\alpha}; \quad \sum_{\iota} \mathcal{S}^{\alpha\iota} = \mathcal{S}^{\alpha}$$

The mass conservation law in equation (1.2) results from applying these identities to the species mass conservation equation. In equation (1.2) the conserved quantity is now the mass of the alpha phase over the total volume. Also, $\mathcal{I}^{\alpha}$ accounts for mass transfer between phases, and $\mathcal{S}^{\alpha}$ incorporates external sources of mass into the model.

$$\frac{\partial}{\partial t}\left(\theta^{\alpha}\rho^{\alpha}\right) = -\nabla \cdot \left(\theta^{\alpha}\rho^{\alpha}\mathbf{v}^{\alpha}\right) + \mathcal{I}^{\alpha} + \mathcal{S}^{\alpha} \tag{1.2}$$

As we are currently concerned solely with single-phase flow, the only possible values for α are either $\alpha = s$ or $\alpha = w$. The $\mathcal{I}^{\alpha}$ term from equation (1.2) is commonly ignored because mass exchange is usually negligible between groundwater and the solid matrix. Furthermore, the solid matrix is generally considered to be immobile, as any movement in the solid is negligible when compared to the movement of the surrounding groundwater. From now on we will focus on mass conservation of the fluid phase only; thus $\alpha = w$.

At this point the three-dimensional model is comprised of one equation containing five unknowns (θ^{w}, ρ^{w}, and the triplet $\mathbf{v}^{w}$), so closure relations involving approximations for four of the unknowns are required to obtain a well-posed model. By

expanding terms, equation (1.2) is equivalent to

$$\theta^w \frac{\partial}{\partial t}\left(\rho^w\right) + \rho^w \frac{\partial}{\partial t}\left(\theta^w\right) = -\rho^w \nabla \cdot \left(\theta^w \mathbf{v}^w\right) - \theta^w \mathbf{v}^w \cdot \nabla\left(\rho^w\right) + \mathcal{S}^w. \tag{1.3}$$

Initially, density is assumed to be a function of the pressure, temperature, and composition of the groundwater; therefore, $\rho^w = \rho^w(p^w, T, \omega^{w\iota})$ where p^w is the macroscopic fluid phase pressure and T denotes temperature. For the majority of natural systems of interest (i.e. in the shallow subsurface), the groundwater temperature is close to the mean annual temperature. Two exceptions to this assumption include (i) the groundwater very near to the surface, and (ii) the existence of certain geothermal conditions. As these exceptions occur rarely in practice, the temperature dependence of density is generally disregarded. Another assumption is that composition effects are negligible, which is true for many dilute systems. This document focuses on single-phase fluid flow; thus, compositional effects are completely ignored. Hence, the density of the fluid phase is approximated as a function of the fluid phase pressure only. The general functional form $\rho^w = \rho^w(p^w)$ represents an equation of state [16, pages 27, 37-38].

When comparing the terms $\rho^w \nabla \cdot (\theta^w \mathbf{v}^w)$ and $\theta^w \mathbf{v}^w \cdot \nabla \rho^w$ from equation (1.3), the low compressibility of water implies that the density gradient should not be very large. Thus another assumption is that

$$|\rho^w \nabla \cdot (\theta^w \mathbf{v}^w)| >> |\theta^w \mathbf{v}^w \cdot \nabla \rho^w|. \tag{1.4}$$

By applying the approximation from equation (1.4) and dividing by ρ^w, equation (1.3) reduces to

$$\frac{\theta^w}{\rho^w}\frac{\partial \rho^w}{\partial t} + \frac{\partial \theta^w}{\partial t} = -\nabla \cdot (\theta^w \mathbf{v}^w) + \mathcal{S}', \tag{1.5}$$

where $\mathcal{S}' = \frac{\mathcal{S}^w}{\rho^w}$. Using the assumption that density depends primarily on pressure changes, we can expand the first term of equation (1.5) such that the equation reduces to

$$\left[\frac{\theta^w}{\rho^w}\frac{\partial \rho^w}{\partial p^w} + \frac{\partial \theta^w}{\partial p^w}\right]\frac{\partial p^w}{\partial t} = -\nabla \cdot (\mathbf{u}^w) + \mathcal{S}' \tag{1.6}$$

where $\mathbf{u}^w = \theta^w \mathbf{v}^w$ is the specific discharge or Darcy velocity of the fluid phase. Under isothermal conditions, the compressibility is given by $\frac{1}{\rho^w}\frac{\partial \rho^w}{\partial p^w}$, and this property of the fluid is easily found in the literature [16, pages 37-38] [36, 91]. It should be noted that over narrow ranges of pressure, the compressibility is an approximately constant.

Further simplification of equation (1.6) follows from the assumption that groundwater flows through the subsurface as predicted by an empirical relation known as Darcy's law. Henry Darcy, a civil engineer, built an experimental set-up similar to Figure 1.2 "to determine the laws of flow of water through sand"[38, page 33]. His goal was to improve the public drinking water system of Dijon, France where the water was purified via sand filtration. Figure 1.2 shows water flowing through a fully saturated cylindrical column packed with a homogeneous porous medium. The volumetric flow rate is $Q\left(\frac{\mathrm{L}^3}{\mathrm{T}}\right)$, while the cross-sectional area of the column is denoted

by A. The Darcy velocity, $\mathbf{u}$, is equal to $\frac{Q}{A}$.

Figure 1.2 shows two tubes called manometers sticking out of the cylinder. The water flowing through the porous medium is able to enter these tubes, and generally speaking, the height to which the water rises in the tube is a measure of the water pressure at the tube inlet. When pressure is expressed in terms of a height of fluid, this quantity is called hydraulic head, $h\,(\mathrm{L})$, and it is the sum of pressure head and elevation head as shown in equation (1.7) [56, page 5900].

$$h = \int_{p_0}^{p} \frac{\mathrm{d}p'}{\rho\,(p')\,g} + z \tag{1.7}$$

Elevation head, z, accounts for the distance between the baseline datum and the tube inlet. Pressure head includes contributions from the pressure of the water column, p, relative to a reference pressure, p_0; density; and acceleration due to gravity, $g = 9.81\frac{\mathrm{m}}{\mathrm{s}^2}$. These forces are what drive the water further up into the manometer. As the manometers are a distance of $\Delta\ell$ apart, we write the dimensionless hydraulic gradient as $\frac{h_1 - h_2}{\Delta\ell}$, which is often generalized over small distances as $\frac{\partial h}{\partial \ell}$. Darcy discovered that the velocity of the water was proportional to the driving force of the hydraulic head gradient.

The Darcy's law formula generalized to three spatial dimensions is given by

$$\mathbf{u} = -K \cdot \nabla h, \tag{1.8}$$

where the proportionality constant, $K\left(\frac{\mathrm{L}}{\mathrm{T}}\right)$, called the hydraulic conductivity, describes the ability of the porous medium to transmit water. The negative sign shows that water tends to flow from areas of high hydraulic head toward areas of low head.

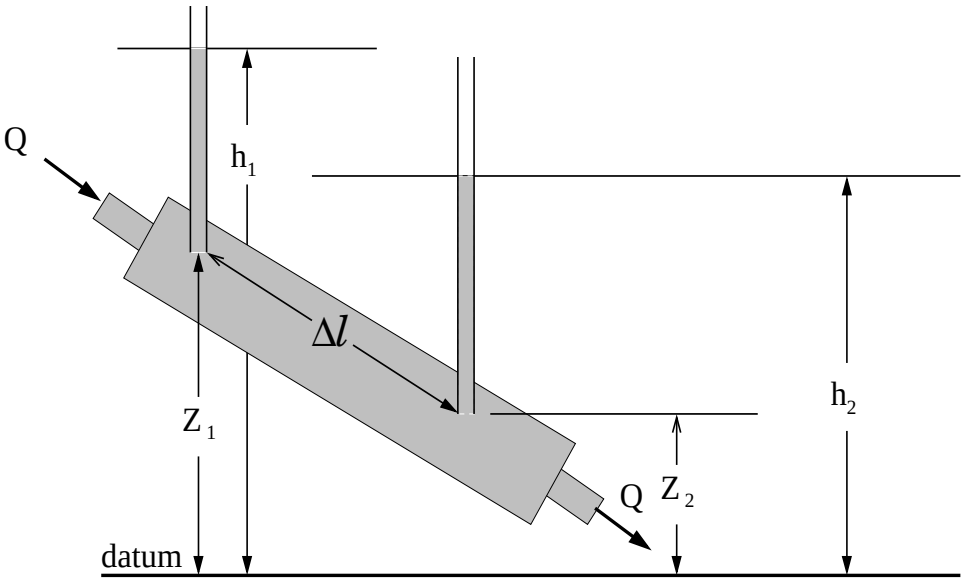

Figure 1.2: Henry Darcy's experiment (adapted from [38, page 34]).

Substituting equation (1.8) into equation (1.6) for $\mathbf{u}^w$ yields

$$\left[\frac{\theta^w}{\rho^w}\frac{\partial \rho^w}{\partial p^w} + \frac{\partial \theta^w}{\partial p^w}\right]\frac{\partial p^w}{\partial h}\frac{\partial h}{\partial t} = \nabla \cdot (K \cdot \nabla h) + \mathcal{S}'. \tag{1.9}$$

The term $\left[\frac{\theta^w}{\rho^w}\frac{\partial \rho^w}{\partial p^w} + \frac{\partial \theta^w}{\partial p^w}\right]\frac{\partial p^w}{\partial h}$ in equation (1.9) is a measurable property of the system called specific storage, which we denote by S_s. For a confined aquifer, S_s is the volume of water released from storage in a unit volume of porous medium material, under a unit decline in hydraulic head [17, page 204]; it accounts for the compressibility of both the fluid and the porous medium. The single-phase flow

equation reduces to

$$S_s \frac{\partial h}{\partial t} = \nabla \cdot (K \cdot \nabla h) + \mathcal{S}', \tag{1.10}$$

which is a single equation for the scalar unknown of hydraulic head. Using Darcy's law as a surrogate for a momentum balance (as in equation (1.9)) implicitly assumes laminar flow conditions. While this is a valid assumption for flow through most granular materials, one practical exception exists near pumping wells where the groundwater velocity is much greater than in the rest of the domain. In fact, the Reynolds number, a dimensionless measure of flow behavior (i.e. laminar or turbulent), can be on the order of 100. A brief justification of this statement follows, including an explanation of the Reynold's number as description of flow behavior.

In general the Reynolds number is proportional to the magnitude of some characteristic velocity, $\mathbf{u}^*$, and inversely proportional to the kinematic viscosity of water, $\nu \left(\frac{\mathrm{L}^2}{\mathrm{T}}\right)$. Assuming that L^* is a characteristic length scale, the Reynolds number is given by

$$\mathrm{Re} = \frac{L^* \mathbf{u}^*}{\nu}. \tag{1.11}$$

This number quantifies the ratio of inertial forces to viscous forces, and as a dimensionless quantity, it is useful in comparing the behavior of flows independent of the scale of the system.

The dynamic viscosity of water, $\mu\left(\frac{\mathrm{M}}{\mathrm{LT}}\right)$, is related to the kinematic viscosity by

$$\nu = \frac{\mu}{\rho}. \tag{1.12}$$

Using the surface average grain diameter of the medium, D [16, page 125], as the characteristic length scale and taking the characteristic velocity to be the unknown velocity, $\mathbf{u}$, the Reynold's number can be formulated as

$$\mathrm{Re} = \frac{\rho D|\mathbf{u}|}{\mu}. \tag{1.13}$$

Darcy's law models slow flow conditions, generally characterized by $0 < \mathrm{Re} < 10$ [16, page 126]. Higher velocity flow data, corresponding to $\mathrm{Re} >> 10$, deviates from the predictions of Darcy's law, as described in Section 1.4. Reynold's numbers outside the Darcy regime can appear in practice, and here it will be shown that near a pumping well it is reasonable to expect a Reynold's number of at least one hundred.

Table 1.1: Range of grain sizes (in millimeters) for various types of gravel [40, page 410].

Fine	4-8
Medium	8-16
Coarse	16-32
Very coarse	32-64

Consider a well with a gravel pack surrounding the well casing as shown in Figure 1.3. Values for density and dynamic viscosity of $1000\frac{\mathrm{kg}}{\mathrm{m}^3}$ and $0.001\frac{\mathrm{kg}}{\mathrm{m-s}}$, respectively,

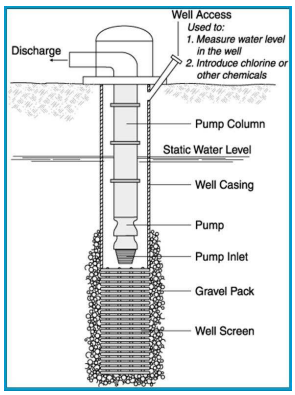

Figure 1.3: The well screen and gravel pack are of particular importance in this picture, as they are key parts of any well (injection or production). Original drawing from [108, page 2]; used here with permission from the Director of Agriculture Communication at North Dakota State University [81].

are used to calculate the Reynold's number near the well. A characteristic velocity and the average grain diameter of the gravel pack are the only parameters from equation (1.13) which remain to be specified. A grain-size classification table is found in [40, page 410], and the portion related to gravel is provided in Table 1.1. Assume that for this calculation the gravel pack is composed of fine gravel with average grain diameter of 4mm. Note that if all other parameters are fixed, the Reynold's number will increase as the average grain size of the gravel pack increases; therefore, this choice of grain size will yield a lower bound on the Reynold's number near the well. As for the characteristic velocity, the average velocity of groundwater should be approximately $0.03\frac{\text{m}}{\text{sec}}$ at the well screen [40, page 450]. In this instance, the Reynold's number at the well screen ($\text{Re} = \frac{1000(0.004)(0.03)}{0.001} = 120$) is certainly outside the Darcy regime.

1.4 Motivating a Nonlinear Approach

1.4.1 Drawbacks to Darcy's Law

The traditional formulation of the single-phase flow problem is advantageous because it only requires solving a scalar equation for the scalar hydraulic head unknown, h. Then the linear differential extension of Darcy's law is used to compute the velocity field across the domain from the hydraulic head solution. However, the shortcomings of Darcy's law are known [17, 56, 107].

Since Darcy's law ($\frac{Q}{A} = \frac{K(h_1 - h_2)}{L}$) was derived experimentally, the conditions under which the experiment was performed should be kept in mind. Darcy studied steady, saturated flow of water through a vertical column packed relatively homogeneously with a porous medium; thus the experimental results apply directly to a system in which (i) the porous medium is well-sorted, (ii) all pore spaces are completely filled by a single fluid phase, (iii) one-dimensional, slow flow conditions are exhibited (i.e. Re $< \mathcal{O}(1)$[16, page 127]), and (iv) all volumetric flow rates and head levels are measured outside of the system of interest at the megascale.

These requirements describe only a very small subset of the groundwater flow problems to which Darcy's law and its various extensions have actually been applied in practice. One should be aware that while in many instances the use of extensions to Darcy's law has resulted in physically reasonable flow fields, rigorous mathematical support for this practice is limited and there is a tendency to ignore the implicit

assumptions made when using Darcy's law. Additionally, Darcy's law breaks down in the case of higher velocities; under very low permeability conditions a minimum gradient is required for flow, independent of Darcy's law [16, page 127]. Furthermore, under high velocity conditions groundwater flows in a nonlinear, indirect path rather than the linear one predicted by the three-dimensional extension to Darcy's law given in equation (1.8) [16, page 177]. As mentioned previously, high velocity conditions can be expected near a pumping well.

Initially, turbulence was suspected as the source of the nonlinearity due to parallels drawn between porous mediium flow and flow in pipes; however, that idea has generally been discounted [66, 107]. Scheidegger provides an argument for why these nonlinearities should instead be attributed to the onset of inertial effects in laminar flow [107, pages 158-160]. Other researchers theorize that microscopic inertial forces [11, 33, 45, 88, 105] or microscale and macroscale drag forces [42, 66, 67, 84, 103] are responsible for the deviations.

1.4.2 Alternatives to Darcy's Law

The short-comings of the traditional groundwater flow model in situations outside of the slow-flow regime motivate an alternative to Darcy's law that will predict linear flow behavior for Re $<<$ 10, while accurately capturing the nonlinear behavior of the data as the Reynolds number increases through the laminar flow regime. Darcy's law was published in 1856 [34], and as early as 1901 other authors published various

Table 1.2: Select early work on nonlinear models for fluid flow through porous media as reported in [16, pages 182-184]

Group I	
Forchheimer (1901)	$J = au + bu^2$, a and b constant
Forchheimer (1901)	$J = au + bu^2 + cu^3$, c also constant
Forchheimer (1930)	$J = au + bu^m$, $1.6 \leq m \leq 2$
Group II	
Rumer and Drinker (1966)	$J = \frac{S_1 C_D u^2}{2g\phi^2}\sqrt{\frac{(1-\phi)}{N_s S_2 k}}$
Bachmat (1965)	$\mathbf{k}\cdot\mathbf{J} = \frac{\nu}{g}\left(1 + \frac{u\beta_g}{\phi\nu}\right)\mathbf{u}$
Group III	
Ergun(1952)	$J = 150\frac{(1-\phi)^2\nu}{\phi^3 g D^2}u + 1.75\frac{(1-\phi)}{\phi^3 g D}u^2$
Schneebeli (1955)	$J = 1100\frac{\nu}{g\varsigma^2}u + \frac{12}{g\varsigma}u^2$

nonlinear alternatives which were shown to out-perform Darcy's law in a variety of experimental situations [16, pages 182-184][107, pages 162-180][41].

Bear separates much of the early work on nonlinear motion equations into categories based upon how the model coefficients relate to fluid and porous medium properties, if at all. In [16, pages 182-184] Bear provides an overview of the nonlinear flow models proposed from 1901-1967, where the models in group I contain coefficients entirely unrelated to fluid and porous medium properties; group II models have coefficients slightly related to fluid and medium properties, but not all parameters are; while all parameters in the group III models are specified in terms of fluid and medium properties.

Table 1.2 provides a subset of Bear's listing, with most models posited in terms of the one-dimensional hydraulic gradient, $J = \frac{h_1 - h_2}{\Delta x}$; however, Bachmat's model

applies to fully three-dimensional flow in an anisotropic porous medium. As a point of reference, Darcy's law in one spatial dimension is stated as $u = KJ$ when using this J notation. To explain the rest of the notation in Table 1.2, ϕ is the porosity, u is the one-dimensional specific discharge or Darcy velocity, the coefficients S_1 and S_2 are volume and surface-shape factors, g is the acceleration due to gravity, ν is the kinematic viscosity, N_s is a factor which accounts for the effects of neighboring particles, C_D is a particle drag coefficient which depends upon Reynolds number, k is the permeability of the porous medium, β_g is a geometrical coefficient accounting for the changing orientation of the fluid flow path, D is the particle diameter, and ς is a constant multiple of the reciprocal of the specific area per unit volume of solid.

The two models which have been the focus of continuing and current research are Forchheimer's equation,

$$J = au + bu^2 + cu^3,$$

and Ergun's equation [19, 66, 88, 95, 114],

$$J = 150\frac{(1-\phi)^2\nu}{\phi^3 g D^2}u + 1.75\frac{(1-\phi)}{\phi^3 g D}u^2$$

which are empirical nonlinear motion models. Forchheimer's equation has been studied in the context of natural convection in which it was shown that the quadratic velocity term was negligible [45, 90, 99], but most other authors take the stance that under different flow conditions it is instead the cubic term which is unnecessary

[48, 84, 96]. Modifications to Ergun's equation have also been made to better fit experimental and simulated data [95].

Several authors have used techniques from continuum mechanics, averaging theory, hybrid mixture theory to derive relations which contain higher order powers of the velocity similar to what appear in the single-phase Forchheimer equation [33, 66, 104]. Furthermore, multiphase and anisotropic extensions to Forchheimer's equation have been derived and used successfully in numerical simulations [19, 109, 113, 114].

In this current work we utilize Forchheimer's quadratic form of the hydraulic gradient. In particular, the model includes both porous medium properties and constants specified by fitting data which is first generated via microscale lattice-Boltzmann simulations and then appropriately averaged to the macroscale [96, page 1].

$$-\nabla p + \rho \mathbf{g} = \frac{\mu}{k_f}\mathbf{u} + \beta \rho \mathbf{u} \|\mathbf{u}\|_2 \tag{1.14}$$

In equation (1.14), the more general quantity $\nabla p - \rho \mathbf{g}$ is considered in place of the hydraulic head gradient which was the focus of the previous discussion on nonlinear extensions to Darcy's law. In this expression for Forchheimer's equation, $\beta(\mathrm{L}^{-1})$ is an inertial coefficient and $k_f(\mathrm{L}^2)$ is the Forchheimer intrinsic permeability. Like the saturated hydraulic conductivity mentioned during the discussion of Darcy's law, intrinsic permeability provides a measure of the medium's ability to transmit a fluid. However, hydraulic conductivity, which is related to the intrinsic permeability via the

formula

$$K = \frac{\rho g k_f}{\mu}, \tag{1.15}$$

is not only a property of the medium, but also of the fluid of interest. The particular values for k_f and β used in the numerical simulations in Chapter 4 are given in [96, page 6].

1.4.3 Additional Nonlinear Effects: Advective Acceleration

The Thermodynamically Constrained Averaging Theory (TCAT [60, 61]) approach to modeling flow through porous media yields a momentum conservation equation with two nonlinearities. One, the inertial term, can be attributed to Forchheimer's expression for the nonlinear relationship between the pressure gradient and the Darcy velocity, $\mathbf{u}$. The other term, the advective acceleration, has the conservative form of

$$\nabla \cdot \left(\frac{\rho \mathbf{u} \otimes \mathbf{u}}{\phi} \right), \tag{1.16}$$

where $\mathbf{u}$ is a row vector, and $\otimes$ is the tensor or dyadic product. In particular, this term in the momentum equation represents how the momentum of the fluid ($\rho\mathbf{u}$) is transported via advection by the pore velocity $\left(\frac{\mathbf{u}}{\phi}\right)$. In the Darcy/non-Darcy flow literature, this term is either missing entirely from the flow model or assumed to be negligible. The reasoning behind this assumption is that porous media flow is, in general, so slow that the term is insignificant in comparison to the other terms in the

equation [16, page 104].

However, in this study we include the advective acceleration term in the flow model (see Section 3.1) to more thoroughly examine its numerical contribution as the velocities of the system increase. In particular, we seek a more formal description of the significance of the nonlinearity in real systems of interest. By "real systems of interest", we refer to heterogeneous porous media. Historically this aspect of non-Darcy flow has been given little attention; in fact, the recent publications by Fourar et al. comprise much of the relevant literature [47, 97] on heterogeneity of the media.

To meet these goals, the plethora of literature on the incompressible Navier-Stokes equations (see Chapter 2) is leveraged throughout this document. Indeed the Navier-Stokes equations include advective acceleration effects and the corresponding literature contains detailed analysis of the form of advective acceleration appropriate for that context,

$$\nabla \cdot (\mathbf{u} \otimes \mathbf{u}) \,. \tag{1.17}$$

Accordingly, much of Section 3.3.3 involves melding the theory required to simulate non-Darcy flow through porous media with the advective acceleration aspects of Navier-Stokes flow. Moreover, notational conventions from the Navier-Stokes literature are adopted in the remainder of this document, as detailed in Chapter 2.

Chapter 2

Background Regarding the Navier-Stokes Equations

This section uses the Navier-Stokes equations as a forum to discuss the advective acceleration term. Moreover, this section will provide a brief introduction to relevant function spaces and the finite element method. Most of the information presented in this section is discussed by Gunzburger in [63, Chapters 1 and 2].

2.1 Equations and Notational Conventions

Recall from Section 1.4.3 that the advective acceleration term, $\nabla \cdot \left(\frac{\rho \mathbf{u} \otimes \mathbf{u}}{\phi} \right)$ (also shown in equation (1.16)), is ignored in the Darcy/non-Darcy flow literature. Section 1.4.3 also mentions that the literature regarding the incompressible Navier-Stokes equations contains detailed analysis of the form of advective acceleration appropriate for that

context, which (repeated from equation (1.17)) is

$$\nabla \cdot (\mathbf{u} \otimes \mathbf{u}) .$$

A perusal of articles regarding the incompressible Navier-Stokes equations will more often than not reference the *advective form* of this term expressed as

$$\mathbf{u} \cdot \nabla \mathbf{u}, \tag{2.1}$$

rather than the conservation form from equation (1.17). This equivalence comes from combining the vector identity [78, Page 1154]

$$\nabla \cdot (\mathbf{a} \otimes \mathbf{b}) = \mathbf{b} \cdot \nabla \mathbf{a} + \mathbf{a} (\nabla \cdot \mathbf{b}) \tag{2.2}$$

with the assumption that the velocity is solenoidal (this assumption is formulated mathematically in equation (2.3b)). A formulation of the incompressible Navier-Stokes equations follows.

$$-\nu \Delta \mathbf{u} + \mathbf{u} \cdot \nabla \mathbf{u} + \nabla \bar{p} = \mathbf{f} \quad \text{in } \Omega \tag{2.3a}$$

$$\nabla \cdot \mathbf{u} = 0 \quad \text{in } \Omega \tag{2.3b}$$

$$\mathbf{u} = 0 \quad \text{on } \Gamma \tag{2.3c}$$

Equation (2.3a) is the Navier-Stokes momentum equation, equation (2.3b) is the incompressibility constraint, and the homogeneous Dirichlet boundary condition on velocity is given by equation (2.3c). The body force per unit mass is denoted by $\mathbf{f}$, ν is the constant kinematic viscosity, as discussed in Section 1.3, and $\bar{p}\left(\frac{\mathrm{L}^2}{\mathrm{T}^2}\right)$ is equal to the pressure, p, divided by the constant density, ρ. The domain, Ω, is assumed to be an open, bounded region in $\mathbb{R}^n$ (n=2 or 3) with boundary denoted by Γ.

In the incompressible Navier-Stokes literature, vectors are assumed to be oriented as row vectors, the gradient operator is defined in [63, Page 6] as

$$[\nabla \mathbf{u}]_{ij} = \frac{\partial u_j}{\partial x_i}, \tag{2.4}$$

and the vector Laplacian is defined by applying the Laplacian operator componentwise to the vector such that

$$[\Delta \mathbf{u}]_i = \Delta u_i. \tag{2.5}$$

2.2 Relevant Function Spaces

In order to discuss the finite element approximation of equations (2.3), various function spaces and their associated norms must first be introduced. Functions that are square integrable over Ω are denoted by $L^2(\Omega)$ and are associated with the following

inner product (equation (2.6)) and norm (equation (2.7)).

$$(a,b) = \int_{\Omega} ab \, \mathrm{d}\Omega \tag{2.6}$$

$$\|a\|_0 = (a,a)^{1/2}. \tag{2.7}$$

A similar inner product is defined for vector-valued functions in $\mathbf{L}^2(\Omega)$ (where each component of the vector is an element of $L^2(\Omega)$) as

$$(\mathbf{a},\mathbf{b}) = \int_{\Omega} \mathbf{a}\cdot\mathbf{b} \, \mathrm{d}\Omega. \tag{2.8}$$

This notation will be particularly useful in rewriting the weak form of the Navier-Stokes equations in a very compact form later in this section.

Additionally, a constraint can be applied to $L^2(\Omega)$ in order to yield another function space. Specifically, including the requirement that the function have zero mean over Ω results in the constrained function space

$$L_0^2(\Omega) = \left\{ a \in L^2(\Omega) : \int_{\Omega} a \, \mathrm{d}\Omega = 0 \right\}. \tag{2.9}$$

From equations (2.3), it is apparent that the Navier-Stokes pressure, $\bar{p}$, is only specified up to an arbitrary additive constant. Thus, one appropriate choice of solution space for pressure is $\bar{p} \in L_0^2(\Omega)$; another option is to look for solutions $\bar{p} \in L^2(\Omega)$ with an additional condition that $\bar{p}$ is fixed at one point in Ω.

The square integrable functions whose derivatives of order less than or equal to i (where $i \geq 0$ is an integer) are also square integrable are of interest as well. This Sobolev space is denoted by

$$H^i(\Omega) = \left\{ a \in L^2(\Omega) : D^\vartheta a \in L^2(\Omega), \ \ \vartheta = 1, \ldots, i \right\} \tag{2.10}$$

where D^ϑ denotes any and all derivatives of order ϑ. The norm associated with $H^i(\Omega)$ is

$$\|a\|_i = \left(\|a\|_0^2 + \sum_{\vartheta \leq i} \|D^\vartheta a\|_0^2 \right)^{1/2}. \tag{2.11}$$

For vector-valued functions where each component of the vector is an element of $H^i(\Omega)$, the vector itself is an element of

$$\mathbf{H}^i(\Omega) = \left[H^i(\Omega) \right]^n = \left\{ \mathbf{v} : v_j \in H^i(\Omega), \ \ j = 1, \ldots, n \right\}. \tag{2.12}$$

The vector norm, denoted $\|\mathbf{v}\|_i$, is defined by

$$\|\mathbf{v}\|_i = \left(\sum_{j=1}^{n} \|v_j\|_i^2 \right)^{1/2}. \tag{2.13}$$

Just as a new function space ($L_0^2(\Omega)$) resulted from applying the zero-mean constraint to the $L^2(\Omega)$ function space, a similar constraint process can generate a new

Sobolev space by constraining the space $H^1(\Omega)$. Specifically,

$$H_0^1(\Omega) = \left\{ a \in H^1(\Omega) : a = 0 \text{ on } \Gamma \right\}, \tag{2.14}$$

where elements of this constrained space not only have one square integrable derivative over the domain, but also vanish on the boundary of the domain. Of course, this Sobolev space also has a vector extension such that elements of $\mathbf{H}_0^1(\Omega)$ are vectors with individual components in $H_0^1(\Omega)$. The norm associated with $H^1(\Omega)$ is

$$\|a\|_1 = \left(\|a\|_0^2 + \sum_{i=1}^{n} \left\| \frac{\partial a}{\partial x_i} \right\|_0^2 \right)^{1/2}, \tag{2.15}$$

and the semi-norm for functions belonging to $H_0^1(\Omega)$ is defined to be

$$|a|_1 = \left(\sum_{i=1}^{n} \left\| \frac{\partial a}{\partial x_i} \right\|_0^2 \right)^{1/2}. \tag{2.16}$$

The dual space $H^{-1}(\Omega)$ consists of bounded linear functionals on $H_0^1(\Omega)$, i.e.

$$H^{-1}(\Omega) = \left\{ a : (a, v) < \infty \text{ for all } v \in H_0^1(\Omega) \right\}. \tag{2.17}$$

A norm for this space is given by

$$\|a\|_{-1} = \sup_{0 \neq v \in H_0^1(\Omega)} \frac{(a, v)}{|v|_1}. \tag{2.18}$$

The trace spaces are also required for the analysis relating to the incompressible Navier-Stokes equations. The trace spaces consist of the restriction of functions in $H^i(\Omega)$ to the boundary Γ. For example, $H^{1/2}(\Gamma)$ consists of traces of functions belonging to $H^1(\Omega)$, and the norm associated with this trace space is given by

$$\|a\|_{1/2,\Gamma} = \inf_{\substack{v \in H^1(\Omega) \\ v=a \text{ on } \Gamma}} \|v\|_1. \tag{2.19}$$

2.3 The Weak Form

To write the weak form of equations (2.3) one considers the velocity $\mathbf{u} \in \mathbf{H}_0^1(\Omega)$, the pressure $\bar{p} \in L_0^2(\Omega)$, and the body force $\mathbf{f} \in \mathbf{H}^{-1}(\Omega)$. Then each equation is multiplied by an appropriate test function and integrated over the domain of interest. To specify the *Galerkin* weak form, the test functions $\mathbf{w}$ and q (associated with velocity and pressure, respectively) are chosen to be elements of the same function spaces as their unknown counterparts. This is contrasted with *Petrov-Galerkin* formulations where each test function need not come from the same function space as the unknown it is associated with.

Nevertheless, executing the steps just described in the process of generating the

Galerkin weak formulation of equations (2.3) results in

$$\int_\Omega -\nu\Delta\mathbf{u}\cdot\mathbf{w}\,\mathrm{d}\Omega + \int_\Omega \mathbf{u}\cdot\nabla\mathbf{u}\cdot\mathbf{w}\,\mathrm{d}\Omega + \int_\Omega \nabla\bar{p}\cdot\mathbf{w}\,\mathrm{d}\Omega = \int_\Omega \mathbf{f}\cdot\mathbf{w}\,\mathrm{d}\Omega \quad \text{(2.20a)}$$
$$\text{for all } \mathbf{w}\in\mathbf{H}_0^1(\Omega)$$

$$\int_\Omega \nabla\cdot\mathbf{u}q\,\mathrm{d}\Omega = 0 \quad \text{in } \Omega \quad \text{for all } q\in L_0^2(\Omega)\,. \quad \text{(2.20b)}$$

The boundary condition on velocity is accounted for by choosing $\mathbf{u}\in\mathbf{H}_0^1(\Omega)$; all elements of that function space are identically zero on the boundary of Ω. To reduce the regularity required of the unknown functions, one integrates the terms with higher-order derivatives by parts. For example, in equation (2.20a) the terms involving the Laplacian of the velocity and the gradient of pressure are integrated by parts, and the result is given in equations (2.21).

$$-\nu\int_\Gamma (\nabla\mathbf{u}\cdot\mathbf{n})\cdot\mathbf{w}\,\mathrm{d}\Gamma + \nu\int_\Omega \nabla\mathbf{u}:\nabla\mathbf{w}\,\mathrm{d}\Omega + \int_\Omega (\mathbf{u}\cdot\nabla\mathbf{u})\cdot\mathbf{w}\,\mathrm{d}\Omega \quad \text{(2.21a)}$$
$$+\int_\Gamma \bar{p}\mathbf{n}\cdot\mathbf{w}\,\mathrm{d}\Gamma - \int_\Omega \bar{p}\nabla\cdot\mathbf{w}\,\mathrm{d}\Omega = \int_\Omega \mathbf{f}\cdot\mathbf{w}\,\mathrm{d}\Omega$$
$$\text{for all } \mathbf{w}\in\mathbf{H}_0^1(\Omega)$$

$$\int_\Omega \nabla\cdot\mathbf{u}q\,\mathrm{d}\Omega = 0 \quad \text{in } \Omega \quad \text{for all } q\in L_0^2(\Omega) \quad \text{(2.21b)}$$

Note that $\mathbf{n}$ denotes the unit outward normal vector to the boundary. New notation

is introduced in equations (2.21), and the definitions follow.

$$\nabla \mathbf{u} : \nabla \mathbf{v} = \sum_{i,j=1}^{n} \frac{\partial u_i}{\partial x_j} \frac{\partial v_i}{\partial x_j} \tag{2.22}$$

$$(\mathbf{v} \cdot \nabla \mathbf{u}) \cdot \mathbf{w} = \sum_{i,j=1}^{n} v_j \frac{\partial u_i}{\partial x_j} w_i \tag{2.23}$$

The choice of function spaces for velocity and pressure cause the boundary terms in equation (2.21a) to vanish. Thus the weak form of the Navier-Stokes equations can be simplified to the following system of equations.

$$\nu \int_{\Omega} \nabla \mathbf{u} : \nabla \mathbf{w} \, \mathrm{d}\Omega + \int_{\Omega} \mathbf{u} \cdot \nabla \mathbf{u} \cdot \mathbf{w} \, \mathrm{d}\Omega - \int_{\Omega} \bar{p} \nabla \cdot \mathbf{w} \, \mathrm{d}\Omega = \int_{\Omega} \mathbf{f} \cdot \mathbf{w} \, \mathrm{d}\Omega \tag{2.24a}$$
$$\text{for all } \mathbf{w} \in \mathbf{H}_0^1(\Omega)$$

$$\int_{\Omega} \nabla \cdot \mathbf{u} q \, \mathrm{d}\Omega = 0 \quad \text{in } \Omega \quad \text{for all } q \in L_0^2(\Omega) \tag{2.24b}$$

Using the vector inner product from equation (2.8), two bilinear forms and a trilinear form can be defined that allow the Navier-Stokes equations to be written in a more compact form.

$$a(\mathbf{u}, \mathbf{w}) = \nu \int_{\Omega} \nabla \mathbf{u} : \nabla \mathbf{w} \, \mathrm{d}\Omega \text{ for all } \mathbf{u}, \mathbf{w} \in \mathbf{H}^1(\Omega) \tag{2.25a}$$

$$b(\mathbf{w}, q) = -\int_{\Omega} q \nabla \cdot \mathbf{w} \, \mathrm{d}\Omega \text{ for all } \mathbf{w} \in \mathbf{H}^1(\Omega) \text{ and } q \in L^2(\Omega) \tag{2.25b}$$

$$c(\mathbf{v}, \mathbf{u}, \mathbf{w}) = \int_{\Omega} \mathbf{v} \cdot \nabla \mathbf{u} \cdot \mathbf{w} \, \mathrm{d}\Omega \text{ for all } \mathbf{u}, \mathbf{v}, \mathbf{w} \in \mathbf{H}^1(\Omega) \tag{2.25c}$$

The weak form of the Navier-Stokes equations from equations (2.24) can be written more succinctly as

$$a(\mathbf{u},\mathbf{w}) + c(\mathbf{u},\mathbf{u},\mathbf{w}) + b(\mathbf{w},\bar{p}) = (\mathbf{f},\mathbf{w}) \quad \text{for all } \mathbf{w} \in \mathbf{H}_0^1(\Omega) \tag{2.26a}$$

$$b(\mathbf{u},q) = 0 \quad \text{for all } q \in L_0^2(\Omega). \tag{2.26b}$$

2.4 Discrete System of Nonlinear Equations

To transition from the continuous, weak finite element problem shown in equations (2.26) to the discrete finite element problem, one chooses a family of finite dimensional spaces $\mathbf{V}_0^\Delta$ and S_0^Δ for the velocity and pressure, respectively. Here, Δ is a measure of the grid spacing associated with the discretization of the domain into elements denoted by Ω_e for $e = 0 \ldots (ne-1)$, where ne is the total number of elements in the domain.

The finite dimensional problem is to find $\mathbf{u}^\Delta \in \mathbf{V}_0^\Delta$ and $\bar{p}^\Delta \in S_0^\Delta$ which satisfy

$$a\left(\mathbf{u}^\Delta,\mathbf{w}^\Delta\right) + c\left(\mathbf{u}^\Delta,\mathbf{u}^\Delta,\mathbf{w}^\Delta\right) + b\left(\mathbf{w}^\Delta,\bar{p}^\Delta\right) = \left(\mathbf{f},\mathbf{w}^\Delta\right) \tag{2.27a}$$

$$\text{for all } \mathbf{w}^\Delta \in \mathbf{V}_0^\Delta$$

$$b\left(\mathbf{u}^\Delta,q^\Delta\right) = 0 \quad \text{for all } q^\Delta \in S_0^\Delta. \tag{2.27b}$$

The final step in the finite element method is to choose bases for $\mathbf{V}_0^\Delta$ and S_0^Δ in order to transform the equation set in (2.27) into a system of nonlinear algebraic equations.

Let $\{q_j(\mathbf{x})\}$, $j = 1, \ldots, \mathbb{J}$ be a basis for S_0^Δ, while $\{\mathbf{w}_i(\mathbf{x})\}$, $i = 1, \ldots, \mathbb{I}$ is a basis for $\mathbf{V}_0^\Delta$. Using these bases, the discrete unknowns $\bar{p}^\Delta$ and $\mathbf{u}^\Delta$ can be written as

$$\bar{p}^\Delta = \sum_{j=1}^{\mathbb{J}} \alpha_j q_j(\mathbf{x}) \tag{2.28}$$

$$\mathbf{u}^\Delta = \sum_{i=1}^{\mathbb{I}} \beta_i \mathbf{w}_i(\mathbf{x}) \tag{2.29}$$

with constant coefficients α_j and β_i. With these basis expansions, equations (2.27) may be rewritten yet again as the following system of equations. Note that the test functions are chosen to be the basis vectors.

$$\sum_{i=1}^{\mathbb{I}} a(\mathbf{w}_i, \mathbf{w}_\xi)\beta_i + \sum_{i,m=1}^{\mathbb{I}} c(\mathbf{w}_m, \mathbf{w}_i, \mathbf{w}_\xi)\beta_i\beta_m + \sum_{j=1}^{\mathbb{J}} b(\mathbf{w}_\xi, q_j)\alpha_j = (\mathbf{f}, \mathbf{w}_\xi) \quad \text{for } \xi = 1, \ldots, \mathbb{I} \tag{2.30a}$$

$$\sum_{i=1}^{\mathbb{I}} b(\mathbf{w}_i, q_\zeta)\beta_i = 0 \quad \text{for } \zeta = 1, \ldots \mathbb{J} \tag{2.30b}$$

The issue of how to choose the finite dimensional spaces $\mathbf{V}_0^\Delta$ and S_0^Δ remains to be addressed. For a *conforming* method one would choose $\mathbf{V}_0^\Delta \subset \mathbf{H}_0^1(\Omega)$ and $S_0^\Delta \subset L_0^2(\Omega)$; in the nonconforming alternative, $\mathbf{V}_0^\Delta \not\subset \mathbf{H}_0^1(\Omega)$ and/or $S_0^\Delta \not\subset L_0^2(\Omega)$. For the Navier-Stokes equations using just any choice of *conforming* spaces may result in an unstable numerical scheme. This is because the Navier-Stokes equations are an example of a mixed finite element method.

A useful definition, due to Roberts and Thomas [102, Page 527], states that

> "...a finite element method is a mixed method if it involves the simultaneous approximation of two or more vector fields defined on the physical domain. These will in general be the principal unknown and an expression involving one or more of its derivatives."

In the case of the Navier-Stokes equations, the interplay between velocity and pressure means that the bases for S_0^Δ and $\mathbf{V}_0^\Delta$ cannot be chosen independently. The two bases must relate to each other in such a way that the *Ladyzhenskaya-Babuška-Brezzi* (LBB) condition is satisfied. This condition is named for the three researchers who quantified the theoretical relationship between the function spaces [5, 6, 7, 25, 83].

2.5 LBB Condition

The LBB condition ([79, Page 234] and [102, Pages 567-573]), also known as the inf-sup condition and the div-stability condition [63, Pages 10-13], provides guidance on how to choose basis combinations for velocity and pressure that will yield a stable numerical scheme. The following mathematical statement is one way to express the LBB condition. Given any $q^\Delta \in S_0^\Delta$,

$$\sup_{0 \neq \mathbf{w}^\Delta \in \mathbf{V}_0^\Delta} \left(\frac{b\left(\mathbf{w}^\Delta, q^\Delta\right)}{\|\mathbf{w}^\Delta\|_1} \right) \geq \eta \|q^\Delta\|_0, \tag{2.31}$$

where η is a positive constant chosen independent of both Δ and q^Δ.

The references above provide very detailed information regarding the div-stability

condition; thus, only an overview of the condition and its applicability to the non-Darcy flow model (shown in Section (3.1)) is provided here. As the name and the appearance of the bilinear operator $b\left(\mathbf{w}^{\Delta}, q^{\Delta}\right)$ in equation (2.31) suggests, the div-stability condition is required due to the appearance of the divergence-free velocity in the steady-state mass conservation equation (2.3b).

Gunzburger clearly states the essence of the div-stability condition as, *"Loosely speaking, the div-stability condition ensures, as* $h \to 0$ *at least, that discretely solenoidal functions tend to solenoidal functions."* [63, Page 13]. The reference to "$h \to 0$" ($\Delta \to 0$ using the notation of this document), is equivalent to "the computational grid is refined". To ensure the stable approximation of a discretely divergence-free velocity, the div-stability condition restricts the allowable combinations of finite element spaces for pressure and velocity. In particular one cannot use the same finite element space defined over the same tessellation of the computational domain to approximate both pressure and velocity.

For those more familiar with finite difference methods, consider using a standard central difference scheme to discretize the continuous equations in (2.3) under the assumption that all unknowns are located at cell-centers. The equivalent idea from the finite element method is using the same finite element space defined over the same grid, and in both cases unphysical pressure oscillations appear in the solution. One way to remove these oscillations for finite difference schemes is to assume that the unknowns are located on a staggered grid, and apply the central difference scheme

to the equations in that case. For the finite element method one can remove the unphysical oscillations by choosing a combination of finite element spaces for velocity and pressure which satisfy the LBB condition. As in the case of finite differences, there exists more than one way to correct the oscillatory pressure field when using the finite element method. One way to circumvent this restrictive condition is to use stabilization techniques which are addressed in Sections 2.6 and 3.3.3.

While the LBB condition is discussed here within the context of the nonlinear Navier-Stokes equations, it should be emphasized that it is the relationship between the unknowns of the problem rather than the nonlinearity that places a restriction on the allowable function spaces. In the next section, stabilization techniques will be illustrated in the context of a linear problem which is also subject to the LBB condition.

2.6 Illustrating Stabilization Techniques Via the Stokes Equations

Stabilization techniques allow the use of any combination of basis functions, without regard to the constraints imposed by the LBB condition. For stabilized equations, the same low-order basis functions can approximate both velocity and pressure and result in a stable discrete system. In this case the steps required to transform the continuous partial differential equations into the corresponding discrete linear or nonlinear system

are greatly simplified.

This section covers a variety of available stabilization techniques at a high level, but does not attempt to detail the extensive literature on this topic [23, 24, 49, 50, 51, 73, 75, 76, 77, 78, 89, 110]. While not exhaustive, this section covers how stabilization circumvents the LBB condition and focuses on multiscale residual stabilization. This technique arises again in Section 3.1 to stabilize the groundwater flow equations.

To simplify the introduction to stabilization, consider the linearization of the Navier-Stokes equations, better known as the Stokes equations.

$$-\nu\Delta\mathbf{u} + \nabla\bar{p} = \mathbf{f} \quad \text{in } \Omega \tag{2.32a}$$

$$\nabla \cdot \mathbf{u} = 0 \quad \text{in } \Omega \tag{2.32b}$$

$$\mathbf{u} = 0 \quad \text{on } \Gamma \tag{2.32c}$$

As one can see, the Stokes equations only differ from the Navier-Stokes equations by the exclusion of the advective term. Furthermore, the same function spaces are considered for approximating the solution to the system of equations, namely those satisfying the LBB condition shown in equation (2.31).

The weak form of the Stokes equations can be derived in the same fashion as in Sections 2.3 and 2.4 for the weak form of the Navier-Stokes equations. Utilizing the bilinear form notation introduced in equations 2.26, the Stokes equations in discrete

weak form can be written as

$$a\left(\mathbf{u}^{\Delta}, \mathbf{w}^{\Delta}\right) + b\left(\mathbf{w}^{\Delta}, \bar{p}^{\Delta}\right) = \left(\mathbf{f}, \mathbf{w}^{\Delta}\right) \quad \text{for all } \mathbf{w}^{\Delta} \in \mathbf{V}_0^{\Delta} \tag{2.33a}$$

$$b\left(\mathbf{u}^{\Delta}, q^{\Delta}\right) = 0 \quad \text{for all } q^{\Delta} \in S_0^{\Delta}. \tag{2.33b}$$

According to [26, Page 3], linear problems of the form

$$\mathcal{A}\left(\widetilde{\mathbf{u}}^{\Delta}, \widetilde{\mathbf{w}}^{\Delta}\right) = \mathcal{F}\left(\widetilde{\mathbf{w}}^{\Delta}\right) \ \ \forall \widetilde{\mathbf{w}}^{\Delta} \in V^{\Delta} \tag{2.34}$$

where $\mathcal{A}(\cdot,\cdot)$ is a continuous, symmetric bilinear form on a space of admissible functions, V^{Δ}, and $\mathcal{F}(\cdot)$ is a linear form on the same space will have a unique solution if the bilinear form is *coercive*.

Definition 2.1. *A bilinear functional $\mathcal{A}(\cdot,\cdot)$ on a normed space E is called* **coercive** *(or sometimes elliptic) if there exists a positive constant α such that*

$$\mathcal{A}(x,x) \geq \alpha \|x\|_E^2 \ \ \forall x \in E. \tag{2.35}$$

The Stokes problem from equations (2.33) can be written as a linear problem of

the form shown in equation (2.34), where $\widetilde{\mathbf{u}}^{\Delta} = \left[\mathbf{u}^{\Delta}, \bar{p}^{\Delta}\right]$ and $\widetilde{\mathbf{w}}^{\Delta} = \left[\mathbf{w}^{\Delta}, q^{\Delta}\right]$.

$$\mathcal{A}\left(\widetilde{\mathbf{u}}^{\Delta}, \widetilde{\mathbf{w}}^{\Delta}\right) = \mathcal{F}\left(\widetilde{\mathbf{w}}^{\Delta}\right) \ \forall \widetilde{\mathbf{w}}^{\Delta} \in V_0^{\Delta} \times S_0^{\Delta} \tag{2.36a}$$

where

$$\mathcal{A}\left(\widetilde{\mathbf{u}}^{\Delta}, \widetilde{\mathbf{w}}^{\Delta}\right) \equiv a\left(\mathbf{u}^{\Delta}, \mathbf{w}^{\Delta}\right) + b\left(\mathbf{w}^{\Delta}, \bar{p}^{\Delta}\right) - b\left(\mathbf{u}^{\Delta}, q^{\Delta}\right) \tag{2.36b}$$

and

$$\mathcal{F}\left(\widetilde{\mathbf{w}}^{\Delta}\right) \equiv \left(\mathbf{f}, \mathbf{w}^{\Delta}\right) \tag{2.36c}$$

The bilinear form $\mathcal{A}\left(\widetilde{\mathbf{u}}^{\Delta}, \widetilde{\mathbf{w}}^{\Delta}\right)$ defined above is not coercive for just any combination of function spaces in $V_0^{\Delta} \times S_0^{\Delta}$. At this point, the LBB condition still must be satisfied. Stabilization techniques circumvent the LBB condition by adding terms to (2.36). These additional terms are chosen in such a way that

1. the new bilinear form is coercive for any choice of basis functions in $V_0^{\Delta} \times S_0^{\Delta}$,
2. and the solution to the new system is consistent with the solution to the Stokes equations.

As an example of how stabilization techniques satisfy these criteria, consider a residual stabilization technique for the Stokes equations proposed by Hughes et. al. in [75]. The description that follows is actually aligned with a simplification of the Hughes theory due to Gunzburger [63, Section 3.5]; however, the simplified version is still a valid stabilization strategy for the discrete Stokes equations in (2.33).

In the Hughes method, an integral term involving the Stokes discrete momentum

equation is added to the incompressibility constraint for each element in the domain. The resulting modified discrete system is

$$\begin{aligned} a\left(\mathbf{u}^{\Delta}, \mathbf{w}^{\Delta}\right) + b\left(\mathbf{w}^{\Delta}, \bar{p}^{\Delta}\right) &= \left(\mathbf{f}, \mathbf{w}^{\Delta}\right) \quad (2.37a) \\ \text{for all } \mathbf{w}^{\Delta} &\in \mathbf{V}_0^{\Delta} \\ b\left(\mathbf{u}^{\Delta}, q^{\Delta}\right) + \varpi \sum_{e=0}^{ne-1} \Delta_e^2 \int_{\Omega_e} \left(\nu \Delta \mathbf{u}^{\Delta} - \nabla \bar{p}^{\Delta} + \mathbf{f}\right) \cdot \nabla q^{\Delta} \, \mathrm{d}\Omega &= 0 \quad (2.37b) \\ \text{for all } q^{\Delta} &\in S_0^{\Delta}, \end{aligned}$$

where ϖ is a constant and Δ_e is the grid spacing associated with element Ω_e. Since the momentum residual vanishes for the solution, $[\mathbf{u}, p]$, of the Stokes problem, equation (2.37b) is satisfied exactly and the method is consistent with the original Stokes problem.

The modified equation set in (2.37) represents a new linear problem,

$$\mathfrak{A}\left(\widetilde{\mathbf{u}}^{\Delta}, \widetilde{\mathbf{w}}^{\Delta}\right) = \mathfrak{F}\left(\widetilde{\mathbf{w}}^{\Delta}\right) \quad \forall \widetilde{\mathbf{w}}^{\Delta} \in V_0^{\Delta} \times S_0^{\Delta} \tag{2.38}$$

where the associated bilinear form is denoted by $\mathfrak{A}(\cdot, \cdot)$. The operators representing the modified problem are defined to be

$$\begin{aligned}\mathfrak{A}\left(\widetilde{\mathbf{u}}^{\Delta},\widetilde{\mathbf{w}}^{\Delta}\right) &\equiv \mathcal{A}\left(\widetilde{\mathbf{u}}^{\Delta},\widetilde{\mathbf{w}}^{\Delta}\right)-\varpi\sum_{e=0}^{ne-1}\Delta_e^2\left(\nu\Delta\mathbf{u}^{\Delta}-\nabla\bar{p}^{\Delta},\nabla q^{\Delta}\right)_{\Omega_e}\\ \mathfrak{F}\left(\widetilde{\mathbf{w}}^{\Delta}\right) &\equiv \mathcal{F}\left(\widetilde{\mathbf{w}}^{\Delta}\right)+\varpi\sum_{e=0}^{ne-1}\Delta_e^2\left(\mathbf{f},\nabla q^{\Delta}\right)_{\Omega_e},\end{aligned}$$

where the subscript Ω_e denotes that the e^{th} element is the limit of the integral of the inner product.

Adding the above stabilization terms will circumvent the LBB restrictions as long as the choice of ϖ guarantees $\mathfrak{A}(\cdot,\cdot)$ is coercive over $V_0^{\Delta}\times S_0^{\Delta}$ with respect to the norm [63, Page 45]

$$\sqrt{|\mathbf{u}^{\Delta}|_1^2+\|\bar{p}^{\Delta}\|_0^2}. \tag{2.39}$$

Under a minor mesh regularity assumption (see [27, Page 226] for details), it can be shown that for small ϖ, $\mathfrak{A}(\cdot,\cdot)$ is coercive for piecewise continuous polynomial basis functions. From [27, Page 227] and [75, Page 90-91], the details required to prove coercivity are as follows.

$$\begin{aligned}\mathfrak{A}\left(\widetilde{\mathbf{u}}^{\Delta},\widetilde{\mathbf{u}}^{\Delta}\right) &= a\left(\mathbf{u}^{\Delta},\mathbf{u}^{\Delta}\right)+b\left(\mathbf{u}^{\Delta},\bar{p}^{\Delta}\right)-b\left(\mathbf{u}^{\Delta},\bar{p}^{\Delta}\right)\\ &\quad -\varpi\sum_{e=0}^{ne-1}\Delta_e^2\left(\nu\Delta\mathbf{u}^{\Delta}-\nabla\bar{p}^{\Delta},\nabla\bar{p}^{\Delta}\right)_{\Omega_e}\\ &= a\left(\mathbf{u}^{\Delta},\mathbf{u}^{\Delta}\right)-\varpi\sum_{e=0}^{ne-1}\Delta_e^2\left(\left(\nu\Delta\mathbf{u}^{\Delta},\nabla\bar{p}^{\Delta}\right)_{\Omega_e}-\|\nabla\bar{p}^{\Delta}\|_{0,\Omega_e}^2\right)\end{aligned}$$

The following assumptions from [75, page 90] are required to simplify this expression

further.

- $\|\Delta \mathbf{u}^{\Delta}\|_{\Omega_e} \leq C_e \Delta_e^{-1} \|\nabla \mathbf{u}^{\Delta}\|_{\Omega_e} \ \ \forall \mathbf{u}^{\Delta} \in V_0^{\Delta}$ where C_e is a nondimensional constant depending upon element type, and
- $0 < \varpi \leq \varpi_e \leq C_e^{-2}, \ \ e = 1, 2, \ldots, ne$, where ϖ is a constant

The term $\varpi \Delta_e^2 \left(\nu \Delta \mathbf{u}^{\Delta}, \nabla \bar{p}^{\Delta}\right)_{\Omega_e}$ can be bounded as follows.

$$\begin{aligned} |\varpi \Delta_e^2 \left(\nu \Delta \mathbf{u}^{\Delta}, \nabla \bar{p}^{\Delta}\right)_{\Omega_e}| &\leq \frac{\varpi \Delta_e^2}{2} \left(\frac{1}{\nu} \|\nu \Delta \mathbf{u}^{\Delta}\|_{\Omega_e}^2 + \nu \|\nabla \bar{p}^{\Delta}\|_{0,\Omega_e}^2 \right) \\ &\leq \frac{\varpi \Delta_e^2}{2} \left(\frac{C_e^2 \Delta_e^{-2}}{\nu} \|\nu \nabla \mathbf{u}^{\Delta}\|_{\Omega_e}^2 + \nu \|\nabla \bar{p}^{\Delta}\|_{0,\Omega_e}^2 \right) \\ &\leq \frac{1}{2\nu} \|\nu \nabla \mathbf{u}^{\Delta}\|_{\Omega_e}^2 + \frac{\varpi \Delta_e^2 \nu}{2} \|\nabla \bar{p}^{\Delta}\|_{0,\Omega_e}^2 \end{aligned}$$

The following is true for $\widehat{C} > 0$.

$$\begin{aligned} a\left(\mathbf{u}^{\Delta}, \mathbf{u}^{\Delta}\right) - \varpi \sum_{e=0}^{ne-1} \Delta_e^2 \left(\nu \Delta \mathbf{u}^{\Delta}, \nabla \bar{p}^{\Delta}\right)_{\Omega_e} + \\ \varpi \sum_{e=0}^{ne-1} \Delta_e^2 \|\nabla \bar{p}^{\Delta}\|_{0,\Omega_e}^2 &\geq a\left(\mathbf{u}^{\Delta}, \mathbf{u}^{\Delta}\right) + \\ &\quad \varpi \sum_{e=0}^{ne-1} \Delta_e^2 \|\nabla \bar{p}^{\Delta}\|_{0,\Omega_e}^2 - \\ &\quad \sum_{e=0}^{ne-1} \frac{1}{2\nu} \|\nu \nabla \mathbf{u}^{\Delta}\|_{\Omega_e}^2 - \sum_{e=0}^{ne-1} \frac{\varpi \Delta_e^2 \nu}{2} \|\nabla \bar{p}^{\Delta}\|_{0,\Omega_e}^2 \\ &\geq \frac{\nu}{2} |\mathbf{u}^{\Delta}|_1^2 + \frac{\widehat{C} \varpi}{2} \sum_{e=0}^{ne-1} \Delta_e^2 \|\nabla \bar{p}^{\Delta}\|_{0,\Omega_e}^2 \end{aligned}$$

For sufficiently small $\varpi > 0$, there exists a constant $\widetilde{C} > 0$ independent of the mesh

size, such that

$$\mathfrak{A}\left(\widetilde{\mathbf{u}}^{\Delta},\widetilde{\mathbf{u}}^{\Delta}\right)\geq\widetilde{C}\left(|\mathbf{u}^{\Delta}|_{1}^{2}+\|\bar{p}^{\Delta}\|_{0}^{2}\right)\ \ \forall\widetilde{\mathbf{u}}^{\Delta}\in\mathbf{V}_{0}^{\Delta}\times S_{0}^{\Delta}.$$

Chapter 3

Saturated Flow through Porous Media

3.1 Groundwater Flow Model Equations

The model for saturated, single-phase groundwater flow is shown in equations (3.4) below where it is assumed that the domain of interest is Ω with boundary $\Gamma = \partial\Omega$. The boundary is partitioned into two regions; Γ_N, where Neumann velocity boundary conditions are applied and Γ_D, where Dirichlet pressure boundary conditions are enforced (see equations (3.4c) and (3.4d)). These two regions partition the boundary

of the domain in the following way.

$$\begin{aligned} \overline{\Gamma_N \cup \Gamma_D} &= \Gamma \\ \overline{\Gamma_N \cap \Gamma_D} &= \emptyset \end{aligned} \tag{3.1}$$

In addition to these geometric conventions, notational conventions must be set with respect to the model equations. The standard notation set forth in the finite element literature for the incompressible Navier-Stokes is followed in this document. Gunzburger ([63, Pages 3-6]) provides an explicit description in which all vectors are assumed to be row vectors and the gradient operator is defined such that

$$[\nabla \mathbf{u}]_{i,j} = \frac{\partial u_j}{\partial x_i}. \tag{3.2}$$

Within this context, the $\otimes$ operator in the advective acceleration term (equation (1.16)) combines two row vectors into a matrix object defined by

$$\mathbf{a} \otimes \mathbf{b} \equiv \mathbf{a}^T \mathbf{b}. \tag{3.3}$$

More information on representing the advective acceleration term is provided in Chapter 2.

Enough geometric and mathematical notation has been established to pose the equations comprising the saturated, single-phase flow model. Equation (3.4a) is the

mass conservation equation and equation (3.4b) ensures momentum conservation.

$$\frac{\partial(\phi\rho)}{\partial t} + \nabla\cdot(\rho\mathbf{u}) = \mathcal{S} \quad \in \Omega \tag{3.4a}$$

$$\frac{\partial(\rho\mathbf{u})}{\partial t} + \nabla\cdot\left(\frac{\rho\mathbf{u}\otimes\mathbf{u}}{\phi}\right) + \phi\left(\nabla p - \rho\mathbf{g}\right) = -\frac{\phi\mu}{k}\mathbf{u} - \phi\beta\rho\|\mathbf{u}\|_2\mathbf{u} \quad \in \Omega \tag{3.4b}$$

$$\mathbf{u}\cdot\mathbf{n} = 0 \quad \in \Gamma_N \tag{3.4c}$$

$$p = p_D \quad \in \Gamma_D \tag{3.4d}$$

At this point, further notational explanation is warranted. In equation (3.4c), $\mathbf{n}$ is the unit outward normal vector to the boundary Γ_N. The Dirichlet boundary conditions for pressure are denoted by p_D. In equation (3.4a), external mass sources/sinks are represented by $\mathcal{S}$. A preview of the scenario considered in the numerical results of this document (Chapter 4), as well as the future work proposed in Section 6.2 will serve to illustrate possible representations for $\mathcal{S}$.

The two-dimensional numerical example considered in Chapter 4 is flow from left to right across a square domain, where the flow is induced by a fixed pressure gradient across the domain. In this case, there are no external sources of mass, so $\mathcal{S} = 0$. The future work proposed in Section 6.2 concerns a three-dimensional domain in which flow is induced across the domain due to the interaction of two pumping wells (see the overhead view of a three-dimensional domain in Figure 3.1). The black dot in the figure represents a production well, or a well that is pumping water (mass) out

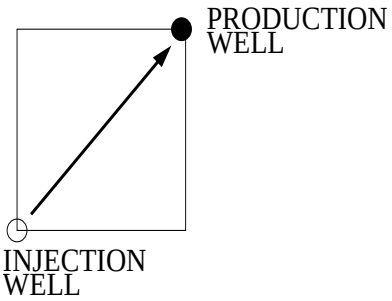

Figure 3.1: Example of how injection and production wells induce flow across the domain. Wells are incorporated in the flow model through a non-zero mass source term ($\mathcal{S}$) in equation (3.4a).

of the subsurface at a given rate. The other dot represents an injection well which is pumping water (mass) into the subsurface at the same rate as the production well is removing it. This set-up will produce a flow field in which the water will flow from the injection well across the domain to the production well. The general expression for the mass source term takes the form

$$\mathcal{S} = \sum_{i=1}^{NW} \rho_i Q_i \delta\left(\mathbf{x} - \mathbf{x}_i\right) \tag{3.5}$$

where there are NW total wells in the domain. For the specific example shown in Figure 3.1, $NW = 2$. Using this expression means that well i, which is pumping with volumetric flow rate Q_i, is modeled as a point source at $\mathbf{x}_i$ in the domain using the Dirac delta function, $\delta\left(\mathbf{x} - \mathbf{x}_i\right)$. This function has the fundamental property that

$$\int_{-\infty}^{\infty} f(x)\delta(x-a)\,\mathrm{d}x = f(a). \tag{3.6}$$

Note also that the right hand side of equation (3.4b) is the Forchheimer relation discussed in Section 1.4.2.

3.2 Incorporating Heterogeneity in the Model

3.2.1 Motivation

The momentum equation introduced in equation (3.4b) of section 3.1 can be considered term by term in the following way.

$$\underbrace{\frac{\partial(\rho\mathbf{u})}{\partial t}}_{\text{acceleration term}} + \underbrace{\nabla\cdot\left(\frac{\rho\mathbf{u}\otimes\mathbf{u}}{\phi}\right)}_{\text{advective acceleration term}} + \phi(\nabla p - \rho\mathbf{g}) + \underbrace{\frac{\phi\mu}{k_f}\mathbf{u}}_{\text{Darcy term}} + \underbrace{\phi\beta\rho\mathbf{u}\|\mathbf{u}\|_2}_{\text{Forchheimer term}} = 0$$

In Chapter 4, all numerical simulations of the flow model shown in equations (3.4) will deal with the steady-state instance. For the momentum equation, which is the focus of this section, this means that one can ignore the acceleration term which is equal to zero at steady-state.

As for the advective acceleration term, its contribution to the momentum equation will increase with the complexity of the flow field; however, the question of whether this term is "significant" in comparison to both the Darcy and Forchheimer terms still remains to be answered. This question is important as we seek to determine which nonlinear terms in the momentum equation have the greatest impact on the solution to the flow model. For this section we determine that the advective term

is "significant" if it is of the same order of magnitude as either the Darcy or the Forchheimer term.

The goal is to determine if, and when, the advective term becomes significant when modeling real systems of interest. In particular, in two spatial dimensions the examination will involve a block heterogeneous media in order to evaluate the effect of advective acceleration over a more complicated flow field.

While it is relatively easy to describe a block heterogeneous system here in words, it is another matter to generate actual values of permeability which are both descriptive of the above two-dimensional problem and can be provided as input to a simulator. The first step in generating a "realistic" system is to assume that the hydraulic conductivity or permeability of most natural porous medium systems is (i) log-normally distributed and (ii) spatially correlated [38, page 38]. This means that if $\mathbb{X}$ is a random variable distributed log-normally, then $\mathbb{Z} = \ln(\mathbb{X})$ is a normally distributed random variable with mean $\mu_{\mathbb{Z}}$ and variance σ^2 ($\mathbb{Z} \in \mathcal{N}(\mu_{\mathbb{Z}}, \sigma^2)$).

As for spatial correlation, Figure 3.2 provides a basic sketch of this concept. If the distance between two points x_1 and x_2 (denoted by $d = |x_1 - x_2|$ where the metric of choice is immaterial) is less than the correlation length, C_L, then the correlation between the two points increases as the distance between them decreases and vice versa. On the other hand, if $d > C_L$ then there is no correlation between the two points regardless of how large d becomes. There are a variety of correlation formulas available, but the simulations in Chapter 4 are based on the Gaussian formulation

shown in equation (3.7).

In the context of determining the permeability of the porous medium contained in a specific domain of interest, two locations in the domain within one correlation length of each other are more likely to have similar permeabilities than if more than one correlation length separated them. This does not rule out the possibility that two locations far from each other in the domain could have similar permeabilities, it is only stating that one is more likely to find localized "neighborhoods" having similar hydraulic properties.

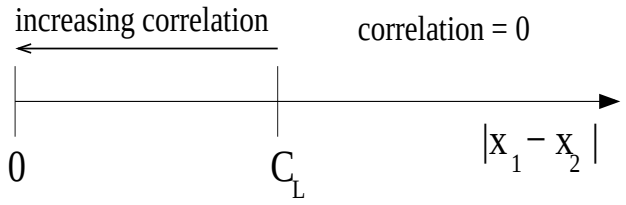

Figure 3.2: When the distance between two points is less than some correlation length, then the distance is inversely proportional to the correlation between the two points. However, when the distance between the two points exceeds the correlation length, the two points are uncorrelated.

Several algorithms exist to generate a random field exhibiting a standard normal distribution with spatial correlation; turning bands, sequential Gaussian algorithm, and the fast Fourier transform (FFT) are a few examples [37, pages 147-148]. The simulations in Chapter 4 use a sequential Gaussian algorithm to generate data from a standard normal distribution. Postprocessing of the data is required before it approximates a permeability field with "realistic" mean and standard deviation.

3.2.2 Random Field Generation

The sequential Gaussian algorithm is explained in [37, section V.2.3], and a specific implementation of this algorithm, `sgsim`, is distributed in the Geostatistical Software LIBrary (GSLIB). GSLIB source code, documentation, and executables can be found at the website `http://www.gslib.com/`, and further documentation is provided in the text [37].

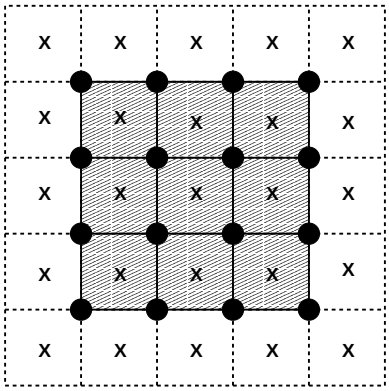

Figure 3.3: GSLIB assumes the data it generates is located at cell centers (marked by an "X"), while all numerical computations in Chapter 4 are performed with nodal (black circles) values. Therefore, an interpolation scheme is required as part of the postprocessing step. The computational domain for the flow simulator, Ω, is represented by the square drawn using solid lines. The squares with dashed boundaries form a "ghost" cell border incorporated into only the GSLIB simulation so that during postprocessing there is enough information to interpolate the data values for the nodes on the boundary of Ω.

Table 3.1 provides an explanation of the input parameters required for `sgsim` in the two-dimensional case. The goal is to generate a log-normally distributed and spatially correlated random field which will approximate a realistic permeability field over the square domain of dimension $[0, 1 \text{ km}] \times [0, 1 \text{ km}]$. Figure 3.3 illustrates how

`sgsim` generates data at cell centers marked in the figure by an "X"; however, all computations in this document deal with unknowns located at nodes on cell edges (represented in Figure 3.3 by black circles). For this reason, the GSLIB domain is slightly larger than the final computational domain of interest so that cell-centered values can be converted to nodal values; in fact, the dimension of the GSLIB domain is $[-5.0, 1005.0 \text{ m}] \times [-5.0, 1005 \text{ m}]$.

By choosing a correlation length of 100 meters and 102 nodes per dimension, we guarantee that there are approximately ten correlation lengths in each dimension and ten nodes per correlation length. A Gaussian model given by

$$G(d) = \mathfrak{S}\left[1 - \exp\left(-\frac{9d^2}{C_L^2}\right)\right] \tag{3.7}$$

is used to determine the correlation between two locations which are separated by the distance d. This model is defined by the sill, $\mathfrak{S}$, and correlation length C_L.

3.2.3 Postprocessing

The output from `sgsim` is a realization of the random variable $\mathbb{Z} \in \mathcal{N}(0, 1)$ at the center of each cell on the grid. These values are ordered in a vector such that the x dimension is cycled through first, then the y dimension, and finally z if one is working in three spatial dimensions (see Figure 3.4).

First the output vector is transformed into a vector of permeability values with the ordering over the computational grid unchanged. Algorithm 3.1, outlining this

Table 3.1: Input parameters for `sgsim` to generate a field variable $\mathbb{Z} \in \mathcal{N}(0,1)$ [37, pages 170-174,330-336].

Parameter	Definition	Value
`idbg`	integer debugging level between 0 and 3	1
`dbgfl`	debugging output file	debug filename
`outfl`	the output grid is written to this file	output filename
`nsim`	number of simulations to generate	1
`nx`	number of nodes in x direction, similarly for y	102
`nz`	number of nodes in z direction	1
`xmn`	location of first x node (origin of x axis), similarly for y and z	-5.0
`xsiz`	spacing of nodes in x direction, similarly for y and z	10.0
`seed`	integer seed to the pseudorandom number generator	69069
`nst`	number of nested variogram structures	1
`c0`	isotropic nugget effect	0
`it`	integer flag specifying type of variogram model	3
`cc`	sill (note: `c0`+`cc`=1.0)	1.0
`ang1`	angle defining orientation of an ellipsoid in 3D	0.0
`ang2`	angle defining orientation of an ellipsoid in 3D	0.0
`ang3`	angle defining orientation of an ellipsoid in 3D	0.0
$\texttt{aa}_{hmax}$	correlation range in horizontal maximum direction	100.0
$\texttt{aa}_{hmin}$	correlation range in horizontal minimum direction	100.0
$\texttt{aa}_{vert}$	correlation range in vertical direction	100.0

transformation following the notation of [44], results in a permeability field with median value coinciding with the computational results of [96].

Algorithm 3.1. *Transform* `sgsim` *output into the random field* k_f *with the mean of* $\ln(k_f)$ *denoted by* μ_f*, and the standard deviation of* $\ln(k_f)$ *denoted by* σ_f*.*

1. *Generate a realization of the random variable* $\mathbb{Z} \in \mathcal{N}(0,1)$ *using* `sgsim`
2. *Convert values of* $\mathbb{Z}$ *to values of* $k_f \in \log -\mathcal{N}(\mu_f, \sigma_f)$ *where* $\mu_f = \log\left(\widetilde{k_f}\right)$ *(*$\widetilde{k_f}$ *is specified in [96, Page 6]) and* σ_f *is the standard deviation. In this document*

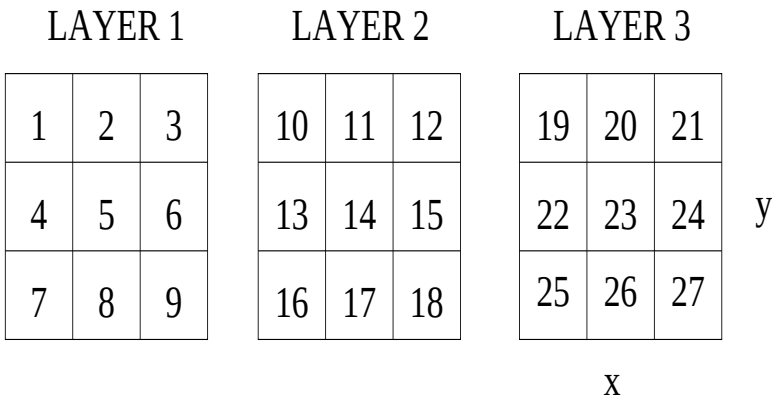

Figure 3.4: GSLIB's scheme for transforming a $3 \times 3 \times 3$ grid into a vector with twenty-seven elements. The various layers represent the discretization in the vertical (z) direction.

increasing levels of heterogeneity are considered, corresponding to variances of

$$\sigma_f^2 = 0.25, 1, 2, 3, \text{ and } 4.$$

The formula for converting realizations of a standard normal distribution to realizations of a specified lognormal distribution is [44, Page 103]

$$\log -\mathcal{N}(\mu_f, \sigma_f) \sim \exp \mu_f \exp(\sigma_f \mathcal{N}(0,1)) \tag{3.8}$$

In the last step of post-processing, the nodal values are generated from the cell-centered values by a simple average (the contribution of the four surrounding cell-centered values are given equal weight).

3.3 Discretization

This section will cover issues pertinent to mixed finite element methods, which were defined on page 33. In formulating an appropriate finite element discretization of the flow equations shown in equations (3.4), one must consider the issues that follow.

1. How will the domain be decomposed into elements? For example, in two dimensions will triangles or rectangles be used? A combination of both is also possible.

2. Given the above meshing strategy, what combination of finite element basis functions will result in a stable discretization in the sense that the classical *LBB condition* is satisfied? (See Section 2.5 for more detailed information on this condition.)

3. And if the appropriate basis functions are somehow inaccessible, what can be done to "fix" the basis function combination that is available?

The above questions will be addressed in the remainder of this section.

3.3.1 Using Available Software to Triangulate the Domain

The question of how to tessellate the continuous domain, Ω, can be a difficult one, but in this case the answer is clear once the computational framework is set. All computations in this document use the Sundance 2.0 symbolic finite element system due to its ease of use in parallel; this software, along with several other software

components required to build the flow simulator, is detailed in Chapter 5. Mesh generation internal to Sundance is limited to the uniform tessellation of lines (1D) and rectangles (2D). In 2D, the interior of the rectangle is divided into uniform triangular elements with cell diameter denoted by Δ. Figure 3.5 provides a coarse example of this case. For more complicated domains or three spatial dimensions the capability exists to read a mesh generated by an external source into the simulator. In this case, the elements still must be simplicial in shape.

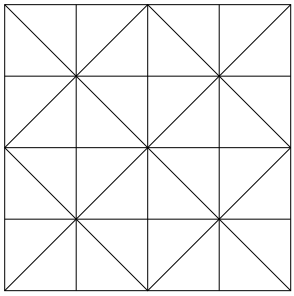

Figure 3.5: Internally Sundance can build a uniform triangulation of the domain of interest as shown here in a coarse mesh example.

In the remainder of this document the tessellation of the domain will be denoted in the following way. The open, bounded domain Ω is subdivided into simplicial elements denoted by Ω_e for $e = 0 \ldots (ne - 1)$, where ne is the total number of elements in the domain. The domain of element interiors will be denoted by $\widetilde{\Omega} = \underset{e}{\cup}\Omega_e$.

3.3.2 Choosing Basis Functions

Raviart-Thomas elements, introduced in [94, 100, 101, 111], are known to be an appropriate basis function pairing for solving the non-Darcy flow equations (equations (3.4)) over a mesh of triangular elements (see [80, 98], [102, Page 550]). The Raviart-Thomas elements also satisfy the LBB condition, introduced in Section 2.5.

While Raviart-Thomas elements are currently unavailable in Sundance 2.0, standard Lagrange interpolating polynomials are readily available and well-tested. These polynomials are elements of $H^1(\Omega)$ and can be computed using the following formula.

$$P(x) = \sum_{j=1}^{n} P_j(x),$$

where

$$P_j(x) = y_j \prod_{\substack{m=1 \\ m \neq j}}^{n} \frac{x - x_m}{x_j - x_m}$$

The Lagrange polynomials of degree one defined over a triangular element will be denoted by $\mathcal{P}_1(\Omega_e)$ (see Figure 3.6). In this document the $\mathcal{P}_1 - \mathcal{P}_1$ combination of finite elements for velocity and pressure, respectively, will be used in the discretization of equations (3.4). The div-stability condition is eluded by modifying the equation set using stabilization techniques [23, Page 324]. Note that the velocity and pressure basis functions are defined over the same discretization of Ω.

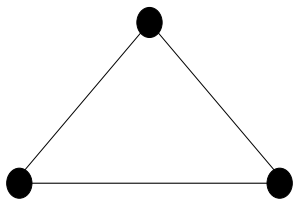

Figure 3.6: A triangular finite element. The black circles represent the locations of the degrees of freedom of the Lagrange interpolation polynomial ($\mathcal{P}_1$ basis functions).

3.3.3 Stabilization

The finite element stabilization literature is extensive, although much of the work focuses on Stokes and Navier-Stokes flow rather than flow described by the Darcy/non-Darcy equations. Section 2.6 was intended to provide the "big picture" information regarding finite element stabilization techniques for the Stokes equations, including some relevant literature and a basic example of how residual-based stabilization provides a work-around for the LBB condition. This section is devoted to details necessary to build a stabilization scheme for the non-Darcy flow model introduced in Section 3.1.

In [23], Bochev and Dohrmann provide a clear overview of several stabilization methods available for the steady-state Darcy flow model

$$\nabla \cdot \mathbf{u} = \mathcal{S}' \in \Omega \tag{3.9a}$$

$$\nabla p + \frac{\mu}{k}\mathbf{u} = 0 \in \Omega \tag{3.9b}$$

$$\mathbf{u} \cdot \mathbf{n} = 0 \in \Gamma. \tag{3.9c}$$

These methods include (i) least-squares formulations, (ii) polynomial pressure projection stabilization, (iii) a weighted average of mixed and Galerkin principles for the particular problem, and (iv) consistently stabilized methods.

These stabilization schemes are advantageous for several reasons. While they provide a means to work around the restrictive div-stability condition, using the same finite element approximations for both velocity and pressure also simplifies the implementation of the finite element method and reduces memory usage. In mentioning these positive features, nothing has yet been said about how the accuracy of the solution is affected by adding stabilizing terms to the original equation set. Through the years individuals in the finite element community have questioned the accuracy of stabilized Galerkin schemes, and in particular, the ability of these schemes to conserve mass. Several recent papers have addressed this question and show that stabilized Galerkin and Petrov-Galerkin schemes do conserve mass both globally and locally [20, 31, 74]. Specifically, the correct way to test mass conservation over a region is to integrate the mass fluxes over all the elements which touch the boundary of the region (see Figure 3.7); if mass is conserved the result will be zero. See section 3.5.1 for a definition of the flux for the multiscale residual-based stabilization method used in the computations in Chapter 4.

The consistently stabilized method is used in the computations in Chapter 4; thus it is the focus of the remainder of this section. The term "consistent" refers to the fact that the stabilized equation set is equivalent to the original equation set at the

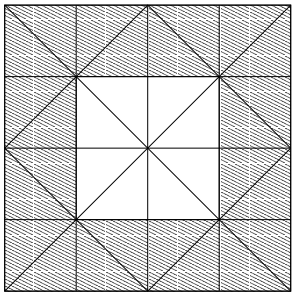

Figure 3.7: To check mass conservation over this region, the mass fluxes should be integrated over the shaded elements.

exact solution. This is because the original equation set is modified by stabilization terms which include the residual of one or more of the original model equations. For example, the non-Darcy flow model in equations (3.4) will be altered by stabilization terms containing the residual of the discrete momentum equation, denoted by

$$\mathbf{r}^{\Delta} = \mathbf{u}^{\Delta} \cdot \nabla \mathbf{u}^{\Delta} + \phi^2 \nabla \bar{p}^{\Delta} + \phi^2 \frac{\nu}{k_f} \mathbf{u}^{\Delta} + \phi^2 \beta \|\mathbf{u}^{\Delta}\|_2 \mathbf{u}^{\Delta}. \tag{3.10}$$

Another example is found in Section 2.6, where the bilinear form associated with the residual-stabilized Stokes equations is shown to be coercive, and therefore stable, for a variety of basis function pairings beyond those allowed by the LBB condition.

The remainder of this section will utilize notation developed in Chapter 2 with respect to the Navier-Stokes/Stokes equations to discuss common stabilized methods. Of particular interest are generalized Galerkin methods applied to an abstract linear

Dirichlet problem [73, Pages 393 and 397]. Given the Dirichlet problem

$$\mathcal{L}\widetilde{\mathbf{u}} = \widetilde{f} \in \Omega \tag{3.11}$$

$$\widetilde{\mathbf{u}} = \widetilde{g} \in \Gamma, \tag{3.12}$$

the generalized Galerkin method takes the form

$$\left(\widetilde{\mathbf{w}}^{\Delta}, \mathcal{L}\widetilde{\mathbf{u}}^{\Delta}\right)_{\Omega} + \sum_{e=0}^{ne-1} \left(\mathbb{L}\widetilde{\mathbf{w}}^{\Delta}, \tau\left(\mathcal{L}\widetilde{\mathbf{u}}^{\Delta} - \widetilde{f}\right)\right)_{\Omega_e} = \left(\widetilde{\mathbf{w}}^{\Delta}, \widetilde{f}\right)_{\Omega}, \tag{3.13}$$

where $\widetilde{\mathbf{w}}$ is the test function, τ is a stabilization parameter [77, 110], $\mathcal{L}\widetilde{\mathbf{u}}^{\Delta} - \widetilde{f}$ is the residual of the original PDE applied to the discrete approximation to the solution, and $\mathbb{L}$ is a differential operator which varies depending on the particular residual-based stabilization strategy used.

Literature associated with Hughes generally provides the following three possibilities for this differential operator [73, 78].

$$\mathbb{L} \equiv \begin{cases} +\mathcal{L} & \text{Galerkin/least-squares (GLS) [76]} \\ +\mathcal{L}_{\text{adv}} & \text{Streamline-Upwind Petrov-Galerkin (SUPG) [28, 76]} \\ -\mathcal{L}^{\dagger} & \text{Multiscale (MS) [50, 78]} \end{cases} \tag{3.14}$$

Again, $\mathcal{L}$ is a the linear operator associated with the original, continuous PDE, $\mathcal{L}_{\text{adv}}$ represents only the advective portion of the original linear operator, and $\mathcal{L}^{\dagger}$ denotes the adjoint of $\mathcal{L}$. This document focuses on the multiscale differential operator; thus,

the formula for the adjoint of a linear operator and an extension to nonlinear operators due to Burýšková are reviewed in Appendix A.

At this point it is helpful to compare this general form to the stabilized Stokes problem detailed in Section 2.6. As in that section, $\widetilde{\mathbf{w}}^{\Delta} = \left[\mathbf{w}^{\Delta}, q^{\Delta}\right]$ are the test functions associated with the unknowns $\widetilde{\mathbf{u}}^{\Delta} = \left[\mathbf{u}^{\Delta}, \bar{p}^{\Delta}\right]$, and $\widetilde{\mathbf{w}}^{\Delta}, \widetilde{\mathbf{u}}^{\Delta} \in \mathbf{V}_0^{\Delta} \times S_0^{\Delta}$. The integral term $\left(\widetilde{\mathbf{w}}^{\Delta}, \mathcal{L}\widetilde{\mathbf{u}}^{\Delta}\right)_{\Omega}$ represents the Dirichlet system of equations after it has been multiplied by the test functions and integrated over the domain, but before any integration by parts is completed. For the Stokes problem,

$$\left(\widetilde{\mathbf{w}}^{\Delta}, \mathcal{L}\widetilde{\mathbf{u}}^{\Delta}\right)_{\Omega} = \int_{\Omega} \left[-\nu\Delta\mathbf{u}^{\Delta} \cdot \mathbf{w}^{\Delta} + \nabla\bar{p}^{\Delta} \cdot \mathbf{w}^{\Delta} + \nabla \cdot \mathbf{u}^{\Delta} q^{\Delta}\right] \mathrm{d}\Omega \quad (3.15a)$$

$$\left(\widetilde{\mathbf{w}}^{\Delta}, \widetilde{f}\right)_{\Omega} = \int_{\Omega} \mathbf{f} \cdot \mathbf{w}^{\Delta} \, \mathrm{d}\Omega. \quad (3.15b)$$

The only difference between the representation in equations (3.15) and the representation shown in equations (2.36) from Section 2.6, i.e.

$$\mathcal{A}\left(\widetilde{\mathbf{u}}^{\Delta}, \widetilde{\mathbf{w}}^{\Delta}\right) = \mathcal{F}\left(\widetilde{\mathbf{w}}^{\Delta}\right) \ \forall \widetilde{\mathbf{w}}^{\Delta} \in V_0^{\Delta} \times S_0^{\Delta}$$

where

$$\mathcal{A}\left(\widetilde{\mathbf{u}}^{\Delta}, \widetilde{\mathbf{w}}^{\Delta}\right) \equiv a\left(\mathbf{u}^{\Delta}, \mathbf{w}^{\Delta}\right) + b\left(\mathbf{w}^{\Delta}, \bar{p}^{\Delta}\right) - b\left(\mathbf{u}^{\Delta}, q^{\Delta}\right)$$

and

$$\mathcal{F}\left(\widetilde{\mathbf{w}}^{\Delta}\right) \equiv \left(\mathbf{f}, \mathbf{w}^{\Delta}\right)$$

is that the first two terms in equations (3.15) have been integrated by parts, and the boundary terms disappear based on the choice of function spaces. The connection between the stabilization term

$$-\varpi \sum_{e=0}^{ne-1} \Delta_e^2 \left(\nu \Delta \mathbf{u}^\Delta - \nabla \bar{p}^\Delta + \mathbf{f}, \nabla q^\Delta\right)_{\Omega_e}$$

introduced in equation (2.37) from Section 2.6 and the generalized Galerkin stabilization term

$$\sum_{e=0}^{ne-1} \left(\mathbb{L}\widetilde{\mathbf{w}}^\Delta, \tau \left(\mathcal{L}\widetilde{\mathbf{u}}^\Delta - \widetilde{f}\right)\right)_{\Omega_e}$$

from equation (3.13) remains to be shown. The residual of the Stokes problem can be written as

$$\mathcal{L}\widetilde{\mathbf{u}}^\Delta - \widetilde{f} = \begin{bmatrix} -\nu \Delta \mathbf{u}^\Delta + \nabla \bar{p}^\Delta - f \\ \nabla \cdot \mathbf{u}^\Delta - 0 \end{bmatrix}. \tag{3.16}$$

This allows the consistent, residual-based stabilization to be based upon either the momentum residual or the incompressibility residual or both, depending on the definition of the τ matrix. Assuming that $\mathbf{u}^\Delta$ has n components, the stabilization parameter is defined as

$$\tau \equiv \begin{bmatrix} \varpi \Delta_e^2 \mathbf{I}_{n \times n} & \mathbf{0}_{n \times 1} \end{bmatrix}, \tag{3.17}$$

and $\mathbb{L}\widetilde{\mathbf{w}}^\Delta \equiv \mathcal{L}_{\text{adv}}\widetilde{\mathbf{w}}^\Delta = \nabla q^\Delta$ according to the SUPG approach, then the Stokes stabilization scheme introduced in Section 2.6 has been recovered using the generalized Galerkin format.

The non-Darcy flow model of interest (shown in equations (3.4)) is an extension of the Darcy flow model from equations (3.9) via the inclusion of both the quadratic Forchheimer term and the Navier-Stokes advective acceleration term. Since the non-Darcy model clearly combines terms from the Darcy and Navier-Stokes models, then an appropriate stabilized non-Darcy model will combine the stabilization strategies applicable to both Darcy and Navier-Stokes. The following section discusses the implementation of this stabilization strategy.

3.4 Weak Form

As all computations in Chapter 4 are at steady-state with constant density and porosity, the non-Darcy flow model from equations (3.4) are rewritten here as

$$\nabla \cdot \mathbf{u} = \mathcal{S}' \quad \in \Omega \tag{3.18a}$$

$$\mathbf{u} \cdot \nabla \mathbf{u} + \phi^2 \left(\nabla \bar{p} - \mathbf{g} \right) = -\frac{\phi^2 \nu}{k_f} \mathbf{u} - \phi^2 \beta \|\mathbf{u}\|_2 \mathbf{u} \quad \in \Omega \tag{3.18b}$$

$$\mathbf{u} \cdot \mathbf{n} = 0 \quad \in \Gamma_N \tag{3.18c}$$

$$\bar{p} = \bar{p}_D \quad \in \Gamma_D \tag{3.18d}$$

where the new variable $\bar{p} = \frac{p}{\rho}$ is introduced as in the Navier-Stokes literature, and $\mathcal{S}'$ is defined as on page 10. Note that the Dirichlet boundary condition for pressure, p_D, has also been modified such that $\bar{p}_D = \frac{p_D}{\rho}$.

With the equations in this form, the Navier-Stokes stabilization terms introduced

in [78, page 1156] directly apply to equations (3.18) while the Darcy and Forchheimer stabilization techniques discussed in Appendix A can easily be modified for this case.

3.4.1 Revisiting the Navier-Stokes Equations

In [78], Hughes and Wells discuss stabilization techniques for the Navier-Stokes equations shown in (2.3),

$$\begin{aligned} -\nu\Delta\mathbf{u} + \mathbf{u}\cdot\nabla\mathbf{u} + \nabla\bar{p} &= \mathbf{f} \quad \text{in } \Omega \\ \nabla\cdot\mathbf{u} &= 0 \quad \text{in } \Omega \\ \mathbf{u} &= 0 \quad \text{on } \Gamma. \end{aligned}$$

Using the bilinear and trilinear forms defined in equations (2.25), the multiscale, residual-stabilized incompressible Navier-Stokes equations can be written as

$$a\left(\mathbf{u}^{\Delta},\mathbf{w}^{\Delta}\right) + c\left(\mathbf{u}^{\Delta},\mathbf{u}^{\Delta},\mathbf{w}^{\Delta}\right) + b\left(\mathbf{w}^{\Delta},\bar{p}^{\Delta}\right) - b\left(\mathbf{u}^{\Delta},q^{\Delta}\right) \tag{3.19a}$$

$$+ \sum_{e=0}^{ne-1}\left(\mathbb{L}\widetilde{\mathbf{w}}^{\Delta},\tau\mathbf{r}^{\Delta}\right)_{\Omega_e} \tag{3.19b}$$

$$- \sum_{e=0}^{ne-1}\left(\mathbf{w}^{\Delta},\tau\mathbf{r}^{\Delta}\cdot\nabla\mathbf{u}^{\Delta}\right)_{\Omega_e} \tag{3.19c}$$

$$+ \sum_{e=0}^{ne-1}\left(\tau\mathbf{r}^{\Delta}\cdot\nabla\mathbf{w}^{\Delta},\tau'\left(\tau\mathbf{r}^{\Delta}\cdot\nabla\mathbf{u}^{\Delta}\right)\right)_{\Omega_e} \tag{3.19d}$$

$$= \left(\mathbf{f},\mathbf{w}^{\Delta}\right), \tag{3.19e}$$

where

$$\mathbb{L}\widetilde{\mathbf{w}}^{\Delta} = \mathbf{u}^{\Delta} \cdot \nabla \mathbf{w}^{\Delta} + \nabla q^{\Delta} + \nu \Delta \mathbf{w}^{\Delta} \tag{3.20a}$$

$$\mathbf{r}^{\Delta} = \mathbf{u}^{\Delta} \cdot \nabla \mathbf{u}^{\Delta} + \nabla \bar{p}^{\Delta} - \nu \Delta \mathbf{u}^{\Delta} - \mathbf{f}. \tag{3.20b}$$

In equation (3.19), lines (3.19a) and (3.19e) combine to form the original unstabilized equation set. Line (3.19b) is the multiscale residual-based stabilization term written in generalized Galerkin form as discussed in Section 3.3.3 and Appendix A. At this point the terms on lines (3.19c) and (3.19d) are new additions to the stabilization discussion. In [78, page 1156] it is explained that the term on line (3.19c) is included to guarantee momentum conservation, while the term on line (3.19d) is necessary to stabilize advection-dominated flows. Note that τ' is a second stabilization parameter, different from τ. Guidelines for specifying τ' can be found in [110, page 170].

3.4.2 Applying the Navier-Stokes Advection Stabilization Terms to Non-Darcy Flow

The non-Darcy flow model was rewritten in equations (3.18) to be as similar as possible in form to the Navier-Stokes equations. This step allows the Navier-Stokes stabilization terms from lines (3.19b)-(3.19d) to directly apply in stabilizing the non-Darcy model by merely changing the definition of $\mathbb{L}\widetilde{\mathbf{w}}^{\Delta}$ and $\mathbf{r}^{\Delta}$. The residual is

defined in equation (3.10) as,

$$\mathbf{r}^{\Delta} = \mathbf{u}^{\Delta} \cdot \nabla \mathbf{u}^{\Delta} + \phi^2 \nabla \bar{p}^{\Delta} + \phi^2 \frac{\nu}{k_f} \mathbf{u}^{\Delta} + \phi^2 \beta \|\mathbf{u}^{\Delta}\|_2 \mathbf{u}^{\Delta},$$

and the differential operator combines Navier-Stokes, Darcy, and Forchheimer adjoint results into

$$\mathbb{L}\widetilde{\mathbf{w}}^{\Delta} = \mathbf{u}^{\Delta} \cdot \nabla \mathbf{w}^{\Delta} + \phi^2 \nabla q^{\Delta} - \phi^2 \frac{\nu}{k_f} \mathbf{w}^{\Delta} - \phi^2 \beta \|\mathbf{u}^{\Delta}\|_2 \mathbf{w}^{\Delta} - \frac{\phi^2 \beta \mathbf{w}^{\Delta} \cdot \mathbf{u}^{\Delta}}{\|\mathbf{u}^{\Delta}\|_2} \mathbf{u}^{\Delta}. \quad (3.21)$$

Thus the weak form of the stabilized, steady-state non-Darcy flow model is given by

$$\begin{aligned}
0 \;=\; & \int_{\Gamma} \left(\mathbf{u}^{\Delta} \cdot \mathbf{n}\right) q^{\Delta} \, \mathrm{d}\Gamma - \int_{\Omega} \mathbf{u}^{\Delta} \cdot \nabla q^{\Delta} \, \mathrm{d}\Omega && (3.22a)\\
& + \int_{\Omega} \left(\mathbf{u}^{\Delta} \cdot \nabla \mathbf{u}^{\Delta}\right) \cdot \mathbf{w}^{\Delta} \, \mathrm{d}\Omega + \int_{\Gamma} \phi^2 \bar{p}^{\Delta} \left(\mathbf{n} \cdot \mathbf{w}^{\Delta}\right) \, \mathrm{d}\Gamma && (3.22b)\\
& - \int_{\Omega} \phi^2 \bar{p}^{\Delta} \left(\nabla \cdot \mathbf{w}^{\Delta}\right) \, \mathrm{d}\Omega + \int_{\Omega} \frac{\phi^2 \nu}{k_f} \left(\mathbf{u}^{\Delta} \cdot \mathbf{w}^{\Delta}\right) \, \mathrm{d}\Omega && (3.22c)\\
& + \int_{\Omega} \phi^2 \beta \|\mathbf{u}^{\Delta}\|_2 \left(\mathbf{u}^{\Delta} \cdot \mathbf{w}^{\Delta}\right) \, \mathrm{d}\Omega && (3.22d)\\
& + \sum_{e=0}^{ne-1} \left(\mathbb{L}\widetilde{\mathbf{w}}^{\Delta}, \tau_{\lambda}(x) \, \mathbf{r}^{\Delta}\right)_{\Omega_e} && (3.22e)\\
& - \sum_{e=0}^{ne-1} \left(\mathbf{w}^{\Delta}, \tau_{\lambda}(x) \, \mathbf{r}^{\Delta} \cdot \nabla \mathbf{u}^{\Delta}\right)_{\Omega_e}\\
& + \sum_{e=0}^{ne-1} \left(\tau_{\lambda}(x) \, \mathbf{r}^{\Delta} \cdot \nabla \mathbf{w}^{\Delta}, \tau' \left(\tau_{\lambda}(x) \, \mathbf{r}^{\Delta} \cdot \nabla \mathbf{u}^{\Delta}\right)\right)_{\Omega_e},
\end{aligned}$$

where lines (3.22a)-(3.22d) comprise the weak form of the non-Darcy flow model and the remaining lines stabilize the weak form. The parameter $\tau_\lambda(x)$ is introduced, explained, and formulated in Appendix A.5. Computations in Chapter 4 use values of τ' and γ (from the definition of $\tau_\lambda(x)$ in Appendix A.5) which are $\mathcal{O}\left(\frac{\Delta_e}{\|\mathbf{r}^\Delta\|_2}\right)$.

3.5 Theory

In this section we prove several theoretical results regarding the stabilized two-dimensional discrete flow model shown in equation (3.22). Specifically, local and global mass conservation, and momentum conservation are proven for the discrete nonlinear equation set containing both the Forchheimer and advective nonlinearities (see sections 3.5.1-3.5.3). This follows the standard practice in the finite element literature.

What remains to be shown is that the stabilization terms serve their intended purpose and result in a stable weak form even when the basis functions do not satisfy the LBB condition. The same steps applied to the linearized Navier-Stokes equations (i.e. the Stokes problem) in section 2.6 are applied here to the linearized non-Darcy flow model. It is standard practice in the finite element literature to prove stability for the linearized problem. Moreover, as we are solving the nonlinear system of equations with Newton's method in Chapter 4, the linearized problem is exactly the equation set involved in the Newton iteration.

In this case, two-dimensional computational results show that the advective accel-

eration term is negligible when compared to the contributions of the Darcy and Forchheimer terms. Thus, to prove stability of the equation set for the two-dimensional problem we ignore the advective acceleration term and its associated stabilization terms altogether. In section 3.5.4 we begin with the linearization of the following nonlinear discrete equation

$$\begin{aligned} 0 \;=\; & \int_{\Gamma} \left(\mathbf{u}^{\Delta}\cdot\mathbf{n}\right) q^{\Delta}\,\mathrm{d}\Gamma - \int_{\Omega} \mathbf{u}^{\Delta}\cdot\nabla q^{\Delta}\,\mathrm{d}\Omega \\ & + \int_{\Gamma} \bar{p}^{\Delta}\left(\mathbf{n}\cdot\mathbf{w}^{\Delta}\right)\,\mathrm{d}\Gamma - \int_{\Omega} \bar{p}^{\Delta}\left(\nabla\cdot\mathbf{w}^{\Delta}\right)\,\mathrm{d}\Omega + \int_{\Omega} \frac{\nu}{k_f}\left(\mathbf{u}^{\Delta}\cdot\mathbf{w}^{\Delta}\right)\,\mathrm{d}\Omega \\ & + \int_{\Omega} \beta\|\mathbf{u}^{\Delta}\|_2\left(\mathbf{u}^{\Delta}\cdot\mathbf{w}^{\Delta}\right)\,\mathrm{d}\Omega + \sum_{e=0}^{ne-1}\left(\mathbb{L}\widetilde{\mathbf{w}}^{\Delta}, \tau_{\lambda}\left(x\right)\mathbf{r}^{\Delta}\right)_{\Omega_e}, \end{aligned}$$

where

$$\mathbb{L}\widetilde{\mathbf{w}}^{\Delta} \equiv \nabla q^{\Delta} - \frac{\nu}{k_f}\mathbf{w}^{\Delta} - \frac{1}{2}\beta\|\mathbf{u}^{\Delta}\|_2\mathbf{w}^{\Delta} - \frac{\beta\left(\mathbf{w}^{\Delta}\cdot\mathbf{u}^{\Delta}\right)}{2\|\mathbf{u}^{\Delta}\|_2}\mathbf{u}^{\Delta}$$

and

$$\mathbf{r}^{\Delta} \equiv \nabla\bar{p}^{\Delta} + \frac{\nu}{k_f}\mathbf{u}^{\Delta} + \beta\|\mathbf{u}^{\Delta}\|_2\mathbf{u}^{\Delta},$$

and from there we prove that the stabilization terms associated with the linearized problem do in fact stabilize the system and result in a coercive bilinear operator.

3.5.1 Local Conservation of Mass

In [20], Berger and Howington prove that mass is conserved locally by the SUPG stabilization approach when the unique mass flux is defined such that it is consistent

with the discrete equations. Here we will prove that local mass conservation holds for the Multiscale stabilization approach when the discrete mass flux, F_e^ρ, through the boundary of element Ω_e is defined by

$$F_e^\rho \equiv \int_{\Omega_e} \left[\rho \mathbf{u}^\Delta \cdot \nabla q_e^\Delta - \tau_\lambda(x)\, \phi^2 \nabla q_e^\Delta \cdot \mathbf{r}^\Delta\right] \mathrm{d}\Omega \tag{3.23}$$

where q_e^Δ is a pressure test function whose support contains the element Ω_e and $\mathbf{r}^\Delta$ is defined in equation (3.10) as

$$\mathbf{r}^\Delta = \mathbf{u}^\Delta \cdot \nabla \mathbf{u}^\Delta + \phi^2 \nabla \bar{p}^\Delta + \phi^2 \frac{\nu}{k_f} \mathbf{u}^\Delta + \phi^2 \beta \|\mathbf{u}^\Delta\|_2 \mathbf{u}^\Delta.$$

As in [20], the motivation for this definition of flux is based on a one-dimensional example. Then the result will be shown in two spatial dimensions. Note that the results for three dimensions are identical to those shown for two dimensions.

One-dimensional Result

The pressure test function, q, is associated with mass conservation since it multiplies the incompressibility equation. The portion of the weak flow equation from (3.22) that involves q and its derivatives is

$$0 = \int_\Gamma \left(\mathbf{u}^\Delta \cdot \mathbf{n}\right) q^\Delta \,\mathrm{d}\Gamma - \int_\Omega \mathbf{u}^\Delta \cdot \nabla q^\Delta \,\mathrm{d}\Omega + \sum_{e=0}^{ne-1} \left(\phi^2 \nabla q^\Delta, \tau_\lambda(x)\, \mathbf{r}^\Delta\right)_{\Omega_e}.$$

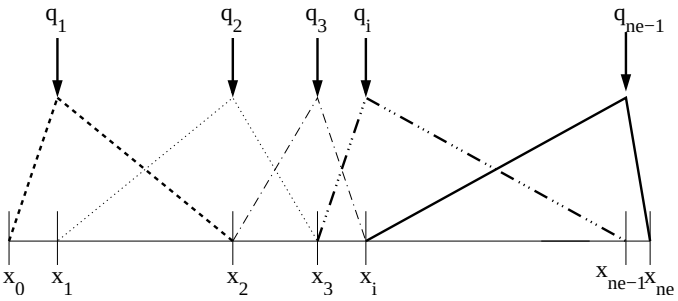

Figure 3.8: One-dimensional $\mathcal{P}_1$ basis functions. The intervals $\Omega_{i-1} = x_i - x_{i-1}$ and $\Omega_i = x_{i+1} - x_i$ provide the *support* of test function q_i.

When translated into a one dimensional system where $\Omega = (0, L)$ and $\Gamma = \{0, L\}$ this reduces to

$$0 = u^{\Delta}(L)q^{\Delta}(L) - u^{\Delta}(0)q^{\Delta}(0) - \int_0^L u^{\Delta}\frac{\mathrm{d}q^{\Delta}}{\mathrm{d}x}\,\mathrm{d}x + \sum_{e=0}^{ne-1}\int_{\Omega_e} \phi^2\tau_{\lambda}(x)\, r^{\Delta}\frac{\mathrm{d}q^{\Delta}}{\mathrm{d}x}\,\mathrm{d}x, \quad (3.24)$$

where r^{Δ} is the one-dimensional version of the momentum residual in equation (3.10).

To develop the mass flux formula at a particular point, x_i, we focus on the equation associated with the test function, q_i^{Δ}. As shown in figure 3.8, this test function is equal to one at x_i and is equal to zero at every other point in the domain. The superscripts $+$ and $-$ will be used to denote approaching a point from the right or the left, respectively.

The portion of equation (3.24) that holds over the support of the test function q_i^{Δ}

(i.e. over the region (x_{i-1}, x_{i+1})) is

$$\begin{aligned}
0 &= u^{\Delta}(x_i^-)q^{\Delta}(x_i^-) - u^{\Delta}(x_{i-1})q^{\Delta}(x_{i-1}) - \int_{x_{i-1}}^{x_i} \left(u^{\Delta}\frac{\mathrm{d}q^{\Delta}}{\mathrm{d}x} - \phi^2\tau_{\lambda}(x)\, r^{\Delta}\frac{\mathrm{d}q^{\Delta}}{\mathrm{d}x} \right) \mathrm{d}x \\
&\quad + u^{\Delta}(x_{i+1})q^{\Delta}(x_{i+1}) - u^{\Delta}(x_i^+)q^{\Delta}(x_i^+) - \int_{x_i}^{x_{i+1}} \left(u^{\Delta}\frac{\mathrm{d}q^{\Delta}}{\mathrm{d}x} - \phi^2\tau_{\lambda}(x)\, r^{\Delta}\frac{\mathrm{d}q^{\Delta}}{\mathrm{d}x} \right) \mathrm{d}x \\
&= u^{\Delta}(x_i^-)q^{\Delta}(x_i^-) - \int_{x_{i-1}}^{x_i} \left(u^{\Delta}\frac{\mathrm{d}q^{\Delta}}{\mathrm{d}x} - \phi^2\tau_{\lambda}(x)\, r^{\Delta}\frac{\mathrm{d}q^{\Delta}}{\mathrm{d}x} \right) \mathrm{d}x \\
&\quad - u^{\Delta}(x_i^+)q^{\Delta}(x_i^+) - \int_{x_i}^{x_{i+1}} \left(u^{\Delta}\frac{\mathrm{d}q^{\Delta}}{\mathrm{d}x} - \phi^2\tau_{\lambda}(x)\, r^{\Delta}\frac{\mathrm{d}q^{\Delta}}{\mathrm{d}x} \right) \mathrm{d}x \\
&= F_{i-1}^{\rho}(x_i^-)q^{\Delta}(x_i^-) - \int_{x_{i-1}}^{x_i} \left(u^{\Delta}\frac{\mathrm{d}q^{\Delta}}{\mathrm{d}x} - \phi^2\tau_{\lambda}(x)\, r^{\Delta}\frac{\mathrm{d}q^{\Delta}}{\mathrm{d}x} \right) \mathrm{d}x \\
&\quad - F_i^{\rho}(x_i^+)q^{\Delta}(x_i^+) - \int_{x_i}^{x_{i+1}} \left(u^{\Delta}\frac{\mathrm{d}q^{\Delta}}{\mathrm{d}x} - \phi^2\tau_{\lambda}(x)\, r^{\Delta}\frac{\mathrm{d}q^{\Delta}}{\mathrm{d}x} \right) \mathrm{d}x,
\end{aligned}$$

where the equation has been split into two portions that correspond to the left and right pieces of the test function. Again, the mass flux across the boundary of element e is denoted by F_e^{ρ}. We require that the flux jump be zero for a single equation constructed for the test function q_i^{Δ}. Since the test function is continuous,

$$F_{i-1}^{\rho}\left(x_i^-\right) - F_i^{\rho}\left(x_i^+\right) \equiv 0$$

must be enforced through the finite element statement. This results in the flux

definition

$$F_{i-1}^{\rho}\left(x_i\right) \equiv -\int_{x_{i-1}}^{x_i}\left(u^{\Delta}\frac{\mathrm{d}q^{\Delta}}{\mathrm{d}x}-\phi^2\tau_{\lambda}\left(x\right)r^{\Delta}\frac{\mathrm{d}q^{\Delta}}{\mathrm{d}x}\right)\mathrm{d}x \tag{3.25a}$$

$$F_{i}^{\rho}\left(x_i\right) \equiv \int_{x_{i}}^{x_{i+1}}\left(u^{\Delta}\frac{\mathrm{d}q^{\Delta}}{\mathrm{d}x}-\phi^2\tau_{\lambda}\left(x\right)r^{\Delta}\frac{\mathrm{d}q^{\Delta}}{\mathrm{d}x}\right)\mathrm{d}x. \tag{3.25b}$$

It doesn't matter whether one chooses the definition corresponding to the element to the left of node x_i or the definition corresponding to the element to the right of node x_i. These are the unique fluxes entering and exiting node x_i as determined by the discrete equations.

By applying this same process in the time-dependent case and using the facts that within a single element $\sum_{j=1}^{i+1} q_j^{\Delta} = 1$ and $\sum_{j=1}^{i+1} \frac{\mathrm{d}q_j^{\Delta}}{\mathrm{d}x} = 0$ one can prove that mass is conserved locally via the equation

$$\int_{x_i}^{x_{i+1}}\frac{\partial\rho}{\partial t}\,\mathrm{d}x + F_i^{\rho}\left(x_{i+1}\right) - F_i^{\rho}\left(x_i\right) = 0 \tag{3.26}$$

where

$$F_i^{\rho}\left(x_j\right) \equiv \int_{x_i}^{x_{i+1}}\left[q_j^{\Delta}\frac{\partial\rho}{\partial t}-\rho u^{\Delta}\frac{\mathrm{d}q_j^{\Delta}}{\mathrm{d}x}+\phi^2\tau_{\lambda}\left(x\right)\rho\frac{\mathrm{d}q_j^{\Delta}}{\mathrm{d}x}r^{\Delta}\right]\mathrm{d}x,\ \ j=i,i+1.$$

Equation (3.26) shows that the mass change in a general element over a time step is exactly balanced by the mass flux over the element faces.

Two-dimensional Result

In two spatial dimensions, the test function at node $\mathbf{x}_3$ which multiplies the incompressibility equation is q_3^Δ, and its support is shown in figure 3.9. The equation corresponding to test function q_3^Δ is

$$\sum_{e=1}^{4} \int_{\Omega_e} -\nabla q_3^\Delta \cdot \mathbf{u}^\Delta \, \mathrm{d}\Omega +$$
$$\sum_{e=1}^{4} \int_{\Omega_e} \phi^2 \tau_\lambda(x) \nabla q^\Delta \cdot \left[\mathbf{u}^\Delta \cdot \nabla \mathbf{u}^\Delta + \phi^2 \left(\nabla \bar{p}^\Delta + \frac{\nu}{k_f} \mathbf{u}^\Delta + \beta \|\mathbf{u}^\Delta\|_2 \mathbf{u}^\Delta \right) \right] \mathrm{d}\Omega = 0.$$

As in the 1D case, the finite element equation is decomposed to estimate the flux.

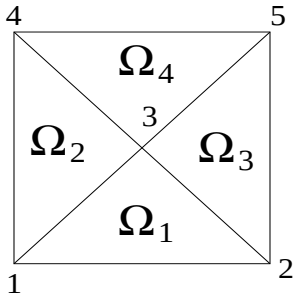

Figure 3.9: The support in 2D for the $\mathcal{P}_1$ basis function associated with node 3, q_3^Δ. The test function, q_3^Δ, is equal to one at node 3 and equal to zero at every other node in the domain.

For the 2D case, this decomposition requires the introduction of the unit outward normal vector for element e (denoted by $\mathbf{n}_e$) and $\mathbf{F}_1$, the discrete flux distribution along the boundary of Ω_1. The contributions from element Ω_1 are separated from the rest of the summation and mass fluxes across the portion of the Ω_1 boundary that intersects the support of the test function q_3^Δ are introduced. Recall that the

boundary of element Ω_e is denoted by $\partial\Omega_e$. At this stage, the finite element equation is

$$\int_{\Omega_1} -\nabla q_3^\Delta \cdot \mathbf{u}^\Delta \,\mathrm{d}\Omega + \sum_{e=2}^{4} \int_{\Omega_e} -\nabla q_3^\Delta \cdot \mathbf{u}^\Delta \,\mathrm{d}\Omega + \int_{\partial\Omega_1} q_3^\Delta \mathbf{F}_1 \cdot \mathbf{n}_1 \,\mathrm{d}l + \sum_{e=2}^{4} \int_{\partial\Omega_e} q_3^\Delta \mathbf{F}_1 \cdot \mathbf{n}_e \,\mathrm{d}l +$$
$$\int_{\Omega_1} \phi^2 \tau_\lambda(x) \nabla q^\Delta \cdot \left[\mathbf{u}^\Delta \cdot \nabla \mathbf{u}^\Delta + \phi^2 \left(\nabla \bar{p}^\Delta + \frac{\nu}{k_f} \mathbf{u}^\Delta + \beta \|\mathbf{u}^\Delta\|_2 \mathbf{u}^\Delta \right) \right] \mathrm{d}\Omega +$$
$$\sum_{e=2}^{4} \int_{\Omega_e} \phi^2 \tau_\lambda(x) \nabla q^\Delta \cdot \left[\mathbf{u}^\Delta \cdot \nabla \mathbf{u}^\Delta + \phi^2 \left(\nabla \bar{p}^\Delta + \frac{\nu}{k_f} \mathbf{u}^\Delta + \beta \|\mathbf{u}^\Delta\|_2 \mathbf{u}^\Delta \right) \right] \mathrm{d}\Omega = 0.$$

Thus the unique partial flux through the interface $\partial\Omega_1$ for test function number 3, denoted by P_3^1, can be computed by either one of the following equivalent formulas.

$$P_3^1 \equiv \int_{\Omega_1} \nabla q_3^\Delta \cdot \mathbf{u}^\Delta - \phi^2 \tau_\lambda(x) \nabla q^\Delta \cdot \left[\mathbf{u}^\Delta \cdot \nabla \mathbf{u}^\Delta + \phi^2 \left(\nabla \bar{p}^\Delta + \frac{\nu}{k_f} \mathbf{u}^\Delta + \beta \|\mathbf{u}^\Delta\|_2 \mathbf{u}^\Delta \right) \right] \mathrm{d}\Omega$$
$$P_3^1 \equiv -\sum_{e=2}^{4} \int_{\Omega_e} \nabla q_3^\Delta \cdot \mathbf{u}^\Delta - \phi^2 \tau_\lambda(x) \nabla q^\Delta \cdot \left[\mathbf{u}^\Delta \cdot \nabla \mathbf{u}^\Delta + \phi^2 \left(\nabla \bar{p}^\Delta + \frac{\nu}{k_f} \mathbf{u}^\Delta + \beta \|\mathbf{u}^\Delta\|_2 \mathbf{u}^\Delta \right) \right] \mathrm{d}\Omega$$

As in 1D, summing the partial fluxes for each test function around an element will result in a flux measure which balances the temporal mass change within the element.

3.5.2 Global Conservation of Mass

We prove that mass is conserved for the weak form of the Forchheimer flow model by substituting $\left(\mathbf{w}^{\Delta}, q^{\Delta}\right) = (\mathbf{0}, 1)$ and showing that any internal sources/sinks of mass are balanced by the flow over the boundary. This procedure is set forth in the work of Hughes and Wells [78, page 1153].

For the two-dimensional heterogeneous flow problem in which flow is induced by the fixed pressure gradient across the domain there are no internal sources/sinks of mass. The mass flow over the boundary in this case should be zero; thus, we want to show that

$$\int_{\Gamma} \left(\mathbf{u}^{\Delta} \cdot \mathbf{n}\right) \, \mathrm{d}\Gamma = 0.$$

Proof:

We begin with the weak form of the equations from equation (3.22).

$$\begin{aligned}
0 \;=\; & \int_{\Gamma} \left(\mathbf{u}^{\Delta} \cdot \mathbf{n}\right) q^{\Delta} \, \mathrm{d}\Gamma - \int_{\Omega} \mathbf{u}^{\Delta} \cdot \nabla q^{\Delta} \, \mathrm{d}\Omega \\
& + \int_{\Omega} \left(\mathbf{u}^{\Delta} \cdot \nabla \mathbf{u}^{\Delta}\right) \cdot \mathbf{w}^{\Delta} \, \mathrm{d}\Omega + \int_{\Omega} \phi^2 \beta \|\mathbf{u}^{\Delta}\|_2 \left(\mathbf{u}^{\Delta} \cdot \mathbf{w}^{\Delta}\right) \, \mathrm{d}\Omega \\
& - \int_{\Omega} \phi^2 \bar{p}^{\Delta} \left(\nabla \cdot \mathbf{w}^{\Delta}\right) \, \mathrm{d}\Omega + \int_{\Omega} \frac{\phi^2 \nu}{k_f} \left(\mathbf{u}^{\Delta} \cdot \mathbf{w}^{\Delta}\right) \, \mathrm{d}\Omega \\
& + \sum_{e=0}^{ne-1} \left(\mathbb{L}\widetilde{\mathbf{w}}^{\Delta}, \tau_{\lambda}(x) \, \mathbf{r}^{\Delta}\right)_{\Omega_e} - \sum_{e=0}^{ne-1} \left(\mathbf{w}^{\Delta}, \tau_{\lambda}(x) \, \mathbf{r}^{\Delta} \cdot \nabla \mathbf{u}^{\Delta}\right)_{\Omega_e} \\
& + \sum_{e=0}^{ne-1} \left(\tau_{\lambda}(x) \, \mathbf{r}^{\Delta} \cdot \nabla \mathbf{w}^{\Delta}, \tau' \left(\tau_{\lambda}(x) \, \mathbf{r}^{\Delta} \cdot \nabla \mathbf{u}^{\Delta}\right)\right)_{\Omega_e}
\end{aligned}$$

Now substitute $\left(\mathbf{w}^{\Delta}, q^{\Delta}\right) = (\mathbf{0}, 1)$.

$$\begin{aligned} 0 &= \int_{\Gamma} \left(\mathbf{u}^{\Delta} \cdot \mathbf{n}\right)(1)\,\mathrm{d}\Gamma - \int_{\Omega} \mathbf{u}^{\Delta} \cdot \nabla(1)\,\mathrm{d}\Omega \\ &\quad + \sum_{e=0}^{ne-1} \left(\nabla(1), \tau_{\lambda}(x)\,\mathbf{r}^{\Delta}\right)_{\Omega_e} \\ &= \int_{\Gamma} \left(\mathbf{u}^{\Delta} \cdot \mathbf{n}\right)\,\mathrm{d}\Gamma \end{aligned}$$

As there are no internal sources or sinks of mass in the domain for the two-dimensional flow problem,

$$\int_{\Gamma} \left(\mathbf{u}^{\Delta} \cdot \mathbf{n}\right)\,\mathrm{d}\Gamma = 0$$

implies that mass is conserved. ■

3.5.3 Conservation of Momentum

We prove that mass is conserved for the weak form of the Forchheimer flow model by substituting $\left(\mathbf{w}^{\Delta}, q^{\Delta}\right) = (\mathbf{e}_i, 0) = \widetilde{\mathbf{e}}$ where $\mathbf{e}_i,\ i = 1, \ldots, n$ denotes the standard orthonormal basis for $\mathbb{R}^n$. Again we want to show that any momentum flux across the boundary is balanced by momentum sources and sinks.

In the derivation of the momentum conservation equation in Appendix B.1, the dynamic momentum exchange term, $\boldsymbol{\tau}^w$, is postulated to have the form $\boldsymbol{\tau}^w = \phi R\mathbf{u}$ (recall that the superscript w denotes the fluid phase, just as the superscript s would represent a solid phase quantity). To describe slow flow conditions (i.e. the Darcy

regime), setting R equal to a constant will suffice. However, as the velocities across the domain increase, a model for R which depends on the magnitude of the velocity is more appropriate. This document focuses on the Forchheimer model, where

$$R = \frac{\nu}{k_f} + \beta \|\mathbf{u}\|_2.$$

So for the momentum equation, the Darcy and Forchheimer terms play the role of momentum source/sink terms [59]. Thus we want to show that the momentum flux across the boundary is balanced by the momentum source/sink terms (i.e. the Darcy and Forchheimer terms). Mathematically this is expressed by

$$0 = \int_\Gamma \left(\rho \mathbf{u}^\Delta \cdot \mathbf{n}\right) \mathbf{u}_i^\Delta \, \mathrm{d}\Gamma + \int_\Omega \frac{\phi^2 \mu}{k_f} \mathbf{u}_i^\Delta \, \mathrm{d}\Omega + \int_\Omega \phi^2 \beta \rho \|\mathbf{u}^\Delta\|_2 \mathbf{u}_i^\Delta \, \mathrm{d}\Omega,$$

or equivalently in the case where density is constant

$$0 = \int_\Gamma \left(\mathbf{u}^\Delta \cdot \mathbf{n}\right) \mathbf{u}_i^\Delta + \int_\Omega \frac{\phi^2 \nu}{k_f} \mathbf{u}_i^\Delta \, \mathrm{d}\Omega + \int_\Omega \phi^2 \beta \|\mathbf{u}^\Delta\|_2 \mathbf{u}_i^\Delta \, \mathrm{d}\Omega.$$

As the equation uses the advective form of the advective acceleration term rather than the conservative form, we also need the following identity.

$$\nabla \cdot (\mathbf{u} \otimes \mathbf{u}) = \mathbf{u} \cdot \nabla \mathbf{u} + \mathbf{u} \nabla \cdot \mathbf{u}$$

This identity shows that the conservative form of the advective acceleration term

would contribute the following terms to the weak form of the momentum equation.

$$\begin{aligned}
\int_\Omega \nabla\cdot\left(\mathbf{u}^\Delta\otimes\mathbf{u}^\Delta\right)\cdot\mathbf{w}^\Delta\,\mathrm{d}\Omega &= \int_\Omega \left(\mathbf{u}^\Delta\cdot\nabla\mathbf{u}^\Delta\right)\cdot\mathbf{w}^\Delta\,\mathrm{d}\Omega+\int_\Omega\left(\mathbf{u}^\Delta\nabla\cdot\mathbf{u}^\Delta\right)\cdot\mathbf{w}^\Delta\,\mathrm{d}\Omega\\
\int_\Gamma\left(\mathbf{u}^\Delta\cdot\mathbf{n}\right)\left(\mathbf{u}^\Delta\cdot\mathbf{w}^\Delta\right)\,\mathrm{d}\Gamma-\int_\Omega\left(\mathbf{u}^\Delta\otimes\mathbf{u}^\Delta\right):\nabla\mathbf{w}^\Delta\,\mathrm{d}\Omega &= \int_\Omega \left(\mathbf{u}^\Delta\cdot\nabla\mathbf{u}^\Delta\right)\cdot\mathbf{w}^\Delta\,\mathrm{d}\Omega+\int_\Omega\left(\mathbf{u}^\Delta\nabla\cdot\mathbf{u}^\Delta\right)\cdot\mathbf{w}^\Delta\,\mathrm{d}\Omega
\end{aligned}$$

Thus,

$$\begin{aligned}
\int_\Omega\left(\mathbf{u}^\Delta\cdot\nabla\mathbf{u}^\Delta\right)\cdot\mathbf{w}^\Delta\,\mathrm{d}\Omega &= \int_\Gamma\left(\mathbf{u}^\Delta\cdot\mathbf{n}\right)\left(\mathbf{u}^\Delta\cdot\mathbf{w}^\Delta\right)\,\mathrm{d}\Gamma \\
&\quad-\int_\Omega\left(\mathbf{u}^\Delta\otimes\mathbf{u}^\Delta\right):\nabla\mathbf{w}^\Delta\,\mathrm{d}\Omega-\int_\Omega\left(\mathbf{u}^\Delta\nabla\cdot\mathbf{u}^\Delta\right)\cdot\mathbf{w}^\Delta\,\mathrm{d}\Omega.
\end{aligned}\tag{3.27}$$

Proof:

We begin with the weak form of the equations from equation (3.22).

$$\begin{aligned}
0 &= \int_\Gamma\left(\mathbf{u}^\Delta\cdot\mathbf{n}\right)q^\Delta\,\mathrm{d}\Gamma-\int_\Omega\mathbf{u}^\Delta\cdot\nabla q^\Delta\,\mathrm{d}\Omega+\int_\Omega\left(\mathbf{u}^\Delta\cdot\nabla\mathbf{u}^\Delta\right)\cdot\mathbf{w}^\Delta\,\mathrm{d}\Omega\\
&\quad-\int_\Omega\phi^2\bar{p}^\Delta\left(\nabla\cdot\mathbf{w}^\Delta\right)\,\mathrm{d}\Omega+\int_\Omega\frac{\phi^2\nu}{k_f}\left(\mathbf{u}^\Delta\cdot\mathbf{w}^\Delta\right)\,\mathrm{d}\Omega\\
&\quad+\int_\Omega\phi^2\beta\|\mathbf{u}^\Delta\|_2\left(\mathbf{u}^\Delta\cdot\mathbf{w}^\Delta\right)\,\mathrm{d}\Omega+\sum_{e=0}^{ne-1}\left(\mathbb{L}\widetilde{\mathbf{w}}^\Delta,\tau_\lambda\left(x\right)\mathbf{r}^\Delta\right)_{\Omega_e}\\
&\quad-\sum_{e=0}^{ne-1}\left(\mathbf{w}^\Delta,\tau_\lambda\left(x\right)\mathbf{r}^\Delta\cdot\nabla\mathbf{u}^\Delta\right)_{\Omega_e}\\
&\quad+\sum_{e=0}^{ne-1}\left(\tau_\lambda\left(x\right)\mathbf{r}^\Delta\cdot\nabla\mathbf{w}^\Delta,\tau'\left(\tau_\lambda\left(x\right)\mathbf{r}^\Delta\cdot\nabla\mathbf{u}^\Delta\right)\right)_{\Omega_e}
\end{aligned}$$

Substitute the right hand side of equation (3.27) into the above weak form.

$$
\begin{aligned}
0 \;=\; & \int_{\Gamma} \left(\mathbf{u}^{\Delta}\cdot\mathbf{n}\right) q^{\Delta}\,\mathrm{d}\Gamma - \int_{\Omega} \mathbf{u}^{\Delta}\cdot\nabla q^{\Delta}\,\mathrm{d}\Omega \\
& \int_{\Gamma} \left(\mathbf{u}^{\Delta}\cdot\mathbf{n}\right)\left(\mathbf{u}^{\Delta}\cdot\mathbf{w}^{\Delta}\right)\,\mathrm{d}\Gamma - \int_{\Omega} \left(\mathbf{u}^{\Delta}\otimes\mathbf{u}^{\Delta}\right) : \nabla\mathbf{w}^{\Delta}\,\mathrm{d}\Omega \\
& - \int_{\Omega} \left(\mathbf{u}^{\Delta}\nabla\cdot\mathbf{u}^{\Delta}\right)\cdot\mathbf{w}^{\Delta}\,\mathrm{d}\Omega - \int_{\Omega} \phi^{2}\bar{p}^{\Delta}\left(\nabla\cdot\mathbf{w}^{\Delta}\right)\,\mathrm{d}\Omega \\
& + \int_{\Omega} \frac{\phi^{2}\nu}{k_{f}}\left(\mathbf{u}^{\Delta}\cdot\mathbf{w}^{\Delta}\right)\,\mathrm{d}\Omega + \int_{\Omega} \phi^{2}\beta\|\mathbf{u}^{\Delta}\|_{2}\left(\mathbf{u}^{\Delta}\cdot\mathbf{w}^{\Delta}\right)\,\mathrm{d}\Omega \\
& + \sum_{e=0}^{ne-1}\left(\mathbb{L}\widetilde{\mathbf{w}}^{\Delta}, \tau_{\lambda}\left(x\right)\mathbf{r}^{\Delta}\right)_{\Omega_{e}} - \sum_{e=0}^{ne-1}\left(\mathbf{w}^{\Delta}, \tau_{\lambda}\left(x\right)\mathbf{r}^{\Delta}\cdot\nabla\mathbf{u}^{\Delta}\right)_{\Omega_{e}} \\
& + \sum_{e=0}^{ne-1}\left(\tau_{\lambda}\left(x\right)\mathbf{r}^{\Delta}\cdot\nabla\mathbf{w}^{\Delta}, \tau'\left(\tau_{\lambda}\left(x\right)\mathbf{r}^{\Delta}\cdot\nabla\mathbf{u}^{\Delta}\right)\right)_{\Omega_{e}}
\end{aligned}
$$

Substitute $\left(\mathbf{w}^{\Delta}, q^{\Delta}\right) = \left(\mathbf{e}_{i}, 0\right) = \widetilde{\mathbf{e}}$.

$$
\begin{aligned}
0 \;=\; & \int_{\Gamma} \left(\mathbf{u}^{\Delta}\cdot\mathbf{n}\right)\left(\mathbf{u}^{\Delta}\cdot\mathbf{e}_{i}\right)\,\mathrm{d}\Gamma - \int_{\Omega} \left(\mathbf{u}^{\Delta}\otimes\mathbf{u}^{\Delta}\right) : \nabla\mathbf{e}_{i}\,\mathrm{d}\Omega - \int_{\Omega} \left(\mathbf{u}^{\Delta}\nabla\cdot\mathbf{u}^{\Delta}\right)\cdot\mathbf{e}_{i}\,\mathrm{d}\Omega \\
& - \int_{\Omega} \phi^{2}\bar{p}^{\Delta}\left(\nabla\cdot\mathbf{e}_{i}\right)\,\mathrm{d}\Omega + \int_{\Omega} \frac{\phi^{2}\nu}{k_{f}}\left(\mathbf{u}^{\Delta}\cdot\mathbf{e}_{i}\right)\,\mathrm{d}\Omega + \int_{\Omega} \phi^{2}\beta\|\mathbf{u}^{\Delta}\|_{2}\left(\mathbf{u}^{\Delta}\cdot\mathbf{e}_{i}\right)\,\mathrm{d}\Omega \\
& + \sum_{e=0}^{ne-1}\left(\mathbf{u}^{\Delta}\cdot\nabla\mathbf{e}_{i} - \phi^{2}\frac{\nu}{k_{f}}\mathbf{e}_{i} - \phi^{2}\beta\|\mathbf{u}^{\Delta}\|_{2}\mathbf{e}_{i} - \frac{\phi^{2}\beta\mathbf{e}_{i}\cdot\mathbf{u}^{\Delta}}{\|\mathbf{u}^{\Delta}\|_{2}}\mathbf{u}^{\Delta}, \tau_{\lambda}\left(x\right)\mathbf{r}^{\Delta}\right)_{\Omega_{e}} \\
& - \sum_{e=0}^{ne-1}\left(\mathbf{e}_{i}, \tau_{\lambda}\left(x\right)\mathbf{r}^{\Delta}\cdot\nabla\mathbf{u}^{\Delta}\right)_{\Omega_{e}} \\
& + \sum_{e=0}^{ne-1}\left(\tau_{\lambda}\left(x\right)\mathbf{r}^{\Delta}\cdot\nabla\mathbf{e}_{i}, \tau'\left(\tau_{\lambda}\left(x\right)\mathbf{r}^{\Delta}\cdot\nabla\mathbf{u}^{\Delta}\right)\right)_{\Omega_{e}}
\end{aligned}
$$

Now use the facts that

1. $\mathbf{r}^{\Delta} = 0$ is the residual of the momentum equation,

2. $\nabla \mathbf{e}_i = 0$, and

3. $\nabla \cdot \mathbf{e}_i = 0$.

$$0 = \int_{\Gamma} \left(\mathbf{u}^{\Delta} \cdot \mathbf{n}\right) \mathbf{u}_i^{\Delta} \, \mathrm{d}\Gamma - \int_{\Omega} \mathbf{u}_i^{\Delta} \left(\nabla \cdot \mathbf{u}^{\Delta}\right) \, \mathrm{d}\Omega + \int_{\Omega} \frac{\phi^2 \nu}{k_f} \mathbf{u}_i^{\Delta} \, \mathrm{d}\Omega + \int_{\Omega} \phi^2 \beta \|\mathbf{u}^{\Delta}\|_2 \mathbf{u}_i^{\Delta} \, \mathrm{d}\Omega$$

Assuming that the incompressibility constraint is solved in such a way that the discrete velocity is divergence-free everywhere in the domain, the above equation reduces to

$$0 = \int_{\Gamma} \left(\mathbf{u}^{\Delta} \cdot \mathbf{n}\right) \mathbf{u}_i^{\Delta} + \int_{\Omega} \frac{\phi^2 \nu}{k_f} \mathbf{u}_i^{\Delta} \, \mathrm{d}\Omega + \int_{\Omega} \phi^2 \beta \|\mathbf{u}^{\Delta}\|_2 \mathbf{u}_i^{\Delta} \, \mathrm{d}\Omega,$$

which says that the momentum flux across the boundary is balanced by the momentum exchange with the solid matrix. ■

3.5.4 Stability

The steady-state Forchheimer flow model linearized about the point $\widetilde{\mathbf{z}} = (\mathbf{z}, \bar{s})$ is given by

$$\begin{aligned} \nabla \bar{p}^{\Delta} + \frac{\nu}{k_f} \mathbf{u}^{\Delta} + \beta \mathbf{u}^{\Delta} \|\mathbf{z}\|_2 + \frac{\beta \left(\mathbf{z} \cdot \mathbf{u}^{\Delta}\right) \mathbf{z}}{\|\mathbf{z}\|_2} &= \beta \mathbf{z} \|\mathbf{z}\|_2 \\ \nabla \cdot \mathbf{u}^{\Delta} &= 0. \end{aligned}$$

The differential operator associated with this system is

$$\mathbb{L}\widetilde{\mathbf{w}}^{\Delta} \equiv \nabla q^{\Delta} - \frac{\nu}{k_f}\mathbf{w}^{\Delta} - \beta \mathbf{w}^{\Delta}\|\mathbf{z}\|_2 - \frac{\beta\left(\mathbf{z}\cdot\mathbf{w}^{\Delta}\right)\mathbf{z}}{\|\mathbf{z}\|_2};$$

thus, the stabilization term is given by

$$\gamma \sum_e \tau_e \left(\nabla q^{\Delta} - \frac{\nu}{k_f}\mathbf{w}^{\Delta} - \beta\|\mathbf{z}\|_2\mathbf{w}^{\Delta} - \frac{\beta\left(\mathbf{z}\cdot\mathbf{w}^{\Delta}\right)\mathbf{z}}{\|\mathbf{z}\|_2}, \nabla \bar{p}^{\Delta} + \frac{\nu}{k_f}\mathbf{u}^{\Delta} + \beta\|\mathbf{z}\|_2\mathbf{u}^{\Delta} + \frac{\beta\left(\mathbf{z}\cdot\mathbf{u}^{\Delta}\right)\mathbf{z}}{\|\mathbf{z}\|_2} \right)_{\Omega_e}.$$

The stabilization parameter, τ_e, is assumed to be constant over individual elements but varying over the entire domain as defined in section A.4.2. As in Section 2.6, we show that the linear operator $\mathfrak{A}$ is coercive over the space $\mathcal{V}_0^{\Delta} \times S_0^{\Delta}$ with respect to the norm

$$\sqrt{\|\mathbf{u}^{\Delta}\|_0^2 + \|\nabla \bar{p}^{\Delta}\|_0^2}.$$

Proof:

$$\begin{aligned}
\mathfrak{A}\left(\widetilde{\mathbf{u}}^{\Delta}, \widetilde{\mathbf{u}}^{\Delta}\right) &= \int_{\Omega} \left(\frac{\nu}{k_f} + \beta\|\mathbf{z}\|_2\right)\left(\mathbf{u}^{\Delta}\cdot\mathbf{u}^{\Delta}\right)\,\mathrm{d}\Omega + \int_{\Omega} \frac{\beta\left(\mathbf{z}\cdot\mathbf{u}^{\Delta}\right)^2}{\|\mathbf{z}\|_2}\,\mathrm{d}\Omega \\
&\quad + \sum_e \int_{\Omega_e} \gamma\tau_e\left(\nabla\bar{p}^{\Delta}\cdot\nabla\bar{p}^{\Delta}\right)\,\mathrm{d}\Omega_e \\
&\quad - \sum_e \int_{\Omega_e} \gamma\tau_e\left(\frac{\nu}{k_f} + \beta\|\mathbf{z}\|_2\right)^2\left(\mathbf{u}^{\Delta}\cdot\mathbf{u}^{\Delta}\right)\,\mathrm{d}\Omega_e \\
&\quad - \sum_e \int_{\Omega_e} \gamma\tau_e\left(3\beta^2 + \frac{2\beta\nu}{\|\mathbf{z}\|_2 k_f}\right)\left(\mathbf{z}\cdot\mathbf{u}^{\Delta}\right)^2\,\mathrm{d}\Omega_e
\end{aligned}$$

Using (1) the fact that $\int\limits_{\Omega} a \, \mathrm{d}\Omega \geq \sum\limits_{e} \int\limits_{\Omega_e} a \, \mathrm{d}\Omega_e$, and (2) the definition of norm, changes the above equality to the following inequality.

$$\begin{aligned}\mathfrak{A}\left(\widetilde{\mathbf{u}}^{\Delta}, \widetilde{\mathbf{u}}^{\Delta}\right) \;\geq\; & \sum_{e} \left(\frac{\nu}{k_f} + \beta\|\mathbf{z}\|_2\right) \|\mathbf{u}^{\Delta}\|^2_{0,\Omega_e} - \sum_{e} \gamma\tau_e \left(\frac{\nu}{k_f} + \beta\|\mathbf{z}\|_2\right)^2 \|\mathbf{u}^{\Delta}\|_{0,\Omega_e} \\ & + \sum_{e} \gamma\tau_e \|\nabla\bar{p}^{\Delta}\|^2_{0,\Omega_e} - \sum_{e} \gamma\tau_e \int\limits_{\Omega_e} \left(3\beta^2 + \frac{2\beta\nu}{\|\mathbf{z}\|_2 k_f}\right) \left(\mathbf{z}\cdot\mathbf{u}^{\Delta}\right)^2 \mathrm{d}\Omega_e\end{aligned}$$

Applying the Cauchy-Schwarz inequality, $|\,(\mathbf{a},\mathbf{b})\,| \leq \|\mathbf{a}\|\|\mathbf{b}\|$, to the terms involving $\left(\mathbf{z}\cdot\mathbf{u}^{\Delta}\right)^2$ results in

$$\begin{aligned}\mathfrak{A}\left(\widetilde{\mathbf{u}}^{\Delta}, \widetilde{\mathbf{u}}^{\Delta}\right) \;\geq\; & \sum_{e} \left(\frac{\nu}{k_f} + \beta\|\mathbf{z}\|_2\right) \|\mathbf{u}^{\Delta}\|^2_{\Omega_e} + \sum_{e} \gamma\tau_e \|\nabla\bar{p}^{\Delta}\|^2_{0,\Omega_e} \\ & - \sum_{e} \gamma\tau_e \left[\left(\frac{\nu}{k_f} + \beta\|\mathbf{z}\|_2\right)^2 + \left(3\beta^2 + \frac{2\beta\nu}{\|\mathbf{z}\|_2 k_f}\right) \|\mathbf{z}\|^2_{\Omega_e}\right] \|\mathbf{u}^{\Delta}\|^2_{\Omega_e}.\end{aligned}$$

Since $\|\mathbf{a}\|_2 \geq \|\mathbf{a}\|_{\Omega_e}$,

$$\mathfrak{A}\left(\widetilde{\mathbf{u}}^{\Delta}, \widetilde{\mathbf{u}}^{\Delta}\right) \;\geq \sum_{e} \left[\left(\tfrac{\nu}{k_f} + \beta\|\mathbf{z}\|_2\right) - \gamma\tau_e \left(\tfrac{\nu}{k_f} + 2\beta\|\mathbf{z}\|_2\right)^2\right] \|\mathbf{u}^{\Delta}\|^2_{\Omega_e} + \sum_{e} \gamma\tau_e \|\nabla\bar{p}^{\Delta}\|^2_{0,\Omega_e}.$$

Let $\mathcal{C}_e \equiv \left(\frac{\nu}{k_f} + \beta\|\mathbf{z}\|_2\right) - \gamma\tau_e \left(\frac{\nu}{k_f} + 2\beta\|\mathbf{z}\|_2\right)^2$. If $\mathcal{C}_e > 0 \;\forall e \in 0, 1, \ldots, ne-1$, then $\mathfrak{A}\left(\widetilde{\mathbf{u}}^{\Delta}, \widetilde{\mathbf{u}}^{\Delta}\right)$ is coercive over $V_0^{\Delta} \times S_0^{\Delta}$. To show this, it is helpful to separate $\sum\limits_{e=0}^{ne-1} \mathcal{C}_e \|\mathbf{u}^{\Delta}\|^2_{\Omega_e}$ into two sums, one over elements in the Darcy regime plus another over elements in the Forchheimer regime (abbreviated in the following summation limits as "Forch."). Recall from its definition that in the Darcy regime $\tau_e = \frac{k_f}{\nu}$ while in the

Forchheimer regime $\tau_e = \frac{1}{\beta\|\mathbf{z}\|_2}$.

$$\begin{aligned}\sum_e \mathcal{C}_e\|\mathbf{u}^\Delta\|^2_{\Omega_e} + \sum_e \gamma\tau_e\|\nabla\bar{p}^\Delta\|^2_{0,\Omega_e} &= \sum_e \gamma\tau_e\|\nabla\bar{p}^\Delta\|^2_{0,\Omega_e} + \sum_{e\in \text{ Darcy}} \mathcal{C}_e\|\mathbf{u}^\Delta\|^2_{\Omega_e} \\ &\quad + \sum_{e\in \text{ Forch.}} \mathcal{C}_e\|\mathbf{u}^\Delta\|^2_{\Omega_e}\end{aligned}$$

Note that in the Darcy regime, $\frac{k_f}{\nu} < \frac{1}{\beta\|\mathbf{z}\|_2}$, while the opposite is true in the Forchheimer regime. This fact can be used to bound the stabilization tuning parameter γ such that $\mathcal{C}_e$ is positive on every element.

$$\begin{aligned}\sum_{e\in \text{ Darcy}} \mathcal{C}_e\|\mathbf{u}^\Delta\|^2_{\Omega_e} &= \sum_{e\in \text{ Darcy}} \left[\left(\frac{\nu}{k_f} + \beta\|\mathbf{z}\|_2\right) - \gamma\left(\frac{k_f}{\nu}\right)\left(\frac{\nu}{k_f} + 2\beta\|\mathbf{z}\|_2\right)^2\right]\|\mathbf{u}^\Delta\|^2_{\Omega_e} \\ &\geq \sum_{e\in \text{ Darcy}} \left[\frac{\nu}{k_f} + \beta\|\mathbf{z}\|_2 - \gamma\left(\frac{\nu}{k_f} + 8\beta\|\mathbf{z}\|_2\right)\right]\|\mathbf{u}^\Delta\|^2_{\Omega_e} \\ &\geq 0 \quad \text{if } \gamma < \frac{1}{8}\end{aligned}$$

$$\begin{aligned}\sum_{e\in \text{ Forch.}} \mathcal{C}_e\|\mathbf{u}^\Delta\|^2_{\Omega_e} &= \sum_{e\in \text{ Forch.}} \left[\left(\frac{\nu}{k_f} + \beta\|\mathbf{z}\|_2\right) - \gamma\left(\frac{1}{\beta\|\mathbf{z}\|_2}\right)\left(\frac{\nu}{k_f} + 2\beta\|\mathbf{z}\|_2\right)^2\right]\|\mathbf{u}^\Delta\|^2_{\Omega_e} \\ &\geq \sum_{e\in \text{ Forch.}} \left[\frac{\nu}{k_f} + \beta\|\mathbf{z}\|_2 - \gamma\left(\frac{5\nu}{k_f} + 4\beta\|\mathbf{z}\|_2\right)\right]\|\mathbf{u}^\Delta\|^2_{\Omega_e} \\ &\geq 0 \quad \text{if } \gamma < \frac{1}{5}\end{aligned}$$

Thus, the bilinear form $\mathfrak{A}\left(\left[\mathbf{u}^\Delta, \bar{p}^\Delta\right], \left[\mathbf{u}^\Delta, \bar{p}^\Delta\right]\right)$ is coercive over $V_0^\Delta \times S_0^\Delta$ for τ_e as defined in section A.4.2 as long as $\gamma < \frac{1}{8}$. ■

Chapter 4

Numerics

The domain of interest, Ω, for all two-dimensional calculations is shown in Figure 4.1 as a square of dimension $[0, 1 \text{ km}] \times [0, 1 \text{ km}]$. The top, right, bottom, and left boundaries of the domain are denoted $\Gamma_T, \Gamma_R, \Gamma_B$, and Γ_L respectively. The fixed pressure boundaries, Γ_D, are Γ_L and Γ_R, while a homogeneous Neumann boundary condition on velocity is applied on $\Gamma_N = \Gamma_T + \Gamma_B$. In particular, for the two-dimensional calculations, equation (3.4c) implies that there is no flow across the top and bottom boundaries.

The model parameters for the two-dimensional simulations are shown in Table 4.1. In this case, the fixed pressure gradient across the domain ($\frac{p_{\text{in}} - p_{\text{out}}(\text{Pa})}{1\text{km}}$) induces flow. To determine a physically reasonable pressure gradient to start with, consider a 1% hydraulic head gradient over the domain as a realistic upper bound. By equation (1.7), a 1% head gradient over a kilometer converts to $p_{\text{in}} - p_{\text{out}} \approx 0.1\text{MPa}$.

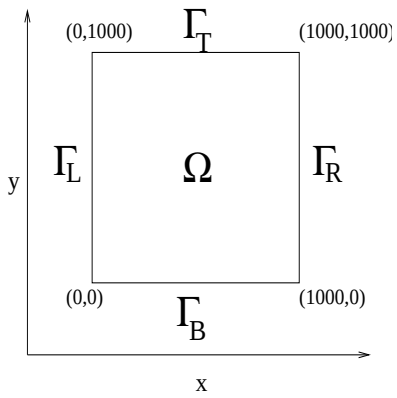

Figure 4.1: Two-dimensional Problem Domain

Table 4.1: Parameters values to be specified in the two-dimensional flow model.

Model Parameters and Numerical Values

Variable	Definition	Value	Units
$\mathcal{S}'$	Source term	0	$\frac{1}{\mathrm{s}}$
$\mathbf{g}$	Gravity vector	$\mathbf{0}$	$\frac{\mathrm{m}}{\mathrm{s}^2}$
ρ	constant density	1000	$\frac{\mathrm{kg}}{\mathrm{m}^3}$
β	inertial coefficient	90.6	mm^{-1}[96, Page 6]
k_f	intrinsic permeability	median (k_f)=4.08e-05	mm^2[96, Page 6]
μ	dynamic viscosity at 1atm and 25°C	8.91e-4	Pa-sec
ν	kinematic viscosity at 1atm and 25°C	8.91e-7	$\frac{\mathrm{m}^2}{\mathrm{s}}$
ϕ	porosity	0.45	dimensionless
$\bar{g}_D$	Dirichlet Pressure Boundary Condition	$\begin{cases} \frac{p_{\mathrm{in}}}{\rho} & \in \Gamma_L \\ \frac{p_{\mathrm{out}}}{\rho} & \in \Gamma_R \end{cases}$	$\frac{\mathrm{m}}{\mathrm{s}^2}$

This pressure difference across the domain is used to induce flow in Simulation A (Section 4.1). The results will illustrate

1. the pressure contours and velocity field,

2. the magnitude of the Darcy, Forchheimer, and advective terms over the domain,

3. and the Reynold's number over the domain.

In Simulation B (Section 4.1), the pressure difference is increased in order to in-

crease the magnitude of the velocity, and accordingly the Reynold's number, over the domain. The point of increasing the pressure difference beyond physically realistic values is to examine the magnitude of the terms at higher Reynold's numbers, specifically on the order of 100. These results will be used to justify the implementation of three-dimensional well simulations which include vertical gradients.

All three simulations use the same intrinsic permeability field, shown in Figure 4.2. The median value of the permeability over the domain is listed in Table 4.1, and the variance is 4.

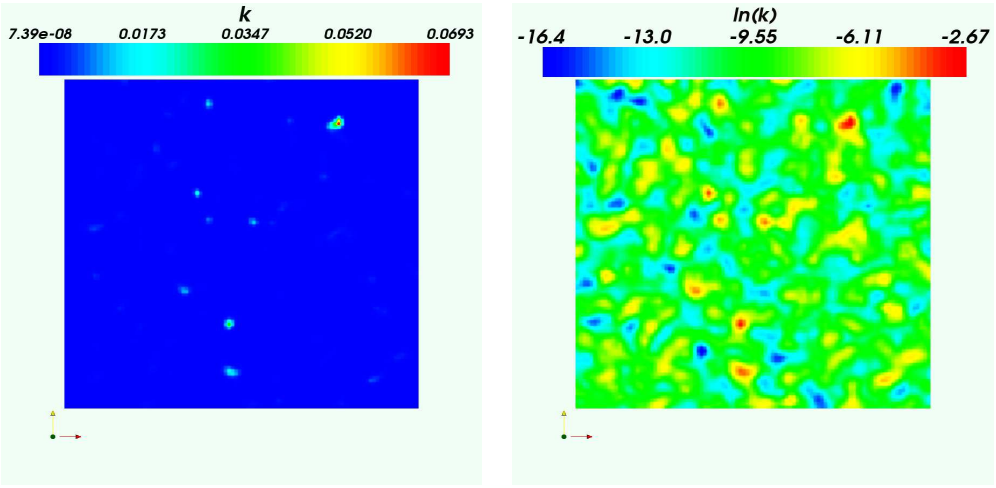

(a) (b)

Figure 4.2: (a) Intrinsic permeability field (in millimeters) used in Simulations A, B, and C; (b) Illustrating the variability in $\ln(k_f)$.

4.1 Simulation A: 1% Hydraulic Head Gradient (Re << 1)

Figure 4.3(a) shows the pressure contours and velocity field at the solution. The Reynold's number, shown in Figure 4.3(b), is much less than one; thus, the velocity field is well within the Darcy regime over the entire domain. The comparison of the Darcy and Forchheimer terms supports this observation; the magnitude of the Forchheimer term is much less than the magnitude of the Darcy term over the entire domain.

Despite these results, the goal of this dissertation is to examine the effect of the advective acceleration term on the solution to the non-Darcy equations. Figure 4.5(a) shows the magnitude of the advective acceleration term over the domain. When compared to the magnitude of both the Darcy and Forchheimer terms as shown in Figure 4.4, the advective acceleration term is clearly much smaller. There is no point in the domain where the magnitude of the advective acceleration term is larger than the other terms in the equation.

In Sections 4.2 and 4.3, the flow field is induced by a higher pressure gradient such that the Reynolds number has a maximum of $\mathcal{O}(10)$ and $\mathcal{O}(100)$, respectively. For both simulations the same quantities are plotted as in this section to examine the relationship among the Darcy, Forchheimer, and advective terms.

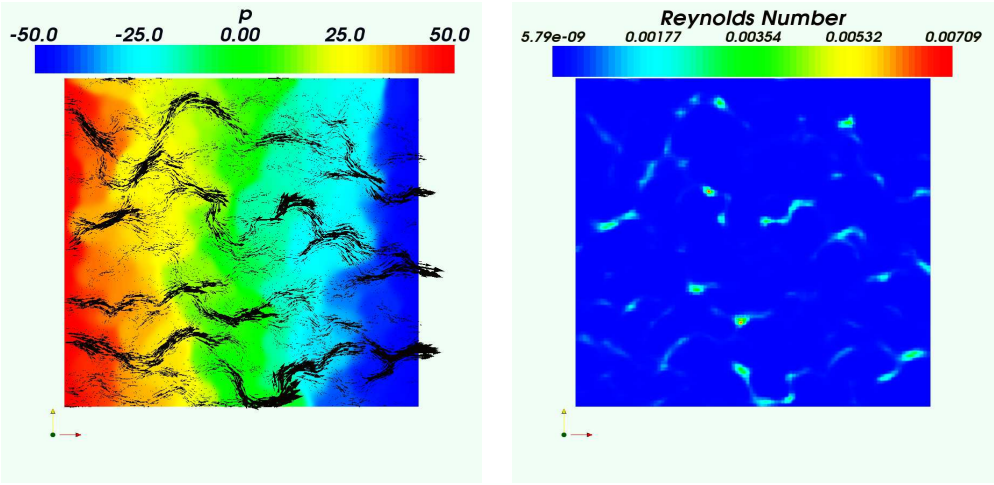

(a) (b)

Figure 4.3: (a) Pressure contours and velocity field. Note that the colorbar label p actually refers to $\bar{p}$ from the non-Darcy equations (3.18). The simulation has units of meters, kilograms, and seconds; (b) Contours of the Reynold's number, $Re = \frac{\sqrt{k_f}\|\mathbf{u}\|_2}{\nu}$

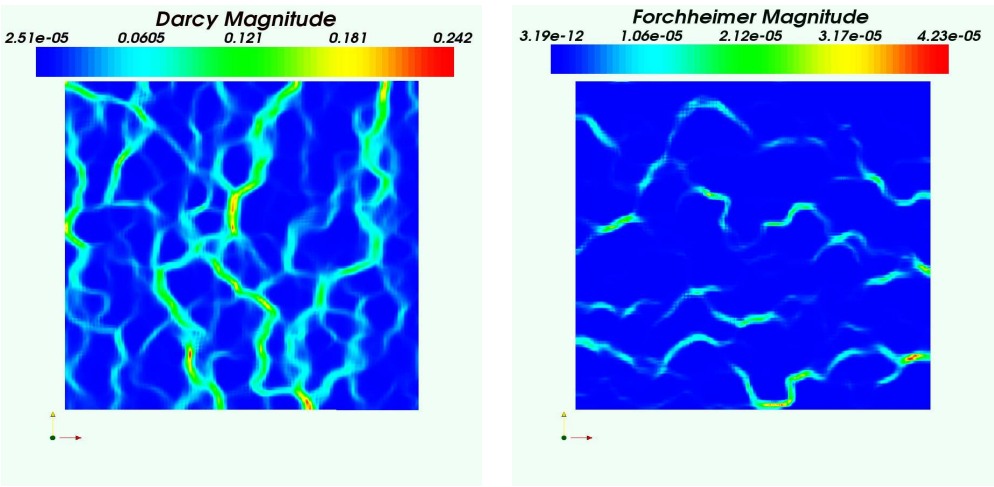

(a) (b)

Figure 4.4: (a) Contours of the magnitude of the linear Darcy term $\frac{\phi^2\nu\mathbf{u}}{k_f}$; (b) Contours of the magnitude of the quadratic Forchheimer term $\phi^2\beta\|\mathbf{u}\|_2\mathbf{u}$

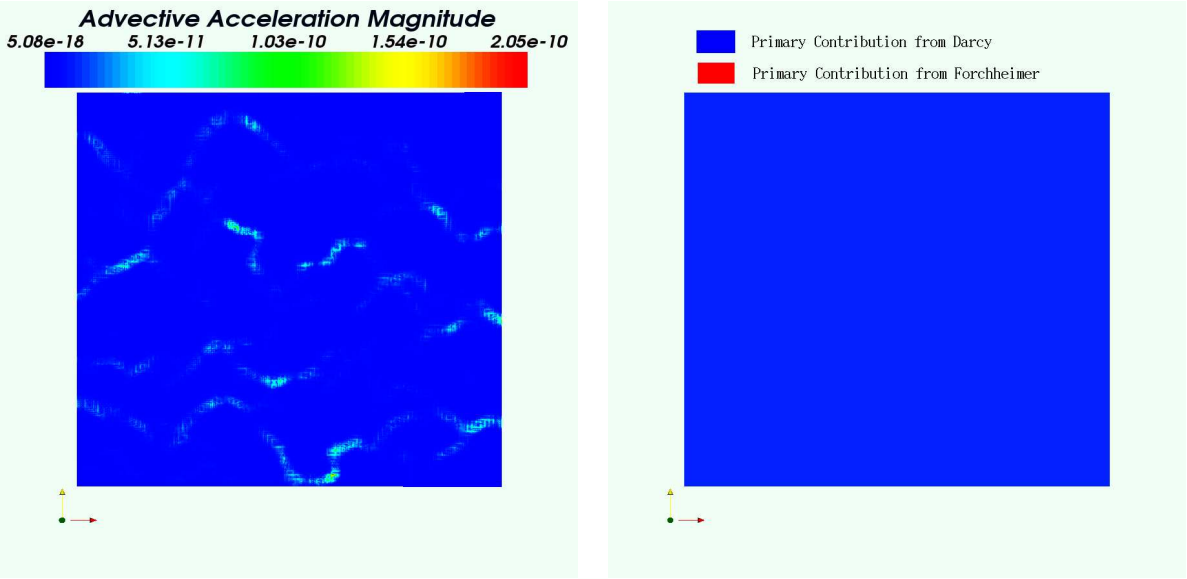

(a) (b)

Figure 4.5: (a) Contours of the magnitude of the advection term, $\mathbf{u} \cdot \nabla \mathbf{u}$; (b) Comparing the contribution of the Darcy term to that of the Forchheimer term over the domain

4.2 Simulation B: Flow for $\mathrm{Re} = \mathcal{O}(10)$

The pressure gradient over the domain has been increased by four orders of magnitude ($p_{\text{in}} - p_{\text{out}} \approx 10^3$MPa) in order to illustrate a flow field with a $\mathcal{O}(10)$ maximum Reynold's number. Figure 4.9 illustrates that in this case for regions of the domain where the Reynolds number is approximately less than 3, the Darcy term predominantly contributes to the flow solution. For Re >= 3, the magnitude of the Forchheimer term is larger than the magnitude of the Darcy term. Still in this case, the magnitude of the advective acceleration term is smaller than both the magnitude of the Darcy term and the magnitude of the Forchheimer term.

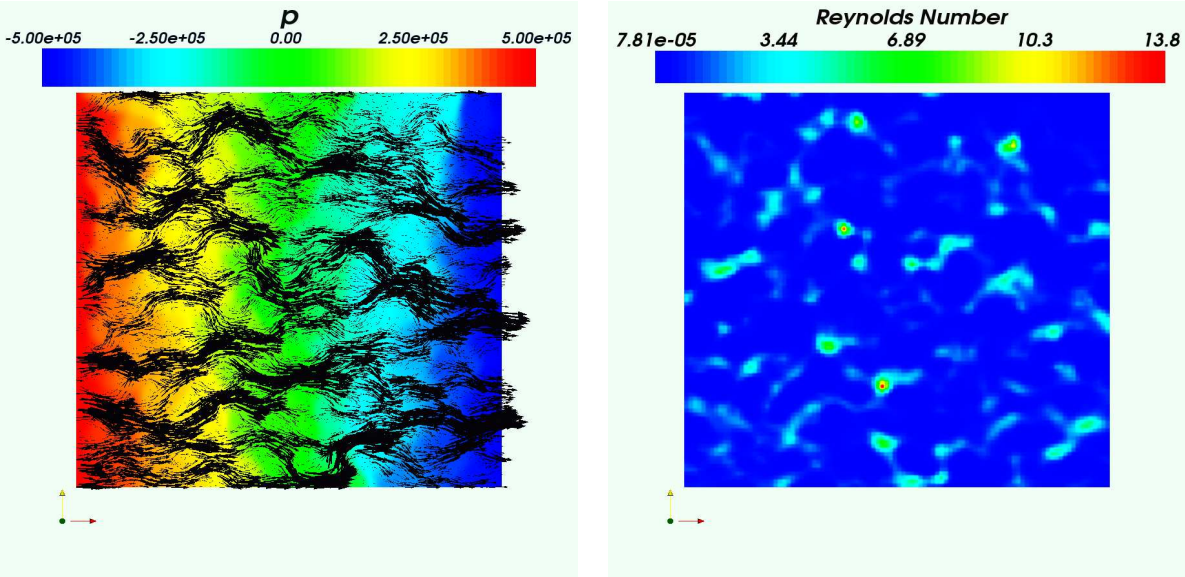

(a) (b)

Figure 4.6: (a) Pressure contours and velocity field. Note that the colorbar label p actually refers to $\bar{p}$ from the non-Darcy equations (3.18). The simulation has units of meters, kilograms, and seconds; (b) Contours of the Reynold's number, $Re = \frac{\sqrt{k_f}\|\mathbf{u}\|_2}{\nu}$

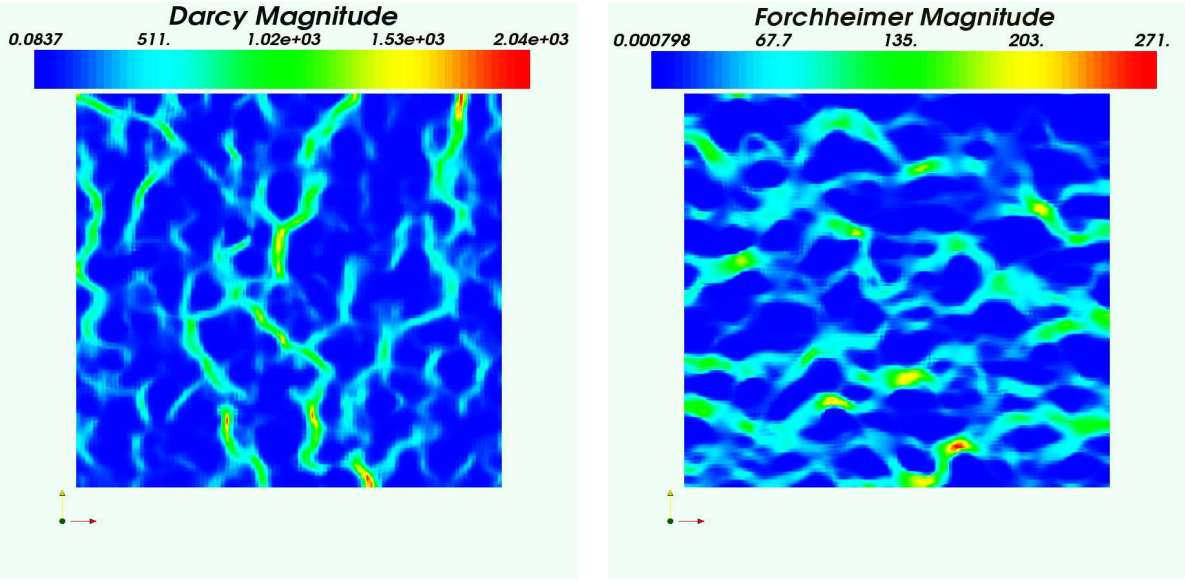

(a) (b)

Figure 4.7: (a) Contours of the magnitude of the linear Darcy term $\frac{\phi^2 \nu \mathbf{u}}{k_f}$; (b) Contours of the magnitude of the quadratic Forchheimer term $\phi^2 \beta \|\mathbf{u}\|_2 \mathbf{u}$

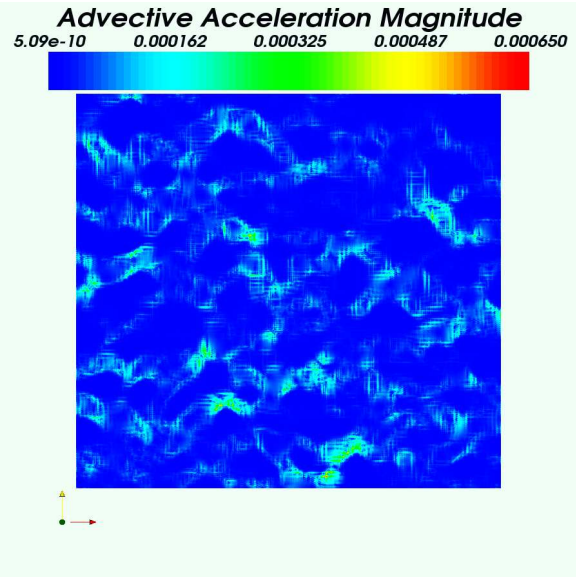

Figure 4.8: Contours of the magnitude of the advection term, $\mathbf{u} \cdot \nabla \mathbf{u}$

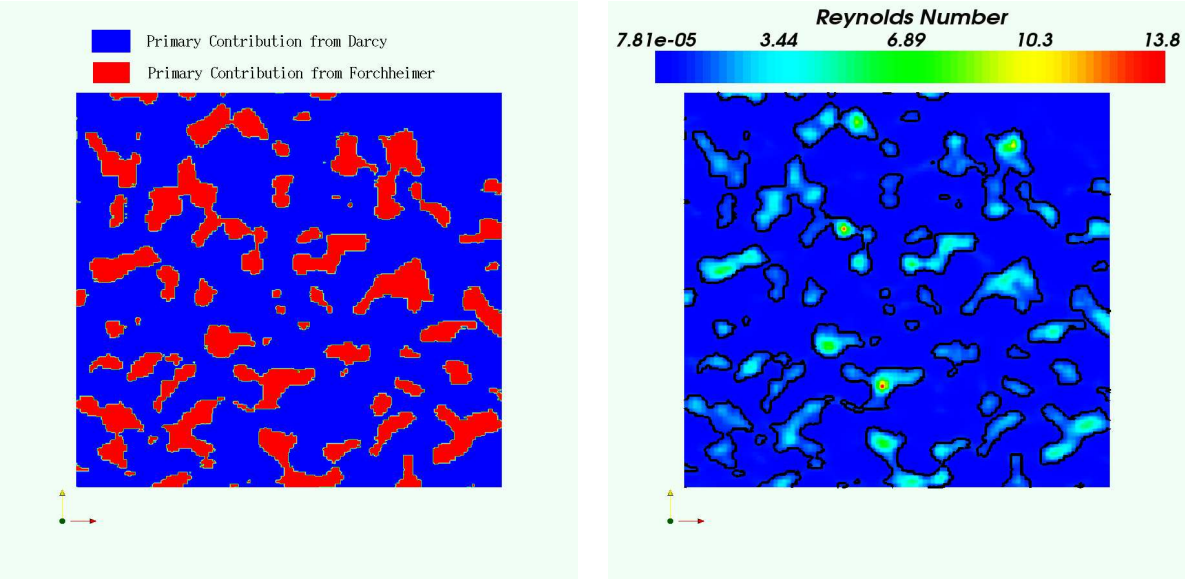

(a) (b)

Figure 4.9: (a) Comparing the contribution of the Darcy term to that of the Forchheimer term over the domain; (b) Illustrating that the Darcy term is larger than the Forchheimer term in regions where the Reynold's number is small.

4.3 Simulation C: Flow for $\mathrm{Re} = \mathcal{O}(100)$

The pressure gradient over the domain has been increased to $p_{\text{in}} - p_{\text{out}} \approx 10^5$MPa which corresponds to a maximum Reynold's number of $\mathcal{O}(100)$. Figure 4.13 illustrates the regions which exhibit Darcy flow behavior, as well as the portions of the domain where the Forchheimer term has more of a contribution. Again, the magnitude of the advective acceleration term is smaller than both the magnitude of the Darcy term and the magnitude of the Forchheimer term.

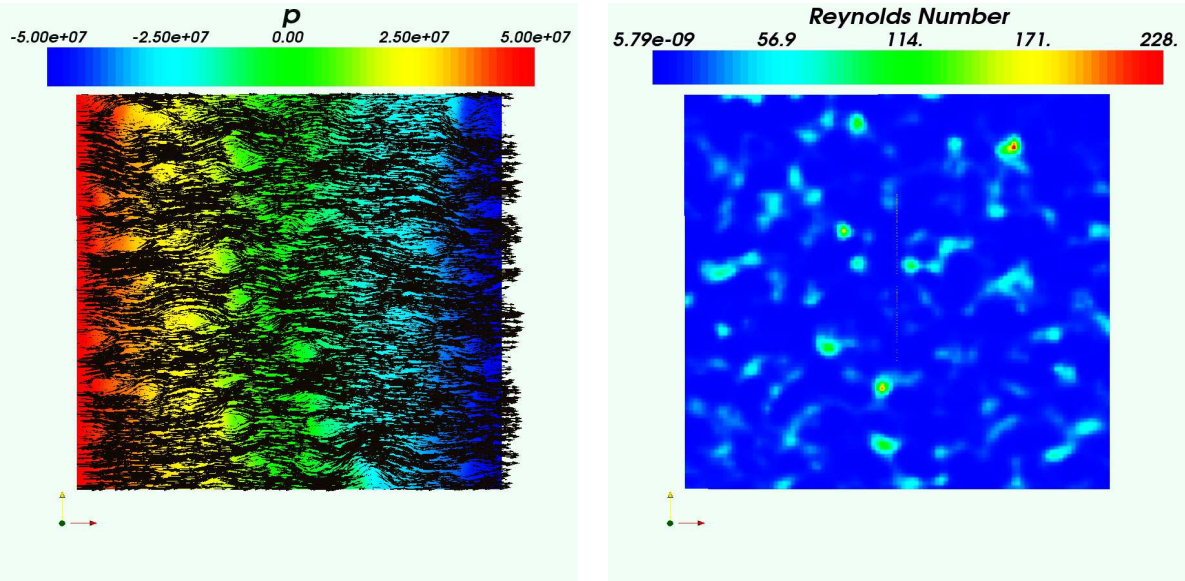

(a) (b)

Figure 4.10: (a) Pressure contours and velocity field. Note that the colorbar label p actually refers to $\bar{p}$ from the non-Darcy equations (3.18). The simulation has units of meters, kilograms, and seconds; (b) Contours of the Reynold's number, $Re = \frac{\sqrt{k_f}\|\mathbf{u}\|_2}{\nu}$

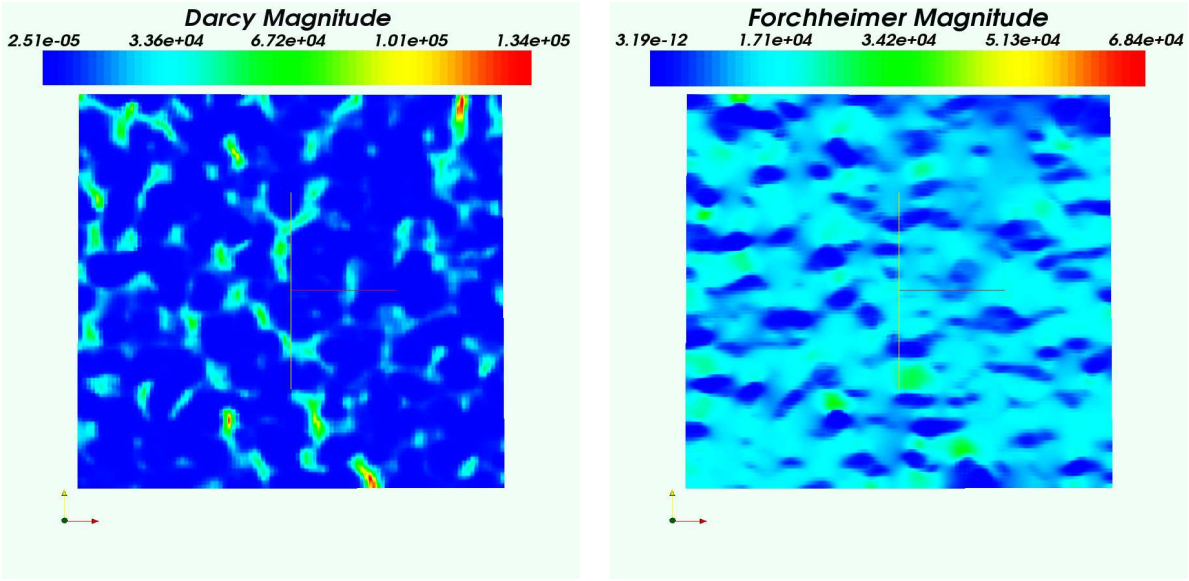

(a) (b)

Figure 4.11: (a) Contours of the magnitude of the linear Darcy term $\frac{\phi^2 \nu \mathbf{u}}{k_f}$; (b) Contours of the magnitude of the quadratic Forchheimer term $\phi^2 \beta \|\mathbf{u}\|_2 \mathbf{u}$

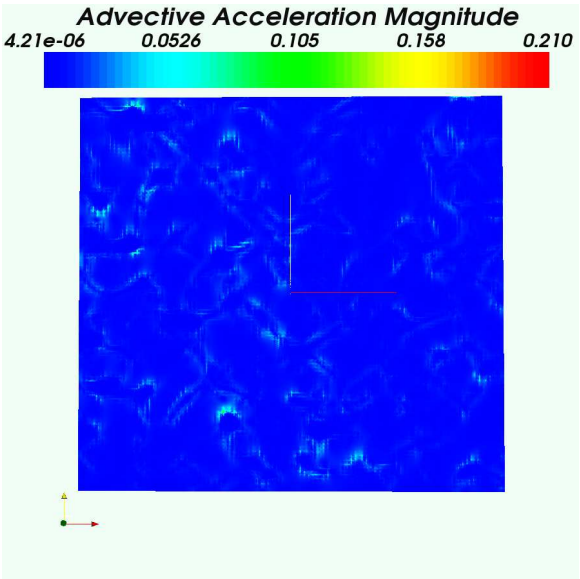

Figure 4.12: Contours of the magnitude of the advection term, $\mathbf{u} \cdot \nabla \mathbf{u}$

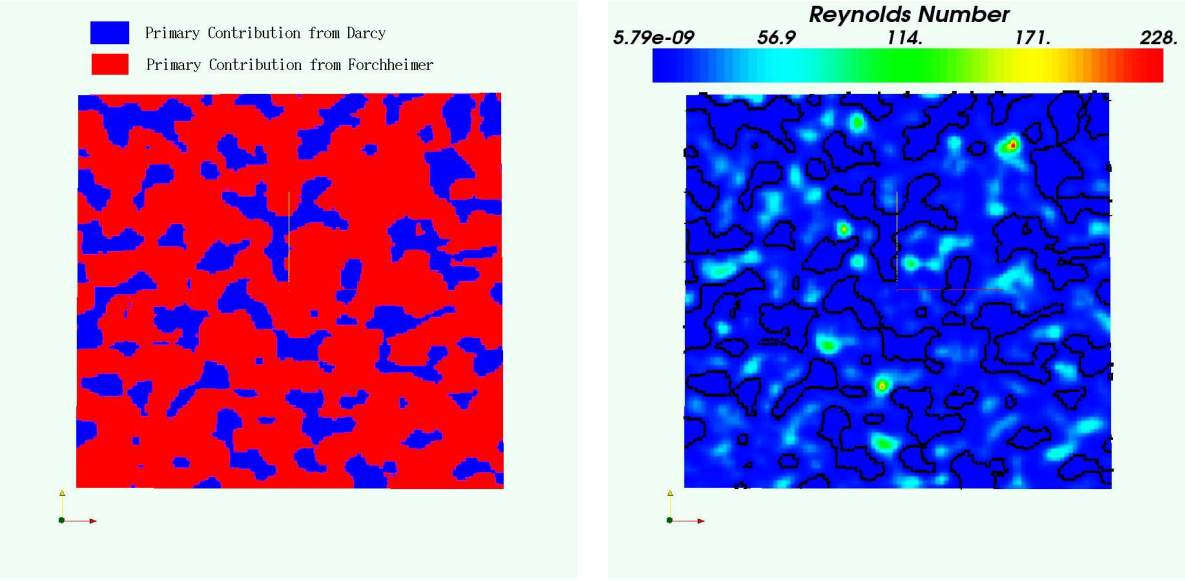

(a) (b)

Figure 4.13: (a) Comparing the contribution of the Darcy term to that of the Forchheimer term over the domain; (b) Illustrating that the Darcy term is larger than the Forchheimer term in regions where the Reynold's number is small.

4.4 Conclusions: 2D Flow

The two dimensional results have supported the general belief that Darcy's law holds for Re $<<$ 1 (see Section 4.1 for a simulation in the Darcy regime). Sections 4.2 and 4.3 show that the quadratic Forchheimer term, $\phi^2\beta\|\mathbf{u}\|_2\mathbf{u}$, contributes more to the flow equation than the Darcy term in regions outside the Darcy regime. The advective acceleration term has been negligible in all two-dimensional flow cases presented. It is hypothesized that for three-dimensional flow the additional complexity due to vertical velocity gradients will cause the advective acceleration term to be significant in certain physically realistic flow scenarios.

Chapter 5

Software

5.1 Introduction to Object-Oriented Programming

Programming practices have progressed over the years from an unstructured style, where all code to complete a task is contained in one main program; to procedural or structured programming. This program design style results in a program composed of interacting functions. The Matlab programming language is an example of a language lending itself to a structured programming style; a program can be partitioned into smaller, more manageable tasks using the `function` keyword.

While a procedural design is better than an unstructured one, the state-of-the art in program design, and the focus of this section, is object-oriented programming (OOP). An object-oriented design is better for large programming projects as it increases flexibility and makes code reuse easier. This section serves as an overview

of object-oriented programming with an assumption of Matlab familiarity and will introduce topics we refer to in the software descriptions in Sections 5.2 and 5.2.3.

Several programming languages have been created for the express purpose of supporting the object-oriented design principles. In this chapter we focus on software packages written in C++, and discuss the many advantages of C++ and OOP, including data abstraction, inheritance, and dynamic binding. Of these three topics, inheritance and dynamic binding are unique to object-oriented programming.

While procedural programming involves interacting procedures (or functions in Matlab), object-oriented programs have interacting objects, with each object controlling its own state. An object is a self-contained entity containing both data and operations on that data, called methods. These methods are the only way an object's data can be modified or accessed by another object. In this way an object-oriented program is composed entirely of interacting objects, communicating by passing messages via methods.

There are a number of design principles which characterize object-oriented programming. When combined, the principles describe OOP; however, individually each is an example of abstraction [92, Page 9].

- Divide and Conquer: A division of labor occurs where complex tasks are broken up into smaller, more manageable units. This strategy increases the likelihood that each task will be completed correctly. This OOP idea is closely related to the divide and conquer algorithm inherent in computer science. Basially, once

the overal problem has been divided into well-defined subproblems, an *object* is designed to solve each subproblem.

- Encapsulation: Each object is designed to fulfill a given type of task, and it contains all the data and methods required to complete its task in a self-contained fashion.

- Interface: An object's calling sequence or interface determines how a single object is used and how multiple objects interact with each other.

- Information Hiding: The implementation of a procedure can be changed without modifying any of the code which calls the procedure, as long as its interface remains the same. The details of how an object completes a task is immaterial to other objects it communicates with, which increases the flexibility of the entire project.

- Generality: Objects are designed to fulfill a certain general task so that as much code as possible can be reused in different specific situations.

- Extensibility: The concept of inheritance is important here, as we hope to inherit as much functionality as possible from other objects in order to extend the capabilities of new object to solve a related task.

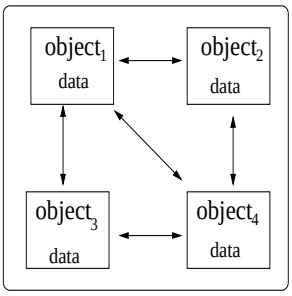

Figure 5.1: OOP Schematic

5.2 Trilinos: Solver Framework

This section discusses software status as of August 2004.

Trilinos, currently under development at Sandia National Laboratories, is an object-oriented product designed to aid the development of parallel solvers and libraries [70, 106]. It is organized into multiple packages, with each package designed to stand alone as an independent piece of software with its own requirements and design team (although there are a small number of dependencies). Some examples of Trilinos packages include ML, a multigrid preconditioning package for solving large, sparse, linear systems; AztecOO, an object-oriented interface to Aztec, a massively parallel solver for sparse, linear systems; NOX, a nonlinear solver package; LOCA, a library of continuation algorithms; and Epetra, a default linear algebra library for all Trilinos solvers. Trilinos also provides a `New_Package` class to aid the inclusion of new packages in future releases.

While each package is stand-alone software, many packages have default options

that use tools contained in other Trilinos packages. For example, LOCA uses tools in NOX to solve the nonlinear systems generated by the continuation algorithms. To represent the nonlinear system and associated linear subsystem, NOX communicates with specific implementations of vectors and matrices indirectly through a variety of linear algebra interfaces. Also, AztecOO contains iterative linear solvers immediately available to NOX.

It is important to understand the difference between a linear algebra *interface* and a linear algebra *implementation*. A linear algebra interface is able to manipulate vectors without any knowledge of the underlying data structure or storage. For example, the Trilinos Solver Framework (known as TSF [12, 14, 87]) is a linear algebra interface which contains many methods for performing vector and matrix operations (see Section 5.2.1 for examples). These methods are independent of the underlying implementation of the linear algebra object; as an example, one should be able to write high level code for a sparse matrix-vector product with no knowledge of how the sparse matrix is stored in memory. That specific fact is entirely dependent upon the user's linear algebra *implementation*. Specific linear algebra implementations include LAPACK [2, 39]; Sandia National Laboratories' Epetra [69, 71]; and Argonne National Laboratory's PETSc [8, 9, 10]).

General software engineering tools required by all packages are located at the Trilinos level and, of these, the most important are the GNU Autotools [52, 53] used configure and compile the code. Autoconf automatically generates the appropriate,

machine-dependent scripts to configure all Trilinos packages for the user's particular platform, and Automake automatically generates the Makefiles for each package.

Trilinos is freely available under the GNU Lesser General Public License from `http://software.sandia.gov/trilinos`.

5.2.1 Linear Algebra Interfaces: TSFCore and TSFExtended

Interest in general abstract linear algebra packages grew in 1996 with the appearance of the Hilbert Class Library (HCL) written by Symes and Gockenbach [54, 55]. The progression from there, as it relates to Trilinos, involves a concrete vector representation called Epetra written by Mike Heroux from Sandia National Laboratories. Epetra is currently the default linear algrebra represention distributed with Trilinos.

In 2001, the addition of the TSF package to the development version of Trilinos expanded the capabilities of the framework through more abstract linear algebra interfaces. Kevin Long from Sandia National Laboratories wrote the original TSF, and over the years it has grown to account for the needs of its users. Recent work has split TSF into three more manageable packages that are currently part of the Trilinos framework: TSFCore, TSFCoreUtils, and TSFExtended.

The TSFCore package contains an abstract interface to basic linear algebra operations on vectors, linear operators, and nonlinear operators. It attempts to support the minimum functionality required to build abstract numerical algorithms (ANAs). In this way, requirements common to ANAs are separated from specific implementations

of the linear algebra. Thus, the user is able to use any linear algebra implementation that can interface with the abstract numerical algorithm. The nonlinear solver NOX was designed to be an ANA, and other examples include iterative linear solvers, stability/bifurcation methods, uncertainty quantification methods, and simultaneous analysis and design (SAND) optimization [12, 15].

Since TSFCore is an interface to a linear algebra library, it requires access to a concrete linear algebra implementation. Epetra is the concrete implementation distributed with Trilinos; thus, it is the linear algebra library most Trilinos users choose in practice. As mentioned earlier, LAPACK and PETSc are other options.

Utilities required for efficient parallel implementation of TSFCore methods are located in the TSFCoreUtils package. One of the most important features is the RTOpPack namespace, which contains efficient templated code for performing reduction and transformation operations [15]. Reduction and transformation operations are important because one can combine them to perform all the standard BLAS operations [2], in addition to any nonstandard operations required by an optimization algorithm or an algorithm for solving nonlinear equations. An example of a nonstandard operation provided in [15] is

$$d_i \leftarrow \begin{cases} (b-u)_i^{1/2} & \text{if} \quad w_i < 0 \quad \text{and} \quad b_i < +\infty \\ 1 & \text{if} \quad w_i < 0 \quad \text{and} \quad b_i = +\infty \\ (u-a)_i^{1/2} & \text{if} \quad w_i \geq 0 \quad \text{and} \quad a_i > -\infty \\ 1 & \text{if} \quad w_i \geq 0 \quad \text{and} \quad a_i = -\infty \end{cases} \quad \text{for } i = 1 \ldots n.$$

The ability to easily handle complicated conditional statements is a major selling point for TSFCore. Furthermore, the implementation of reduction and transformation operations in TSFCore strives to reduce the overall number of temporary vector copies required to compute complicated operations.

Examples of Reduction/Transformation Operations:

1. element-wise transformation: $op_T\left(i, v_i^0, \ldots, v_i^{p-1}, z_i^0, \ldots, z_i^{q-1}\right) \rightarrow z_i^0, \ldots, z_i^{q-1}$

   Examples: vector addition, linear combinations, scaling

2. element-wise reduction: $op_R\left(i, v_i^0, \ldots, v_i^{p-1}, z_i^0, \ldots, z_i^{q-1}\right) \rightarrow \beta$

   Examples: norm, dot product

3. reduction of intermediates: $op_{RR}\left(\hat{\beta}, \tilde{\beta}\right) \rightarrow \tilde{\beta}$

Here $v^0, \ldots, v^{p-1} \in \mathbb{R}^n$ are p non-mutable input vectors; $z^0, \ldots, z^{q-1} \in \mathbb{R}^n$ are q mutable input/output vectors; $i = 1 \ldots n$; and β is a reduction target which can be a simple scalar, a more complicated non-scalar (e.g. a set of scalars), or NULL. Mutable is a C++ keyword, which allows the modification of a data member belonging to a constant object.

The TSFExtended package provides an abstract interface to vectors, operators, and solvers through wrappers and extensions to TSFCore [12, 14]. A goal of TSFExtended is Matlab-like syntax, yielding intuitive syntax and more readable code. Moreover, TSFExtended's use of *handle classes* makes TSFCore and TFEXtended interchangeable and memory management automatic.

Essentially a handle class contains both a pointer to the object being handled as well as a counter that tracks the number of valid references to the object that are in the code at any given time. As soon as the object is no longer referenced at any point in the code, the handle will recognize that the counter is currently at zero, and the space allocated for the object will automatically be deleted. Thus the user will use the `new` command to allocate space, but will never delete objects or deallocate space. This idea will be familiar to Java users.

In TSFExtended, the handle class wraps a pointer to a TSFCore object, so the user is not responsible for the minute details of pointer syntax. Also TSFExtended code has minimal explicit use of pointers, so the code is more readable and user-friendly. A final benefit of the handle classes in TSFExtended is that they allow TSFCore and TSFExtended to be interchangeable. For example, assume a user has access to a TSFCore object, but would like to perform a TSFExtended operation on the object. First, the TSFCore object is used to construct the equivalent TSFExtended object. Then the TSFExtended operation is applied to this new object.

On the other hand, consider the case where the user wants to perform TSFCore operations, but only has access to TSFExtended objects. The handle class comes into play in this instance, as every handle to a TSFExtended object contains a pointer to the equivalent underlying TSFCore object. The pointer can be used to access the TSFCore object and perform TSFCore operations on it.

5.2.2 NOX

NOX is an object-oriented software package designed to efficiently solve nonlinear problems of the form

$$F(x) = 0, \;\; F : \mathbb{R}^n \rightarrow \mathbb{R}^n,$$

using any available linear algebra package which conforms to the NOX calling sequence. NOX does not require information about the Jacobian, F', although when this information is available the performance of the nonlinear solver improves. Here $F'_{i,j} = \frac{\partial F_i}{\partial x_j}(x)$.

The methods a linear algebra package must support are defined through the NOX abstract base classes (ABCs) `NOX_Abstract_Vector` and `NOX_Abstract_Group`. All standard vector operations that NOX expects a linear algebra package to handle are defined within the Vector class. All other nonlinear solver operations are encapsulated in the Group class.

For example, the concrete implementation of the `NOX_Abstract_Group` class contains specific methods to compute $F(x)$ at a particular point $x \in \mathbb{R}^n$, as well as $F'(x)$, if available. Assuming Jacobian information is provided, a method should be specified for computing the Newton direction and possibly the gradient for the problem. The Newton direction is the solution, s, of $F's = -F$, which can be computed with either a direct linear solver or an iterative method like GMRES. If the nonlinear problem is

formulated as the optimization problem,

$$\min f(x) = \frac{1}{2}\|F(x)\|_2^2,$$

NOX will compute and store the gradient, $g = (F')^T F$, of $f(x)$.

In order for NOX to communicate with a particular linear algebra package, concrete implementations of the required methods must be coded by the user in classes derived from the abstract base classes. To allow NOX to communicate with vectors implemented by the linear algebra package LAPACK, for example, the class `NOX_LAPACK_Vector` must be derived from `NOX_Abstract_Vector` and implement all required vector methods using LAPACK. Similarly, `NOX_LAPACK_Group` must derive from `NOX_Abstract_Group` and implement all of its pure abstract methods.

5.2.3 My Contribution to Trilinos

Sundance 2.0 is a high-level C++ software package under development at Sandia National Laboratories. Its purpose is to provide a partial differential equation (PDE) simulation/optimization framework using the finite element method (FEM), which hides most of the FEM details from the user. The code is object-oriented, allowing the user to describe the finite element problem in terms of objects like a mesh, the weak form of the PDE, and function spaces, rather than by computing each individual entry of the stiffness matrix or load vector [85, 86].

Sundance depends upon Trilinos, Sandia's parallel solver framework, for linear

algebra and solver support. This dependence requires the user to first successfully install Trilinos on their system before installing Sundance. The current version of Sundance contains interfaces to TSFExtended vectors, linear and nonlinear operators, linear solvers, and preconditioners. There are also interfaces to more sophisticated linear solvers and preconditioners in AztecOO and nonlinear solvers based in NOX, as well as hooks for preconditioning with ML and IFPACK.

Sundance is available for download under the GNU Lesser General Public License (LPGL) from `http://software.sandia.gov/sundance`. The current version of Sundance supports only equal-order elements. This is not a hindrance for most applications; however, when solving nonlinear fluid flow applications spurious oscillations in the pressure field will appear unless mixed-order elements are used to satisfy the LBB compatibility condition (see Section 3.3.2). Adding a pressure-stabilization term to the fluid flow model is a feasible work-around to Sundance's current restriction to equal-order elements. Information on stabilization techniques for the finite element method is included in Section 3.3.3.

The following information provides some technical details regarding Sundance.

- Sundance takes advantage of a hybrid *symbolic-automatic functional differentiation* scheme to allow users to write high-level, yet computationally efficient code. Derivatives are computed at evaluation time rather than requiring symbolic expressions in expanded form.

  Automatic differentiation, detailed in [13, 21, 22, 72, 112], is included in Sun-

dance with a variety of beneficial results. For optimization problems, adjoints can be computed automatically for the user. More pertinent to this document is the question of how to handle the Jacobian when solving a system of non-linear equations. Can the Jacobian be specified exactly or does it have to be approximated by some means like finite differences? If it can be approximated, is it computationally feasible to do so? With Sundance, these questions become insignificant; the Jacobian is always computed efficiently using symbolic automatic differentiation.

- *Handle classes* are used throughout Sundance to simplify user-level code and yield automatic and intelligent memory management. For example, Sundance symbolic objects are represented with the `Expr` (Expression) handle class. The different symbolic types all derive from the base class `ExprBase`, but after being constructed they are all used through the `Expr` handle only.

```
Expr x = new CoordExpr(0);
Expr f = x + 3.0*sin(x);
Expr dx = new Derivative(0);
Expr df = dx*f;
```

The `Expr` handle assumes total responsibility for the "pointers" created above, including any required copying, memory management, and eventual deletion. Large data structures like meshes, matrices, and degree-of-freedom maps are

shallow-copied (original and copy refer to the same chunk of memory) rather than deep-copied (the copy occupies a portion of memory entirely separate from the original object). Reference counted "smart pointers" are used to keep track of the number of references to a given object so that the object is deleted only when there are no more references to it in the entire program.

- One goal in developing Sundance is to make parallelism as transparent as possible to the user. The only necessary differences between a serial code and a parallel one is the use of parallel linear algebra and a partitioned mesh.

- To solve *time-dependent* partial differential equations, the user writes the PDE in terms of the weak form for the spatial derivatives and the finite difference approximation to all time derivatives. The user is then responsible for coding a standard C++ loop structure to evolve the equations in time, while Sundance solves the spatial portion of the equation at each time step. Thus, it is up to the user to implement fixed or adaptive time-stepping and satisfy the stability condition on the ratio of time step to mesh width.

- The object-oriented nature of Sundance enables the user to generate a finite element *mesh* with any available meshing tool, with Sundance accessing the mesh information through the `MeshSource` interface. The default mesh reading capability within Sundance reads text-based NetCDF format; however, reading any other mesh format is as simple as the user writing a routine, derived from

the `MeshSourceBase` class, to do so.

- There is built-in functionality through the FieldWriter class for writing solutions to a file for easier *visualization*. Two default FieldWriters are VTKWriter which writes to a `*.vtu` file (visualized with any VTK viewer like Paraview) and MatlabWriter which writes to a Matlab `*.dat` file. Of course, a user can write other FieldWriter classes which extend from the FieldWriterBase class as needed.

Chapter 6

Conclusions

6.1 Two-Dimensional Finite Element Simulation

We have simulated regional groundwater flow through heterogeneous porous media using stabilization techniques implemented in the finite element simulation framework, Sundance. We have found that the practice of simplifying the momentum balance equation by excluding the advective acceleration term, $\mathbf{u} \cdot \nabla \mathbf{u}$, is valid for this type of flow regime. When compared to the magnitude of both the Darcy and Forchheimer terms over a range of Reynold's numbers ($\mathrm{Re} \in (0, \mathcal{O}(100))$), the magnitude of the advective acceleration term is much smaller.

Focusing on the stabilization strategy implemented in this work, we have applied the work of Burýšková on general adjoint operators to express the negative adjoint of the quadratic Forchheimer term. The negative adjoint is what sets the multiscale

stabilization method apart from other residual-based stabilization schemes, like GLS and SUPG.

6.2 Future Work: Three-Dimensional Finite Element Simulation

We will extend the two dimensional work shown in Chapter 4 to three spatial dimensions where flow through the domain is induced by a production well (see Figure 1.3). We hypothesize that vertical flow gradients which can only be identified in 3D will contribute to increasing the magnitude of the advective acceleration term. It remains to be seen if the contribution of the advective term will be increased enough for it to be significant to the simulation when compared to both the Darcy and Forchheimer terms.

A two-dimensional "Quarter Five Spot" simulation will provide the boundary conditions for the three-dimensional simulation. The 3D grid can be generated using CUBIT, a mesh generation tool developed at Sandia National Laboratories. This meshing tool was chosen because Sundance already includes an interface to CUBIT.

References

[1] Analytic & Computational Research, Inc., 1931 Stradella Rd., Bel Air, CA 90077. *PORFLOW: a software tool for multiphase fluid flow, heat and mass transport in fractured porous media*, March 2002. Version 5.0. `http://www.acricfd.com`.

[2] E. Anderson, Z. Bai, C. Bischof, S. Blackford, J. Demmel, J. Dongarra, J. Du Croz, A. Greenbaum, S. Hammarling, A. McKenney, and D. Sorensen. *LAPACK Users' Guide*. Society for Industrial and Applied Mathematics, Philadelphia, PA, third edition, 1999.

[3] George B. Arfken and Hans J. Weber. *Mathematical Methods for Physicists*. Elsevier Academic Press, Boston, sixth edition, 2005.

[4] S. F. Ashby, R. D. Falgout, S. G. Smith, and A. F. B. Tompson. Modeling groundwater flow on MPPs. Technical Report UCRL-JC-115602, Lawrence Livermore National Laboratory, 1993.

[5] Ivo Babuška and A. K. Aziz. Survey lectures on the mathematical foundations

of the finite element method. In *The Mathematical Foundations of the Finite Element Method with Applications to Partial Differential Equations (Proc. Sympos., Univ. Maryland, Baltimore, Md., 1972)*, pages 1–359. Academic Press, New York, 1972. With the collaboration of G. Fix and R. B. Kellogg.

[6] Ivo Babuška. Error-bounds for finite element method. *Numerische Mathematik*, 16(4):322–333, January 1971.

[7] Ivo Babuška. The finite element method with Lagrange multipliers. *Numerische Mathematik*, 20(3):179–192, June 1973.

[8] Satish Balay, Kris Buschelman, Victor Eijkhout, William D. Gropp, Dinesh Kaushik, Matthew G. Knepley, Lois Curfman McInnes, Barry F. Smith, and Hong Zhang. PETSc users manual. Technical Report ANL-95/11 - Revision 2.1.5, Argonne National Laboratory, 2004.

[9] Satish Balay, Kris Buschelman, William D. Gropp, Dinesh Kaushik, Matthew G. Knepley, Lois Curfman McInnes, Barry F. Smith, and Hong Zhang. PETSc Web page, 2001. http://www.mcs.anl.gov/petsc.

[10] Satish Balay, William D. Gropp, Lois Curfman McInnes, and Barry F. Smith. Efficient management of parallelism in object oriented numerical software libraries. In E. Arge, A. M. Bruaset, and H. P. Langtangen, editors, *Modern Software Tools in Scientific Computing*, pages 163–202. Birkhäuser Press, 1997.

[11] A.Z. Barak. High-velocity flow in porous media - Comments. *Transport in Porous Media*, 2(6):533–535, December 1987.

[12] R. A. Bartlett. TSFCore::Nonlin : Interfaces extending TSFCore for the development of nonlinear abstract numerical algorithms and interfacing to nonlinear applications. Technical Report SAND2003-1377, Sandia National Laboratories, 2003.

[13] R. A. Bartlett, D. M. Gay, and E. T. Phipps. Automatic differentiation of C++ codes for large-scale scientific computing. In *Computational Science - ICCS 2006*, volume 3994 of *Lecture Notes in Computer Science*, pages 525–532. Springer Berlin / Heidelberg, 2006.

[14] R. A. Bartlett, M. A. Heroux, and K. R. Long. TSFCore : A package of lightweight object-oriented abstractions for the development of abstract numerical algorithms and interfacing to linear algebra libraries and applications. Technical Report SAND2003-1378, Sandia National Laboratories, 2003.

[15] Roscoe A. Bartlett, Bart G. Van Bloemen Waanders, and Michael A. Heroux. Vector Reduction/Transformation Operators. *ACM Transactions on Mathematical Software (TOMS)*, 30(1):62–85, March 2004.

[16] Jacob Bear. *Dynamics of Fluids in Porous Media*. Dover Publications, Inc. , New York, 1972.

[17] Jacob Bear. *Hydraulics of Groundwater*. McGraw-Hill Book Co., New York, 1979.

[18] A. Ben-Tal and M. Teboulle. A smoothing technique for nondifferentiable optimization problems. In *Optimization (Varetz, 1988)*, volume 1405 of *Lecture Notes in Mathematics*, pages 1–11. Springer, Berlin, 1989.

[19] L. S. Bennethum and T. Giorgi. Generalized Forchheimer equation for two-phase flow based on hybrid mixture theory. *Transport in Porous Media*, 26:261–275, 1997.

[20] R. C. Berger and S. E. Howington. Discrete fluxes and mass balance in finite elements. *Journal of Hydraulic Engineering*, 128(1):87–92, January 2002.

[21] C. H. Bischof, A. Carle, P. Khademi, and A. Mauer. ADIFOR 2.0: Automatic differentiation of Fortran 77 programs. *IEEE Computational Science & Engineering*, 3(3):18–32, 1996.

[22] Christian H. Bischof, Paul D. Hovland, and Boyana Norris. Implementation of automatic differentiation tools. *ACM SIGPLAN Notices*, 37(3):98–107, March 2002.

[23] Pavel B. Bochev and Clark R. Dohrmann. A computational study of stabilized, low-order C^0 finite element approximations of Darcy equations. *Computational Mechanics*, 38:323–333, 2006.

[24] Pavel B. Bochev and R. B. Lehoucq. Regularization and stabilization of discrete saddle-point variational problems. *Electronic Transactions on Numerical Analysis*, 22:97–113, 2006.

[25] Franco Brezzi. On the existence, uniqueness, and approximation of saddle-point problems arising from Lagrange multipliers. *RAIRO Anal. Numer.*, 8:129–151, 1974.

[26] Franco Brezzi and Michel Fortin. *Mixed and Hybrid Finite Element Methods*. Number 15 in Springer Series in Computational Mathematics. Springer-Verlag, New York, 1991.

[27] Franco Brezzi and Jim Douglas, Jr. Stabilized mixed methods for the Stokes problem. *Numerische Mathematik*, 53:225–235, 1988.

[28] Alexander N. Brooks and Thomas J. R. Hughes. Streamline upwind/Petrov-Galerkin formulations for convection dominated flows with particular emphasis on the incompressible Navier-Stokes equations. *Comput. Methods Appl. Mech. Engrg.*, 32(1-3):199–259, 1982. FENOMECH '81, Part I (Stuttgart, 1981).

[29] Věra Burýšková. Definition und grundlegende Eigenschaften des nichtlinearen adjungierten Operators. *Časopis Pěst. Mat.*, 103(2):186–201, 203, 1978.

[30] Věra Burýšková. Some properties of nonlinear adjoint operators. *Rocky Mountain Journal of Mathematics*, 28(1):41–59, Spring 1998.

[31] Graham F. Carey. Some further properties of the superconvergent flux projection. *Communications in Numerical Methods in Engineering*, 18:241–250, 2002.

[32] Xin Chen, Houduo Qi, Liqun Qi, and Kok-Lay Teo. Smooth convex approximation to the maximum eigenvalue function. *Journal of Global Optimization*, 30:253–270, 2004.

[33] Vladimir D. Cvetković. A continuum approach to high-velocity flow in a porous-medium. *Transport in Porous Medium*, 1(1):63–97, 1986.

[34] Henry Darcy. *Les Fontaines Publiques de la Ville de Dijon*. Dalmont, Paris, 1856.

[35] Henry Darcy. Determination of the laws of flow of water through sand. In R. A. Freeze and W. Back, editors, *Physical Hydrogeology*, Benchmark papers in geology ; 72. Hutchinson Ross Pub. Co., 1983.

[36] Ghislain de Marsily. *Quantitative Hydrogeology*, page 102. Academic Press, Orlando, FL, 1986.

[37] Clayton V. Deutsch and André G. Journel. *GSLIB Geostatistical Software Library and User's Guide*. Applied Geostatistics Series. Oxford University Press, New York, second edition, 1998.

[38] Patrick A. Domenico and Franklin W. Schwartz. *Physical and Chemical Hydrogeology*. John Wiley and Sons, Inc., New York, NY, second edition, 1998.

[39] Jack J. Dongarra, James R. Bunch, Cleve B. Moler, and G.W. Stewart. *LINPACK Users' Guide*. SIAM, Philadelphia, PA, 1979.

[40] Fletcher G. Driscoll. *Groundwater and Wells*. Johnson Divison, St. Paul, MN, second edition, 1986.

[41] F. A. L. Dullien. Single phase flow through porous media and pore structure. *The Chemical Engineering Journal*, 10(1):1–34, 1975.

[42] A. J. E. J. Dupuit. *Études Théoriques et Pratiques sur le Mouvement des aux dans les Canaux Découvert et a Travers les Terrains Perméables*. Victor Dalmont, Paris, 1863.

[43] S. Ergun. Fluid flow through packed columns. *Chemical Engineering Progress*, 48(2):89–94, 1952.

[44] Merran Evans, Nicholas Hastings, and Brian Peacock. *Statistical Distributions*, chapter 25: Lognormal Distribution, pages 102–105. John Wiley & Sons, Inc., second edition, 1993.

[45] Mouaouia Firdaouss, Jean-Luc Guermond, and Patrick Le Quéré. Nonlinear corrections to Darcy's law at low Reynold's numbers. *Journal of Fluid Mechanics*, 343:331–350, 1997.

[46] P. Forchheimer. Wasserbewegun durch boden. *Z. Ver. Deutsch. Ingen.*, 45:1782–1788, 1901.

[47] M. Fourar, R. Lenormand, M. Karimi-Fard, and R. Horne. Inertia effects in high-rate flow through heterogeneous porous media. *Transport in Porous Media*, 60:353–370, 2005.

[48] M. Fourar, G. Radilla, R. Lenormand, and C.Moyne. On the non-linear behavior of a laminar single-phase flow through two and three-dimensional porous media. *Advances in Water Resources*, 27(6):669–677, 2004.

[49] L. P. Franca and T. J. R. Hughes. Convergence analysis of Galerkin least squares methods for the symmetric advective-diffusive form of the Stokes and incompresible Navier-Stokes equations. *Computer Methods in Applied Mechanics and Engineering*, 2:285–298, 1993.

[50] Leopoldo P. Franca, Sergio L. Frey, and Thomas J. R. Hughes. Stabilized finite element methods: I. Application to the advective-diffusion model. *Computer Methods in Applied Mechanics and Engineering*, 95:253–276, 1992.

[51] Leopoldo P Franca, Thomas J. R. Hughes, and Rolf Stenberg. *Incompressible Computational Fluid Dynamics: Trends and Advances*, chapter Stabilized Finite Element Methods, pages 87–107. Cambridge University Press, 1993.

[52] GNU. Autoconf home page, `http://www.gnu.org/software/autoconf/`, September 25, 2006.

[53] GNU. Automake home page, `http://www.gnu.org/software/automake/`, September 25, 2006.

[54] M. S. Gockenbach and W. W. Symes. Hilbert Class Library: A library of abstract C++ classes for optimization and inversion. *Computers & Mathematics with Applications*, 32(6):1–13, September 1996.

[55] Mark S. Gockenbach, Matthew J. Petro, and William W. Symes. C++ classes for linking optimization with complex simulations. *ACM Transactions on Mathematical Software*, 25(2):191–212, June 1999.

[56] W. G. Gray and C. T. Miller. Examination of Darcy's law for flow in porous media with variable porosity. *Environmental Science & Technology*, 38(22):5895–5901, 2004.

[57] William G. Gray. On the definition and derivatives of macroscale energy for the description of multiphase systems. *Advances in Water Resources*, 25(8-12):1091–1104, August 2002.

[58] William G. Gray. Personal communication, December 2004.

[59] William G. Gray and Cass T. Miller. Multiphase transport phenomena. Department of Environmental Sciences and Engineering, University of North Carolina, unpublished lecture notes for ENVR265, 2003.

[60] William G. Gray and Cass T. Miller. Thermodynamically Constrained Aver-

aging Theory approach for modeling flow and transport phenomena in porous medium systems: 1. Motivation and overview. *Advances in Water Resources*, 28:161–180, 2005.

[61] William G. Gray and Cass T. Miller. Thermodynamically Constrained Averaging Theory approach for modeling flow and transport phenomena in porous medium systems: 2. Foundation. *Advances in Water Resources*, 28:181–202, 2005.

[62] William G. Gray, Andrew F. B Tompson, and Wendy E. Soll. Closure conditions for two-fluid flow in porous media. *Transport in Porous Media*, 47(1):29–65, April 2002.

[63] Max D. Gunzburger. *Finite Element Methods for Viscous Incompressible Flows: A Guide to Theory, Practice, and Algorithms*. Computer Science and Scientific Computing. Academic Press, Inc., Boston, 1989.

[64] A. W. Harbaugh, E. R. Banta, M. C. Hill, and M. G. McDonald. *MODFLOW-2000, the U.S. Geological Survey modular ground-water model – User guide to modularization concepts and the Ground-Water Flow Process*. U. S. Geological Survey, 2000. Open-File Report 00-92.

[65] A.W. Harbaugh and M.G. McDonald. User's documentation for modflow-96, an update to the u.s. geological survey modular finite-difference ground-water flow model. Open-File Report OFR 96-485, U.S. Geological Survey, 1996.

[66] S. M. Hassanizadeh and W. G. Gray. High velocity flow in porous media. *Transport in Porous Media*, 2(6):521–531, 1987.

[67] S. M. Hassanizadeh and W. G. Gray. High-velocity flow in porous-media by Hassanizadeh and Gray - Reply. *Transport in Porous Media*, 3:319–321, 1988.

[68] S. M. Hassanizadeh and W. G. Gray. *Bioremediation: Principles and Practice*, volume 1 (Fundamentals and Applications), chapter Basic Equations of Flow and Transport in Porous Media, pages 19–57. Technomic Publishing Company, Inc., 1998.

[69] Michael Heroux, Roscoe Bartlett, Vicki Howle Robert Hoekstra, Jonathan Hu, Tamara Kolda, Richard Lehoucq, Kevin Long, Roger Pawlowski, Eric Phipps, Andrew Salinger, Heidi Thornquist, Ray Tuminaro, James Willenbring, and Alan Williams. An Overview of Trilinos. Technical Report SAND2003-2927, Sandia National Laboratories, 2003.

[70] Michael A. Heroux and James M. Willenbring. Trilinos users guide. SAND REPORT SAND2003-2952, Sandia National Laboratories, August 2003.

[71] Michael A. Heroux and James M. Willenbring. Trilinos Users Guide. Technical Report SAND2003-2952, Sandia National Laboratories, 2003.

[72] P. Hovland, C. Bischof, D. Spiegelman, and M. Casella. Efficient derivative codes through automatic differentiation and interface contraction: An applica-

tion in biostatistics. *SIAM Journal on Scientific Computing*, 18(4):1056–1066, July 1997.

[73] Thomas J. R. Hughes. Multiscale phenomena: Green's functions, the Dirichlet-to-Neumann formulation, subgrid scale models, bubbles and the origins of stabilized methods. *Computer Methods in Applied Mechanics and Engineering*, 127:387–401, 1995.

[74] Thomas J. R. Hughes, Gerald Engel, Luca Mazzei, and Mats G. Larson. The continuous Galerkin method is locally conservative. *Journal of Computational Physics*, 163(2):467–488, September 2000.

[75] Thomas J. R. Hughes, Leopoldo P. Franca, and Marc Balestra. A new finite element formulation for computational fluid dynamics: V. Circumventing the Babuška-Brezzi condition: A stable Petrov-Galerkin formulation of the Stokes problem accommodating equal-order interpolations. *Computer Methods in Applied Mechanics and Engineering*, 59:85–99, 1986.

[76] Thomas J. R. Hughes, Leopoldo P. Franca, and Gregory M. Hulbert. A new finite element formulation for computational fluid dynamics: VIII. The Galerkin/Least-squares method for advective-diffusive equations. *Computer Methods in Applied Mechanics and Engineering*, 73:173–189, 1989.

[77] Thomas J. R. Hughes, Michel Mallet, and Akira Mizukami. A new finite element

formulation for computational fluid dynamics: II. Beyond SUPG. *Computer Methods in Applied Mechanics and Engineering*, 54:341–355, 1986.

[78] Thomas J. R. Hughes and Garth N. Wells. Conservation properties for the Galerkin and stabilised forms of the advection-diffusion and incompressible Navier-Stokes equations. *Computer Methods in Applied Mechanics and Engineering*, 194(9-11):1141–1159, March 2005.

[79] Claes Johnson. *Numerical Solution of partial differential equations by the finite element method*. Cambridge University Press, New York, 1987.

[80] M.-Y. Kim and E.-J. Park. Fully discrete mixed finite element approximations for non-Darcy flows in porous media. *Computers and Mathematics with Applications*, 38:113–129, 1999.

[81] Becky Koch. Email communication on 09.11.06, September 2006. "North Dakota State University grants permission to Jill Paula Reese to use the irrigation well graphic for the educational, non-commercial purpose in her thesis as described. Please credit NDSU, the publication [108] and the author as appropriate.".

[82] B. W. Kort and D. P. Bertsekas. A new penalty function algorithm for constrained minimization. In *Proceedings of the 1972 IEEE Conference on Decision and Control*, New Orleans, LA, 1972.

[83] O. Ladyzhenskaya, editor. *The Mathematical Theory of Viscous Incompressible Flow*, volume 2 of *Mathematics and Its Applications*. Gordon and Breach, New York, second edition, 1969.

[84] J. L. Lage and B. V. Antohe. Darcy's experiments and the deviation to nonlinear flow regime. *Journal of Fluids Engineering*, 122:619–625, September 2000.

[85] Kevin Long. Solving partial differential equations with Sundance, 2004.

[86] Kevin Long. Sundance 2.0 tutorial. Unlimited Release SAND2004-4793, Sandia National Laboratories, July 2004.

[87] Kevin Long, Roscoe A. Bartlett, Paul T. Boggs, Michael A. Heroux, Victoria E. Howle, and Jill P. Reese. TSFExtended user's guide. Technical report, Sandia National Laboratories, 2004. In preparation.

[88] I. F. Macdonald, M. S. El-Sayed, K. Mow, and F. A. L. Dullien. Flow through porous media - the Ergun equation revisited. *Industrial Engineering and Chemistry Fundamentals*, 18(3):199–208, 1979.

[89] Arif Masud and Thomas J. R. Hughes. A stabilized mixed finite element method for Darcy flow. *Computer Methods in Applied Mechanics and Engineering*, 191:4341–4370, 2002.

[90] C. C. Mei and J. L. Auriault. The effect of weak inertia on flow through a porous-medium. *Journal of Fluid Mechanics*, 222:647–663, 1991.

[91] Cass T. Miller. Groundwater hydrology. Department of Environmental Sciences and Engineering, University of North Carolina, unpublished lecture notes for ENVR153, 2002.

[92] Ralph Morelli. *Java, Java, Java: Object-Oriented Problem Solving*. Prentice Hall, Upper Saddle River, NJ, 2000.

[93] M. Muskat. *The Flow of Homogeneous Fluids Through Porous Media*. J. W. Edwards, Inc., 1946.

[94] J. C. Nédélec. Mixed finite elements in $\mathbb{R}^3$. *Numerische Mathematik*, 35:315–341, 1980.

[95] Chongxun Pan, Markus Hilpert, and Cass T. Miller. Pore-scale modeling of saturated permeabilities in random sphere packings. *Physcial Review E*, 64(6):1–9, December 2001.

[96] Chongxun Pan, James E. McClure, William G. Gray, and Cass T. Miller. Lattice Boltzmann simulation of non-Darcy flow. In Philip J. Binning, Peter K. Engesgaard, Helge K. Dahle, George F. Pinder, and William G. Gray, editors, *Proceedings of the XVI International Conference on Computational Methods in Water Resources*, Copenhagen, Denmark, June 2006.

[97] M. Panfilov and M. Fourar. Physical splitting of nonlinear effects in high-velocity stable flow through porous media. *Advances in Water Resources*, 29:30–41, 2006.

[98] Eun-Jae Park. Mixed finite element methods for generalized Forchheimer flow in porous media. *Numerical Methods for Partial Differential Equations*, 21(2):213–228, March 2005.

[99] Dimos Poulikakos and Adrian Bejan. The departure from Darcy flow in natural convection in a vertical porous layer. *Physics of Fluids*, 28(12):3477–3484, December 1985.

[100] P.-A. Raviart and J.-M. Thomas. *A mixed finite element method for second order elliptic problems*, volume 606 of *Lecture Notes in Mathematics*, pages 292–315. Springer-Verlag, Berlin, 1977.

[101] P.-A. Raviart and J.-M. Thomas. Primal hybrid finite element methods for second order elliptic equations. *Mathematics of Computation*, 31(138):391–413, 1977.

[102] J. E. Roberts and J.-M. Thomas. *Handbook of Numerical Analysis*, volume II: Finite Element Methods (Part I), chapter Mixed and Hybrid Methods, pages 523–640. Elsevier Science Publishers B. V., Amsterdam, The Netherlands, 1991. Edited by P. G. Ciarlet and J. L. Lions.

[103] S. Rojas and J. Koplik. Nonlinear flow in porous media. *Physical Review E*, 58(4):4776–4782, October 1998.

[104] D.W. Ruth and H. Ma. On the derivation of the Forchheimer equation by means of the averaging theorem. *Transport in Porous Media*, 7(3):255–264, 1992.

[105] D.W. Ruth and H. Ma. The microscopic analysis of high Forchheimer number flow in porous-media. *Transport in Porous Media*, 13(2):139–160, November 1993.

[106] Marzio Sala, Michael A. Heroux, and David Day. Trilinos 4.0 tutorial. SAND REPORT SAND2004-2189, Sandia National Laboratories, May 2004.

[107] Adrian E. Scheidegger. *The Physics of Flow Through Porous Media*. The Macmillan Company, New York, 1960.

[108] Tom Scherer. Care and maintenance of irrigation wells. Technical Report AE-97 (Revised), NDSU Extension Service, North Dakota State University, Fargo, North Dakota 58105, July 2005.

[109] Erik Skjetne and Jean-Louis Auriault. New insights on steady, non-linear flow in porous media. *European Journal of Mechanics (B: Fluids)*, 18(1):131–145, 1999.

[110] Charles A. Taylor, Thomas J. R. Hughes, and Christopher K. Zarins. Finite element modeling of blood flow in arteries. *Computer Methods in Applied Mechanics and Engineering*, 158:155–196, 1998.

[111] J.-M. Thomas. *Sur l'analyse numérique des méthodes d'eléments finis hybrides et mixtes*. Thèse d'Etat, Université Pierre et Marie Curie, Paris, 1977.

[112] E. Tijskens, D. Roose, H. Ramon, and J. De Baerdemaeker. Automatic differen-

tiation for solving nonlinear partial differential equations: an efficient operator overloading approach. *Numerical Algorithms*, 30:259–301, 2002.

[113] X. Wang, F. Thauvin, and K. K. Mohanty. Non-Darcy flow through anisotropic porous media. *Chemical Engineering Science*, 54:1859–1869, 1999.

[114] Y. S. Wu. Numerical simulation of single-phase and multiphase non-Darcy flow in porous and fractured reservoirs. *Transport in Porous Media*, 49(2):209–240, 2002.

Appendices

Appendix A

Deriving Linear and Nonlinear Adjoints for the Generalized Galerkin Stabilization Method

Recall the generalized Galerkin stabilization method from equation (3.13) in the discussion of stabilization strategies from Section 3.3.3.

$$\left(\widetilde{\mathbf{w}}^{\Delta}, \mathcal{L}\widetilde{\mathbf{u}}^{\Delta}\right)_{\Omega} + \sum_{e=0}^{ne-1} \left(\mathbb{L}\widetilde{\mathbf{w}}^{\Delta}, \tau\left(\mathcal{L}\widetilde{\mathbf{u}}^{\Delta} - \widetilde{f}\right)\right)_{\Omega_e} = \left(\widetilde{\mathbf{w}}^{\Delta}, \widetilde{f}\right)_{\Omega},$$

The expression for $\mathbb{L}$ depends upon the specific implementation of stabilization in the following way (again, see Section 3.3.3 for details).

$$\mathbb{L} \equiv \begin{cases} +\mathcal{L} & \text{Galerkin/least-squares (GLS)} \\ +\mathcal{L}_{\text{adv}} & \text{Streamline-Upwind Petrov-Galerkin (SUPG)} \\ -\mathcal{L}^{\dagger} & \text{Multiscale (MS)} \end{cases}$$

The multiscale version of $\mathbb{L}$ is used to stabilize the Darcy and Forchheimer terms from the non-Darcy flow equations (3.4) as shown in Section 3.4. This appendix provides the derivation of the adjoint for both the linear Darcy and quadratic Forchheimer terms.

A.1 Linear Adjoint Operator

According to [3, Page 622],the adjoint operator of a linear, second-order ordinary differential operator of the form

$$\mathcal{L}a\left(x\right) = b_0\left(x\right)\frac{\mathrm{d}^2 a\left(x\right)}{\mathrm{d}x^2} + b_1\left(x\right)\frac{\mathrm{d}a\left(x\right)}{\mathrm{d}x} + b_2\left(x\right)a\left(x\right), \tag{A.1}$$

is given by

$$\mathcal{L}^{\dagger}a\left(x\right) = b_0\left(x\right)\frac{\mathrm{d}^2 a\left(x\right)}{\mathrm{d}x^2} + \left(2\frac{\mathrm{d}b_0\left(x\right)}{\mathrm{d}x} - b_1\left(x\right)\right)\frac{\mathrm{d}a\left(x\right)}{\mathrm{d}x} + \left(\frac{\mathrm{d}^2 b_0\left(x\right)}{\mathrm{d}x^2} - \frac{\mathrm{d}b_1\left(x\right)}{\mathrm{d}x} + b_2\left(x\right)\right)a\left(x\right). \tag{A.2}$$

To find the adjoint of the linear Darcy portion of the non-Darcy momentum equation shown in (3.4b) (i.e. the momentum equation from the Darcy problem, shown in equation 3.9b), this one-dimensional example is extended to higher spatial dimensions in the following way. As in previous sections, $\widetilde{\mathbf{w}}^{\Delta} = \left[\mathbf{w}^{\Delta}, q^{\Delta}\right]$.

$$\begin{aligned} \mathcal{L}^{\dagger}\widetilde{\mathbf{w}}^{\Delta} &= \left[\mathcal{L}\mathbf{w}^{\Delta}\right]^{\dagger} + \left[\mathcal{L}q^{\Delta}\right]^{\dagger} \\ &= \left[\frac{\mu}{k}\mathbf{w}^{\Delta}\right]^{\dagger} + \left[\nabla q^{\Delta}\right]^{\dagger} \\ &= \frac{\mu}{k}\mathbf{w}^{\Delta} - \nabla q^{\Delta} \end{aligned} \tag{A.3}$$

The negative of this expression is shown by Masud and Hughes in [89, Page 4345] to be the multiscale differential operator required in the residual-based stabilization of the Darcy equations (shown in equations (3.9)).

The extension of the above ideas to a nonlinear adjoint operator is necessary stabilize the nonlinear Forchheimer term, $\beta\rho\|\mathbf{u}\|_2\mathbf{u}$, in the non-Darcy flow model. The work of Burýšková provides a formula for computing the nonlinear adjoint, provided some initial conditions are satisfied [30].

A.2 Definition of the Nonlinear Adjoint Operator

In [30], Burýšková discusses the adjoint, $F^{\dagger}$, of a general operator, F. The operator F associates an element of a Banach space with an element of the respective dual space. The details required to treat adjoint operators in the full generality neces-

sary to achieve results over arbitrary Banach spaces are left to the given reference. They are not necessary to determine the adjoint of the nonlinear operator associated with Forchheimer portion of the nonlinear non-Darcy flow model in three spatial dimensions, namely

$$F\left(\widetilde{\mathbf{u}}\right) = \begin{bmatrix} \nabla p + \frac{\mu}{k_f}\mathbf{u} + \beta\rho\mathbf{u}\|\mathbf{u}\|_2 \\ -\nabla\cdot\mathbf{u} \end{bmatrix}. \tag{A.4}$$

Furthermore, the stabilization of the Forchheimer portion of the model is determined separately from the stabilization for the advective acceleration term. For this reason, the advective acceleration terms can be left out of equation (A.4) with no ill effects.

From [30, Definition 1.6], in order for the adjoint operator $F^{\dagger}\left(\widetilde{\mathbf{u}}\right)$ to exist for the given operator $F\left(\widetilde{\mathbf{u}}\right)$, it must be true that

1. $F(0) = 0$, and
2. the directional derivative of $F\left(\widetilde{\mathbf{u}}\right)$ evaluated at $\mathbb{T}\widetilde{\mathbf{u}}$ ($\mathbb{T} \in [0,1]$) is integrable for arbitrary (but fixed) $\widetilde{\mathbf{u}}$ in any direction.

Assuming that the velocity vector $\mathbf{u}$ is bounded away from zero over the entire domain Ω, the operator defined in equation (A.4) has an adjoint operator which is defined by

$$F^{\dagger}\left(\bar{x}\right) = \int_0^1 \left[F'\left(\mathbb{T}x\right)\right]^{\dagger}\left(\bar{x}\right)\,\mathrm{d}\mathbb{T}, \tag{A.5}$$

where F' is the standard Jacobian of the nonlinear operator ($F'_{i,j} = \frac{\partial F_i}{\partial x_j}$). The assumption that the velocity is nonzero over the entire domain is valid for the groundwater

flow application at hand.

Table A.1: Multiscale Residual-Based Stabilization. The linear problem is given by $\mathcal{L}\widetilde{\mathbf{u}} = \widetilde{f}$, while the nonlinear problem is specified by $F(\widetilde{\mathbf{u}}) = 0$.

Multiscale Linear Stabilization Term
$\sum_{e=0}^{ne-1} \left(-\mathcal{L}^{\dagger}\widetilde{\mathbf{w}}^{\Delta}, \tau_e \left(\mathcal{L}\widetilde{\mathbf{u}}^{\Delta} - \widetilde{f} \right) \right)_{\Omega_e}$
Multiscale Nonlinear Stabilization Term
$\sum_{e=0}^{ne-1} \left(-F^{\dagger}(\widetilde{\mathbf{w}}), \tau_e F\left(\widetilde{\mathbf{u}}^{\Delta} \right) \right)_{\Omega_e}$

Now the adjoint formula from equation (A.5) can be put in the context of the finite element discretization with unknowns $\widetilde{\mathbf{u}}$ and test functions $\widetilde{\mathbf{w}}$. The linear stabilization term was reiterated at the beginning of this appendix as

$$\sum_{e=0}^{ne-1} \left(\mathbb{L}\widetilde{\mathbf{w}}^{\Delta}, \tau \left(\mathcal{L}\widetilde{\mathbf{u}}^{\Delta} - \widetilde{f} \right) \right)_{\Omega_e},$$

where the linear differential operator, $\mathbb{L}$, acting on the test functions is equal to $-\mathcal{L}^{\dagger}\widetilde{\mathbf{w}}^{\Delta}$ in the linear multiscale case. In the nonlinear case, $\mathbb{L}\widetilde{\mathbf{w}}^{\Delta} = -F^{\dagger}(\widetilde{\mathbf{w}})$, as shown in Table A.1. Note that the nonlinear adjoint formula

$$F^{\dagger}(\widetilde{\mathbf{w}}) = \int_0^1 \left[F'(\mathbb{T}\widetilde{\mathbf{u}}) \right]^{\dagger}(\widetilde{\mathbf{w}}) \, \mathrm{d}\mathbb{T},$$

approximates the directional derivative of $F(\widetilde{\mathbf{u}})$ in the direction of the test functions.

A.3 Computing the Adjoint Operator of $\beta\rho\|\mathbf{u}\|_2\mathbf{u}$

Consider the three-dimensional steady-state model equations shown in (3.4) written component-wise. If contributions from advective acceleration are ignored, then

$$F\left(\widetilde{\mathbf{u}}\right) = \begin{bmatrix} \nabla p + \frac{\mu}{k_f}\mathbf{u} + \beta\rho\mathbf{u}\|\mathbf{u}\|_2 \\ -\nabla\cdot\mathbf{u} \end{bmatrix}.$$

Assuming the variable order to be $\widetilde{\mathbf{u}} = [\mathbf{u}, p]^T$ and assuming that density is constant, the Jacobian of the nonlinear operator is

$$F'\left(\widetilde{\mathbf{u}}\right) = \begin{bmatrix} \frac{\mu}{k_f} + \beta\rho\|\mathbf{u}\|_2 + \frac{\beta\rho u_1^2}{\|\mathbf{u}\|_2} & \frac{\beta\rho u_1 u_2}{\|\mathbf{u}\|_2} & \frac{\beta\rho u_1 u_3}{\|\mathbf{u}\|_2} & \frac{\partial}{\partial x} \\ \frac{\beta\rho u_1 u_2}{\|\mathbf{u}\|_2} & \frac{\mu}{k_f} + \beta\rho\|\mathbf{u}\|_2 + \frac{\beta\rho u_2^2}{\|\mathbf{u}\|_2} & \frac{\beta\rho u_2 u_3}{\|\mathbf{u}\|_2} & \frac{\partial}{\partial y} \\ \frac{\beta\rho u_1 u_3}{\|\mathbf{u}\|_2} & \frac{\beta\rho u_2 u_3}{\|\mathbf{u}\|_2} & \frac{\mu}{k_f} + \beta\rho\|\mathbf{u}\|_2 + \frac{\beta\rho u_3^2}{\|\mathbf{u}\|_2} & \frac{\partial}{\partial z} \\ & -\nabla\cdot & & 0 \end{bmatrix}.$$

$$
\begin{aligned}
F^{\dagger}\left(\widetilde{\mathbf{w}}\right) &= \int_{\mathbb{T}=0}^{\mathbb{T}=1} \left[F'\left(\mathbb{T}\widetilde{\mathbf{u}}\right)\right]^{\dagger} \begin{bmatrix} \mathbf{w} \\ q \end{bmatrix} \, \mathrm{d}\mathbb{T} \\
&= \int_{\mathbb{T}=0}^{\mathbb{T}=1} \begin{bmatrix}
\frac{\mu}{k_f} + \mathbb{T}\beta\rho\|\mathbf{u}\|_2 + \frac{\mathbb{T}\beta\rho u_1^2}{\|\mathbf{u}\|_2} & \frac{\mathbb{T}\beta\rho u_1 u_2}{\|\mathbf{u}\|_2} & \frac{\mathbb{T}\beta\rho u_1 u_3}{\|\mathbf{u}\|_2} & -\frac{\partial}{\partial x} \\
\frac{\mathbb{T}\beta\rho u_1 u_2}{\|\mathbf{u}\|_2} & \frac{\mu}{k_f} + \mathbb{T}\beta\rho\|\mathbf{u}\|_2 + \frac{\mathbb{T}\beta\rho u_2^2}{\|\mathbf{u}\|_2} & \frac{\mathbb{T}\beta\rho u_2 u_3}{\|\mathbf{u}\|_2} & -\frac{\partial}{\partial y} \\
\frac{\mathbb{T}\beta\rho u_1 u_3}{\|\mathbf{u}\|_2} & \frac{\mathbb{T}\beta\rho u_2 u_3}{\|\mathbf{u}\|_2} & \frac{\mu}{k_f} + \mathbb{T}\beta\rho\|\mathbf{u}\|_2 + \frac{\mathbb{T}\beta\rho u_3^2}{\|\mathbf{u}\|_2} & -\frac{\partial}{\partial z} \\
\nabla\cdot & & & 0
\end{bmatrix} \begin{bmatrix} w_1 \\ w_2 \\ w_3 \\ q \end{bmatrix} \mathrm{d}\mathbb{T} \\
&= \int_{\mathbb{T}=0}^{\mathbb{T}=1} \begin{bmatrix}
\frac{\mu w_1}{k_f} + \mathbb{T}\beta\rho w_1\|\mathbf{u}\|_2 + \frac{\mathbb{T}\beta\rho u_1^2 w_1}{\|\mathbf{u}\|_2} + \frac{\mathbb{T}\beta\rho u_1 u_2 w_2}{\|\mathbf{u}\|_2} + \frac{\mathbb{T}\beta\rho u_1 u_3 w_3}{\|\mathbf{u}\|_2} - \frac{\partial q}{\partial x} \\
\frac{\mu w_2}{k_f} + \mathbb{T}\beta\rho w_2\|\mathbf{u}\|_2 + \frac{\mathbb{T}\beta\rho u_2^2 w_2}{\|\mathbf{u}\|_2} + \frac{\mathbb{T}\beta\rho u_1 u_2 w_1}{\|\mathbf{u}\|_2} + \frac{\mathbb{T}\beta\rho u_2 u_3 w_3}{\|\mathbf{u}\|_2} - \frac{\partial q}{\partial y} \\
\frac{\mu w_3}{k_f} + \mathbb{T}\beta\rho w_3\|\mathbf{u}\|_2 + \frac{\mathbb{T}\beta\rho u_3^2 w_3}{\|\mathbf{u}\|_2} + \frac{\mathbb{T}\beta\rho u_1 u_3 w_1}{\|\mathbf{u}\|_2} + \frac{\mathbb{T}\beta\rho u_2 u_3 w_2}{\|\mathbf{u}\|_2} - \frac{\partial q}{\partial z} \\
\nabla\cdot\mathbf{w}
\end{bmatrix} \mathrm{d}\mathbb{T} \\
&= \left[\begin{array}{c}
\mathbb{T}\frac{\mu w_1}{k_f} + \frac{\mathbb{T}^2}{2}\beta\rho w_1\|\mathbf{u}\|_2 + \frac{\mathbb{T}^2\beta\rho u_1^2 w_1}{2\|\mathbf{u}\|_2} + \frac{\mathbb{T}^2\beta\rho u_1 u_2 w_2}{2\|\mathbf{u}\|_2} + \frac{\mathbb{T}^2\beta\rho u_1 u_3 w_3}{2\|\mathbf{u}\|_2} - \mathbb{T}\frac{\partial q}{\partial x} \\
\frac{\mathbb{T}\mu w_2}{k_f} + \frac{\mathbb{T}^2}{2}\beta\rho w_2\|\mathbf{u}\|_2 + \frac{\mathbb{T}^2\beta\rho u_2^2 w_2}{2\|\mathbf{u}\|_2} + \frac{\mathbb{T}^2\beta\rho u_1 u_2 w_1}{2\|\mathbf{u}\|_2} + \frac{\mathbb{T}^2\beta\rho u_2 u_3 w_3}{2\|\mathbf{u}\|_2} - \mathbb{T}\frac{\partial q}{\partial y} \\
\frac{\mathbb{T}\mu w_3}{k_f} + \frac{\mathbb{T}^2}{2}\beta\rho w_3\|\mathbf{u}\|_2 + \frac{\mathbb{T}^2\beta\rho u_3^2 w_3}{2\|\mathbf{u}\|_2} + \frac{\mathbb{T}^2\beta\rho u_1 u_3 w_1}{2\|\mathbf{u}\|_2} + \frac{\mathbb{T}^2\beta\rho u_2 u_3 w_2}{2\|\mathbf{u}\|_2} - \mathbb{T}\frac{\partial q}{\partial z} \\
\mathbb{T}\nabla\cdot\mathbf{w}
\end{array}\right]_{\mathbb{T}=0}^{\mathbb{T}=1} \\
&= \begin{bmatrix}
\frac{\mu w_1}{k_f} + \frac{1}{2}\beta\rho w_1\|\mathbf{u}\|_2 + \frac{\beta\rho u_1^2 w_1}{2\|\mathbf{u}\|_2} + \frac{\beta\rho u_1 u_2 w_2}{2\|\mathbf{u}\|_2} + \frac{\beta\rho u_1 u_3 w_3}{2\|\mathbf{u}\|_2} - \frac{\partial q}{\partial x} \\
\frac{\mu w_2}{k_f} + \frac{1}{2}\beta\rho w_2\|\mathbf{u}\|_2 + \frac{\beta\rho u_2^2 w_2}{2\|\mathbf{u}\|_2} + \frac{\beta\rho u_1 u_2 w_1}{2\|\mathbf{u}\|_2} + \frac{\beta\rho u_2 u_3 w_3}{2\|\mathbf{u}\|_2} - \frac{\partial q}{\partial y} \\
\frac{\mu w_3}{k_f} + \frac{1}{2}\beta\rho w_3\|\mathbf{u}\|_2 + \frac{\beta\rho u_3^2 w_3}{2\|\mathbf{u}\|_2} + \frac{\beta\rho u_1 u_3 w_1}{2\|\mathbf{u}\|_2} + \frac{\beta\rho u_2 u_3 w_2}{2\|\mathbf{u}\|_2} - \frac{\partial q}{\partial z} \\
\nabla\cdot\mathbf{w}
\end{bmatrix} \\
&= \begin{bmatrix}
-\nabla q + \frac{\mu\mathbf{w}}{k_f} + \frac{1}{2}\beta\rho\|\mathbf{u}\|_2\mathbf{w} + \frac{1}{2}\frac{\beta\rho\mathbf{w}\cdot\mathbf{u}}{\|\mathbf{u}\|_2}\mathbf{u} \\
\nabla\cdot\mathbf{w}
\end{bmatrix}
\end{aligned} \tag{A.6}
$$

A.4 Choosing the Stabilization Parameter τ

Equation (A.6) provides $-\mathbb{L}\widetilde{\mathbf{w}}$ which is required to stabilize the non-Darcy model. The stabilization for the Darcy and Forchheimer terms takes the form

$$\sum_{e=0}^{ne-1} \left(\mathbb{L}\widetilde{\mathbf{w}}^{\Delta}, \tau \mathbf{r}^{\Delta} \right)_{\Omega_e} =$$
$$\sum_{e=0}^{ne-1} \left(\left(-\tfrac{\mu}{k_f}\mathbf{w}^{\Delta} + \nabla q^{\Delta} - \tfrac{1}{2}\beta\rho\|\mathbf{u}^{\Delta}\|_2 \mathbf{w}^{\Delta} - \tfrac{1}{2}\tfrac{\beta\rho \mathbf{w}^{\Delta}\cdot\mathbf{u}^{\Delta}}{\|\mathbf{u}^{\Delta}\|_2}\mathbf{u}^{\Delta} \right), \tau \mathbf{r}^{\Delta} \right)_{\Omega_e},$$

where $\mathbf{r}^{\Delta}$ is defined in equation (3.10).

It remains to specify the stabilization parameter, τ. For the Darcy equations, Masud and Hughes show that $\tau = \frac{k}{2\mu}$, and they also illustrate how τ changes for a different model. As an example, they consider the Brinkman model [89, Pages 4345 and 4348].

$$\frac{\mu}{k}\mathbf{u} + \nabla p = \mu\Delta\mathbf{u} \tag{A.7a}$$

$$\nabla \cdot \mathbf{u} = 0 \tag{A.7b}$$

A.4.1 Example: Brinkman Model

For the linear Brinkman model, the differential operator $\mathbb{L}\mathbf{w}^{\Delta} = -\frac{\mu}{k}\mathbf{w}^{\Delta} + \nabla q^{\Delta} + \mu\Delta\mathbf{w}^{\Delta}$, and the stabilization parameter becomes element dependent ($\tau = \tau_e$). Thus

the stabilization term becomes

$$\sum_{e=0}^{ne-1}\left(\mathbb{L}\widetilde{\mathbf{w}}^{\Delta},\tau\mathbf{r}^{\Delta}\right)_{\Omega_e}=\sum_{e=0}^{ne-1}\left(\left(-\frac{\mu}{k_f}\mathbf{w}^{\Delta}+\nabla q^{\Delta}+\mu\Delta\mathbf{w}^{\Delta}\right),\tau_e\left(\frac{\mu}{k}\mathbf{u}^{\Delta}+\nabla p^{\Delta}-\mu\Delta\mathbf{u}^{\Delta}\right)\right)_{\Omega_e}, \tag{A.8}$$

where

$$\tau_e=\min_{x\in\Omega_e}\left\{\frac{\gamma\Delta_e^2}{2\mu\left(x\right)},\frac{k\left(x\right)}{2\mu\left(x\right)}\right\}. \tag{A.9}$$

The non-dimensional constant γ depends upon the element type. One can see that the pattern is to choose τ_e by looking at the reciprocal of the coefficient of each velocity term and setting the parameter to be one-half of the minimum value over each element. The grid spacing, Δ_e, is included to balance any derivative terms; thus, the term $\frac{\gamma\Delta_e^2}{\mu(x)}$ can be viewed as the reciprocal of the coefficient of a finite difference approximation to the second derivative, $\mu\Delta\mathbf{u}^{\Delta}$.

A.4.2 The Darcy/Forchheimer Stabilization Parameter

Consider the coefficients of the Darcy and Forchheimer terms in the non-Darcy flow model (3.4), namely $\frac{\mu}{k_f}$ and $\beta\|\mathbf{u}\|_2$, respectively. Following the Brinkman example developed in Section A.4.1, the appropriate stabilization parameter for the non-Darcy model is

$$\tau_e=\min_{x\in\Omega_e}\left\{\frac{\gamma k_f\left(x\right)}{\mu},\frac{\gamma}{\beta\|\mathbf{u}\left(x\right)\|_2}\right\}. \tag{A.10}$$

One can see that in the Darcy regime where the velocities are assumed to be small in magnitude, $\tau_e=\frac{\gamma k_f(x)}{\mu(x)}$ and the Darcy stabilization has been recovered. On the

other hand, outside the Darcy regime the magnitude of the velocities increase, the Forchheimer term will impact the non-Darcy model, and there will be regions in the domain where

$$\frac{1}{\beta \|\mathbf{u}(x)\|_2} << \frac{k_f(x)}{\mu}.$$

A.5 Approximating τ in Sundance

While the formula for the non-Darcy stabilization parameter shown in equation (A.10) is correct for the problem at hand, it is not computationally feasible within the current Sundance framework. While both $\frac{\gamma k_f(x)}{\mu}$ and $\frac{\gamma}{\beta\|\mathbf{u}(x)\|_2}$ can be computed at each point in the computational domain, Sundance does not have the functionality to determine the minimum of the two functions over each element.

To avoid this limitation, the stabilization parameter τ_e will be replaced by $\tau_\lambda(x)$, a differentiable approximation to the min function. This formulation combines the differentiable approximation to the max function from [32, Page 255] and [18, 82] with the fact that

$$\min\{a, b\} = -\max\{-a, -b\}.$$

The form of $\tau_\lambda(x)$ implemented for the numerical results in Chapter 4 finds the minimum of $\frac{\gamma k_f(x)}{\mu}$ and $\frac{\gamma}{\beta\|\mathbf{u}(x)\|_2}$ at each node in the computational grid. Thus $\tau_\lambda(x)$ is a function associated with the nodes rather than a piecewise constant function over the elements as Masud and Hughes intended τ_e to be. The parameter λ is equal to

10^{-2} or 10^{-3}.

$$\tau_\lambda(x) = -\lambda \ln\left(\exp\left(\frac{-\gamma k_f(\mathbf{x})}{\lambda\mu}\right) + \exp\left(\frac{-\gamma}{\lambda\beta\|\mathbf{u}(x)\|_2}\right)\right) \tag{A.11}$$

Further details on specifying τ can be found in [110, page 170].

Appendix B

TCAT Single Phase Flow Model

B.1 Derivation

We make use of the following constitutive forms and variable definitions [68, pages 35 and 36], where the compressibility coefficients β^w and β^s describe how the fluid and solid densities, respectively, change in response to an isothermal change in fluid pressure [16, page 37].

$$\frac{\partial \rho^w}{\partial p^w} = \rho^w \beta^w \tag{B.1}$$

$$\frac{\partial \rho^s}{\partial p^w} = \rho^s \beta^s \tag{B.2}$$

$$\Upsilon \frac{\partial p^w}{\partial t} = \nabla \cdot \mathbf{v}^s \tag{B.3}$$

Let C, the porous medium compressibility coefficient, equal $\phi\beta^w + (1-\phi)\,\beta^s + \Upsilon$, and recall that the Darcy velocity is given by $\mathbf{u}^w = \phi\,(\mathbf{v}^w - \mathbf{v}^s)$. Here the velocity is

referenced with respect to the velocity of the solid matrix.[16]

B.1.1 Flow Equation

Conservation of Mass for the water phase, $\alpha = w$:

$$\frac{\partial \left(\epsilon^w \rho^w\right)}{\partial t} + \nabla \cdot \left(\epsilon^w \rho^w \mathbf{v}^w\right) = \rho^w \mathcal{S}' \tag{B.4}$$

The conservation of mass equation for the solid is similar, with w superscripts replaced with s superscripts and no source term. For single phase flow, the volume fraction of the water phase, ϵ^w, is equivalent to the porosity, ϕ, of the porous medium. Therefore, we can write the mass conservation equations for the fluid and the solid as

$$\frac{\partial \left(\phi \rho^w\right)}{\partial t} + \nabla \cdot \left(\phi \rho^w \mathbf{v}^w\right) = \rho^w \mathcal{S}' \tag{B.5}$$

$$\frac{\partial \left[\left(1-\phi\right) \rho^s\right]}{\partial t} + \nabla \cdot \left(\left(1-\phi\right) \rho^s \mathbf{v}^s\right) = 0 \tag{B.6}$$

Applying the product rule to equations (B.5) and (B.6), we find that

$$\phi \frac{\partial \rho^w}{\partial t} + \rho^w \frac{\partial \phi}{\partial t} + \nabla \cdot \left(\phi \rho^w \mathbf{v}^w\right) = \rho^w \mathcal{S}' \tag{B.7}$$

$$\rho^s \frac{\partial \phi}{\partial t} = \left(1-\phi\right) \frac{\partial \rho^s}{\partial t} + \left(1-\phi\right) \mathbf{v}^s \cdot \nabla \rho^s + \rho^s \nabla \cdot \left[\left(1-\phi\right) \mathbf{v}^s\right]. \tag{B.8}$$

(B.8) shows that the change in porosity can be due to either the compressibility of the solid matrix or the movement of the solid grains with respect to each other. Both are

determined by the state of stress and the stress-strain relationship within the solid matrix. Eliminate the time derivative of porosity using (B.8) along with (B.7).

$$\phi\frac{\partial\rho^w}{\partial t}+\frac{\rho^w}{\rho^s}\left(\left(1-\phi\right)\frac{\partial\rho^s}{\partial t}+\left(1-\phi\right)\mathbf{v}^s\cdot\nabla\rho^s+\rho^s\nabla\cdot\left[\left(1-\phi\right)\mathbf{v}^s\right]\right) \tag{B.9}$$
$$+\nabla\cdot\left(\phi\rho^w\mathbf{v}^w\right)=\rho^w\mathcal{S}'$$

Applying the following constitutive forms (B.1)-(B.3) to the above equation (B.9) yields

$$\phi\frac{\partial\rho^w}{\partial p^w}\frac{\partial p^w}{\partial t}+\frac{\rho^w}{\rho^s}\left(\left(1-\phi\right)\frac{\partial\rho^s}{\partial p^w}\frac{\partial p^w}{\partial t}+\left(1-\phi\right)\mathbf{v}^s\cdot\nabla\rho^s+\rho^s\nabla\cdot\left[\left(1-\phi\right)\mathbf{v}^s\right]\right)$$
$$+\nabla\cdot\left(\phi\rho^w\mathbf{v}^w\right)=\rho^w\mathcal{S}'$$
$$\left[\phi\rho^w\beta^w+\rho^w\left(1-\phi\right)\beta^s\right]\frac{\partial p^w}{\partial t}+\frac{\rho^w}{\rho^s}\left(1-\phi\right)\mathbf{v}^s\cdot\nabla\rho^s+\rho^w\nabla\cdot\left[\left(1-\phi\right)\mathbf{v}^s\right]$$
$$+\nabla\cdot\left(\phi\rho^w\mathbf{v}^w\right)=\rho^w\mathcal{S}'$$
$$\left[\phi\rho^w\beta^w+\rho^w\left(1-\phi\right)\beta^s\right]\frac{\partial p^w}{\partial t}+\frac{\rho^w}{\rho^s}\left(1-\phi\right)\mathbf{v}^s\cdot\nabla\rho^s+\rho^w\nabla\cdot\mathbf{v}^s-\rho^w\nabla\cdot\left(\phi\mathbf{v}^s\right)$$
$$+\rho^w\nabla\cdot\left(\phi\mathbf{v}^w\right)+\phi\mathbf{v}^w\cdot\nabla\rho^w=\rho^w\mathcal{S}'$$
$$\left[\phi\beta^w+\left(1-\phi\right)\beta^s\right]\frac{\partial p^w}{\partial t}+\frac{\left(1-\phi\right)\mathbf{v}^s}{\rho^s}\cdot\nabla\rho^s+\Upsilon\frac{\partial p^w}{\partial t}+\nabla\cdot\left[\phi\left(\mathbf{v}^w-\mathbf{v}^s\right)\right]$$
$$+\frac{\phi\mathbf{v}^w}{\rho^w}\cdot\nabla\rho^w=\mathcal{S}'$$
$$\left[\phi\beta^w+\left(1-\phi\right)\beta^s+\Upsilon\right]\frac{\partial p^w}{\partial t}+\frac{\left(1-\phi\right)\mathbf{v}^s}{\rho^s}\cdot\nabla\rho^s+\nabla\cdot\left[\phi\left(\mathbf{v}^w-\mathbf{v}^s\right)\right]$$
$$+\frac{\phi\mathbf{v}^w}{\rho^w}\cdot\nabla\rho^w=\mathcal{S}'$$

Introducing the porous medium compressibility coefficient and the Darcy velocity defined earlier, we have

$$\begin{aligned} C\frac{\partial p^w}{\partial t} + \nabla\cdot\mathbf{u}^w + \frac{(1-\phi)\,\mathbf{v}^s}{\rho^s}\cdot\nabla\rho^s + \frac{\phi\mathbf{v}^w}{\rho^w}\cdot\nabla\rho^w &= \mathcal{S}' \\ C\frac{\partial p^w}{\partial t} + \nabla\cdot\mathbf{u}^w + \frac{(1-\phi)\,\mathbf{v}^s}{\rho^s}\cdot\frac{\partial\rho^s}{\partial p^w}\frac{\partial p^w}{\partial x_j} + \frac{\phi\mathbf{v}^w}{\rho^w}\cdot\frac{\partial\rho^w}{\partial p^w}\frac{\partial p^w}{\partial x_j} &= \\ C\frac{\partial p^w}{\partial t} + \nabla\cdot\mathbf{u}^w + \left[(1-\phi)\,\beta^s\mathbf{v}^s + \phi\beta^w\mathbf{v}^w\right]\cdot\nabla p^w &= \end{aligned}$$

Since the compressibilities and velocities are generally small, the term

$$\left[(1-\phi)\,\beta^s\mathbf{v}^s + \phi\beta^w\mathbf{v}^w\right]\cdot\nabla p^w$$

is usually neglected.

Thus the flow equation is given by

$$C\frac{\partial p^w}{\partial t} + \nabla\cdot\mathbf{u}^w = \mathcal{S}'.$$

B.1.2 Momentum Conservation

$$\frac{D^w\left(\phi\rho^w\mathbf{v}^w\right)}{Dt} + \phi\rho^w\mathbf{v}^w\mathbf{d}^w : \mathbf{I} + \phi\left(\nabla p^w - \rho\mathbf{g}\right) = -\boldsymbol{\tau}^w$$

A valid assumption is that the solid matrix is relatively immobile, so only the fluid contributes to momentum conservation in the system.

$$\frac{D^w\left(\rho^w \mathbf{u}^w\right)}{Dt} + \rho^w \mathbf{u}^w \mathbf{d}^w : \mathbf{I} + \phi\left(\nabla p^w - \rho \mathbf{g}\right) = -\boldsymbol{\tau}^w$$

The following notation definition is required:

$$\mathbf{d}^w : \mathbf{I} = \nabla \cdot \mathbf{v}^w = \nabla \cdot \frac{\mathbf{u}^w}{\phi} = \frac{1}{\phi} \nabla \cdot \mathbf{u}^w - \frac{\mathbf{u}^w}{\phi^2} \cdot \nabla \phi$$

For an isotropic medium the Darcy-type approximation yields the constitutive relation

$$\boldsymbol{\tau}^w = \phi R^w \mathbf{u}^w$$

where $\boldsymbol{\tau}^w$ is the dynamic momentum exchange term [62], and R^w incorporates properties of both the fluid and porous medium, but not the flow conditions. For high velocity flow it can be shown that

$$R^w = r + a\left|\mathbf{u}^w - \mathbf{u}^s\right|$$

where r and a are properties of the fluid and porous medium. Thus the momentum equation becomes

$$\frac{D^w\left(\rho^w \mathbf{u}^w\right)}{Dt} + \rho^w \mathbf{u}^w \mathbf{d}^w : \mathbf{I} + \phi\left(\nabla p^w - \rho \mathbf{g}\right) = -\phi R^w \mathbf{u}^w$$

B.2 Model Representations

The following model representations were completed with Bill Gray [58].

B.2.1 Three-dimensional Model

The single-phase, single species TCAT groundwater flow model is given by

$$C\frac{\partial p}{\partial t} + \nabla \cdot \mathbf{u} = \sum_{i=1}^{NW} Q_i \delta\left(\mathbf{x} - \mathbf{x}_i\right) \tag{B.10}$$

$$\frac{\partial\left(\rho \mathbf{u}\right)}{\partial t} + \nabla \cdot \left(\frac{\rho \mathbf{u} \otimes \mathbf{u}}{\phi}\right) + \phi\left(\nabla p - \rho \mathbf{g}\right) \;\; = \;\; -\phi R \mathbf{u}, \tag{B.11}$$

where the first equation in the system has units of $\frac{1}{\text{time}}$ and the two remaining equations have units of $\frac{\text{mass}}{\text{length}^2\text{time}^2}$. In this formula and all those that follow, the resistance tensor, R, has units of $\frac{\text{mass}}{\text{length}^3\text{time}}$.

B.2.2 Two Dimensional Model

In order to solve the two dimensional "Quarter of Five Spot" problem in Section 6.2, we derive the two dimensional model by integrating the PDE system (B.10)-(B.11)

over the vertical direction, z.

$$\begin{cases} \int\limits_z \left[C\frac{\partial p}{\partial t} + \nabla\cdot\mathbf{u}\right]\,\mathrm{d}z = \int\limits_z \sum\limits_{i=1}^{NW} Q_i\delta\left(\mathbf{x}-\mathbf{x}_i\right)\,\mathrm{d}z \\ \int\limits_z \left[\frac{\partial(\rho\mathbf{u})}{\partial t} + \nabla\cdot\left(\frac{\rho\mathbf{u}\otimes\mathbf{u}}{\phi}\right) + \phi\left(\nabla p - \rho\mathbf{g}\right)\right]\,\mathrm{d}z = -\int\limits_z \left[\phi R\mathbf{u}\right]\,\mathrm{d}z \end{cases}$$

Thus,

$$\begin{cases} \ell_z C\frac{\partial p}{\partial t} + \ell_z\nabla\cdot\mathbf{u} = \sum\limits_{i=1}^{NW} Q_i\delta\left(\mathbf{x}-\mathbf{x}_i\right) \\ \ell_z\frac{\partial(\rho\mathbf{u})}{\partial t} + \ell_z\nabla\cdot\left(\frac{\rho\mathbf{u}\otimes\mathbf{u}}{\phi}\right) + \ell_z\phi\left(\nabla p - \rho\mathbf{g}\right) = -\ell_z\phi R\mathbf{u}, \end{cases}$$

where ℓ_z is the thickness of the aquifer in the vertical (z) direction and $\delta\left(\mathbf{x}-\mathbf{x}_i\right)$ now has units of $\frac{1}{\text{length}^2}$ rather than $\frac{1}{\text{length}^3}$ as in the three-dimensional case. In two spatial dimensions the first equation has units of $\frac{\text{length}}{\text{time}}$, while the units of the momentum equation are $\frac{\text{mass}}{\text{lengthtime}^2}$.

B.2.3 One Dimensional Model

For the one dimensional test case of groundwater flow through a column packed with porous medium from Section 1.3, we derive an appropriate version of the TCAT model by integrating the PDE system (B.10)-(B.11) over two horizontal spatial directions, x and y. We also neglect the well source terms since they do not apply in one spatial dimension.

$$\begin{cases} \int\limits_x\int\limits_y \left[C\frac{\partial p}{\partial t} + \nabla\cdot\mathbf{u}\right]\,\mathrm{d}y\,\mathrm{d}x = 0 \\ \int\limits_x\int\limits_y \left[\frac{\partial(\rho\mathbf{u})}{\partial t} + \nabla\cdot\left(\frac{\rho\mathbf{u}\otimes\mathbf{u}}{\phi}\right) + \phi\left(\nabla p - \rho\mathbf{g}\right)\right]\,\mathrm{d}y\,\mathrm{d}x = -\int\limits_x\int\limits_y \phi R\mathbf{u}\,\mathrm{d}y\,\mathrm{d}x \end{cases}$$

Thus,

$$\begin{cases} \ell_x \ell_y C \frac{\partial p}{\partial t} + \ell_x \ell_y \frac{\partial u}{\partial z} = 0 \\ \ell_x \ell_y \frac{\partial (\rho u)}{\partial t} + \ell_x \ell_y \left(\frac{2\rho u \frac{\partial u}{\partial z}}{\phi} \right) + \ell_x \ell_y \phi \left(\frac{\partial p}{\partial z} - \rho g \right) = -\ell_x \ell_y \phi R u, \end{cases}$$

where $\ell_x \ell_y$ is the cross-sectional area of the column. The equations have units of $\frac{\text{length}^2}{\text{time}}$ and $\frac{\text{mass}}{\text{time}^2}$, respectively.

B.2.4 Dimensionless Model

In certain instances dealing with a dimensionless version of the model can lend insight into the physics of the model and simplify its implementation and analysis. The derivation of the dimensionless version of the two-dimensional steady-state TCAT model follows.

We first consider how to transform

$$\ell_z \nabla \cdot \mathbf{u} = \sum_{i=1}^{NW} Q_i \delta \left(\mathbf{x} - \mathbf{x}_i \right) \tag{B.12}$$

into its dimensionless equivalent.

Let

$$\nabla = \nabla^* \frac{1}{\mathrm{L}} \tag{B.13}$$

$$\ell_z = \ell_z^* \ell_z \tag{B.14}$$

$$\delta = \delta^* \frac{1}{\mathrm{L}^2} \tag{B.15}$$

$$\mathbf{u} = \mathbf{u}^* \frac{h}{\mathrm{t}^\mathrm{r}} \tag{B.16}$$

$$Q_i = Q_i^* \frac{\mathrm{B}^3}{\mathrm{t}^\mathrm{r}} \tag{B.17}$$

where L, h, ℓ_z, and B denote generic length scale variables, t^r is a representative time scale variable, and the superscript $*$ denotes a dimensionless quantity.

We substitute the defined dimensionless variables into (B.12) in the following way.

$$\begin{aligned}
\nabla \cdot \mathbf{u} &= \sum_{i=1}^{NW} \frac{Q_i}{\ell_z} \delta\left(\mathbf{x} - \mathbf{x}_i\right) \\
\nabla^* \cdot \mathbf{u}^* \frac{h}{\mathrm{t}^\mathrm{r}\mathrm{L}} &= \sum_{i=1}^{NW} \frac{Q_i^* \mathrm{B}^3}{\ell_z^* \ell_z \mathrm{t}^\mathrm{r} \mathrm{L}^2} \delta^*\left(\mathbf{x} - \mathbf{x}_i\right) \\
\nabla^* \cdot \mathbf{u}^* &= \sum_{i=1}^{NW} \frac{Q_i^* \delta^*\left(\mathbf{x} - \mathbf{x}_i\right)}{\ell_z^*} \left[\frac{\mathrm{B}^3}{\ell_z \mathrm{L} h}\right]
\end{aligned}$$

The following are reasonable choices for variable relationships.

$h = \mathrm{L}$: since both are horizontal lengths

$\mathrm{B}^3 = \ell_z \mathrm{L}^2 \phi$: the volume B^3 is equal to the void volume available for flow

Using these equivalent relations and the fact that $\ell_z^* = 1$ in (B.14), we have the

dimensionless formulation of (B.12).

$$\boxed{\frac{\nabla^* \cdot \mathbf{u}^*}{\phi} = \sum_{i=1}^{NW} Q_i^* \delta^* \left(\mathbf{x} - \mathbf{x}_i\right)} \tag{B.18}$$

Moving on to the momentum equation, we have

$$\begin{aligned} \ell_z \nabla \cdot \left(\frac{\rho \mathbf{u} \otimes \mathbf{u}}{\phi}\right) + \ell_z \phi \left(\nabla p - \rho \mathbf{g}\right) &= -\ell_z \phi R \mathbf{u} \\ \frac{\ell_z \mathbf{u}}{\phi} \cdot \nabla \left(\rho \mathbf{u}\right) + \ell_z \rho \mathbf{u} \nabla \cdot \left(\frac{\mathbf{u}}{\phi}\right) + \ell_z \phi \left(\nabla p - \rho \mathbf{g}\right) &= -\ell_z \phi R \mathbf{u} \end{aligned}$$

Using our choices for h and B^3 to simplify some of the definitions in (B.13)-(B.15), we have

$$\mathbf{u} = \mathbf{u}^* \frac{L}{\mathrm{t^r}} \tag{B.19}$$

$$Q_i = Q_i^* \frac{\ell_z \mathrm{L}^2 \phi}{\mathrm{t^r}} \tag{B.20}$$

$$p = p^* \mathbb{P} \tag{B.21}$$

Substituting (B.13)-(B.15) and (B.19)-(B.21) into the two-dimensional steady-state momentum equation yields

$$\begin{aligned} \frac{\ell_z^* \mathbf{u}^*}{\phi} \cdot \nabla^* \left(\rho \mathbf{u}^*\right) \frac{\ell_z \mathrm{L}}{\left(\mathrm{t^r}\right)^2} + \rho \ell_z^* \mathbf{u}^* \nabla^* \cdot \left(\frac{\mathbf{u}^*}{\phi}\right) \frac{\ell_z \mathrm{L}}{\left(\mathrm{t^r}\right)^2} + \ell_z^* \nabla^* p^* \frac{\phi \ell_z \mathbb{P}}{\mathrm{L}} - \phi \ell_z \rho \mathbf{g} \ell_z^* &= \\ -\phi R \ell_z^* \mathbf{u}^* \frac{\ell_z \mathrm{L}}{\left(\mathrm{t^r}\right)} \end{aligned} \tag{B.22}$$

Multiply (B.22) by $\frac{(\mathrm{t^r})^2}{\phi\rho\ell_z \mathrm{L}}$, recall that $\ell_z^* = 1$, and simplify to find

$$\frac{\mathbf{u}^*}{\phi}\cdot\nabla^*\left(\frac{\mathbf{u}^*}{\phi}\right)+\frac{\mathbf{u}^*}{\phi}\nabla^*\cdot\left(\frac{\mathbf{u}^*}{\phi}\right)+\nabla^* p^*\frac{\mathbb{P}\left(\mathrm{t^r}\right)^2}{\rho \mathrm{L}^2}-\mathbf{g}\frac{\left(\mathrm{t^r}\right)^2}{\mathrm{L}}=-\phi R\frac{\mathbf{u}^*\left(\mathrm{t^r}\right)}{\phi\rho}. \tag{B.23}$$

Substitute the following definition of the actual pore velocity into (B.23).

$$\bar{\mathbf{u}}=\frac{\mathbf{u}^*}{\phi}$$

Now we have a simplified equation in which $\mathbf{e}$ denotes the unit vector in the direction of gravity.

$$\bar{\mathbf{u}}\cdot\nabla^*\bar{\mathbf{u}}+\bar{\mathbf{u}}\nabla^*\cdot\bar{\mathbf{u}}+\nabla^* p^*\left[\frac{\mathbb{P}\left(\mathrm{t^r}\right)^2}{\rho \mathrm{L}^2}\right]-g\mathbf{e}\left[\frac{\left(\mathrm{t^r}\right)^2}{\mathrm{L}}\right]=-R\bar{\mathbf{u}}\left[\frac{\phi\left(\mathrm{t^r}\right)}{\rho}\right]. \tag{B.24}$$

The following are reasonable choices for variable relationships.

$(\mathrm{t^r})=\frac{\phi\ell_z \mathrm{L}^2}{Q_i}$: void volume divided by the volumetric flow rate yields the *residence time*, or the average length of time it takes for a particle of water to travel through the system

$\mathbb{P}=\rho g \mathrm{L}$: so the same coefficient multiplies the pressure and gravity terms

$$\boxed{\bar{\mathbf{u}}\cdot\nabla^*\bar{\mathbf{u}}+\bar{\mathbf{u}}\nabla^*\cdot\bar{\mathbf{u}}+\nabla^* p^*\left[\frac{g\ell_z^2\phi^2\mathrm{L}^3}{Q_i^2}\right]-\left[\frac{g\ell_z^2\phi^2\mathrm{L}^3}{Q_i^2}\right]\mathbf{e}=-R\bar{\mathbf{u}}\left[\frac{\ell_z\phi^2\mathrm{L}^2}{\rho Q_i}\right]} \tag{B.25}$$

The unknowns of the system are now $p^*=\frac{p}{\rho g \mathrm{L}}$ and $\bar{\mathbf{u}}=\frac{\mathbf{u}\ell_z \mathrm{L}}{Q_i}$, and we know the conversions between the dimensionless variables p^* and $\bar{\mathbf{u}}$ and their corresponding original variables p and $\mathbf{u}$. Now we have to consider computing the resistance tensor

in a dimensionless fashion.

For the resistance tensor we consider the modified Ergun formulation from [95]

$$R = \left(A + B \frac{\mathrm{Re}}{\mathrm{Re} + \mathrm{Re}_0} \frac{\mathrm{Re}}{1-\phi} \right) \left(\frac{\mu \left(1-\phi\right)^2}{D^2 \phi^4} \right)$$

which should allow the model to account for transitions from linear to nonlinear flow behavior since

$$-R\bar{\mathbf{u}} \left[\frac{\ell_z \phi^2 \mathrm{L}^2}{\rho Q_i} \right] \approx C_1 \bar{\mathbf{u}} + C_2 \bar{\mathbf{u}} |\bar{\mathbf{u}}|. \tag{B.26}$$

Here C_1 is a constant coefficient while C_2 will vary over the domain as it depends upon the Reynolds number. The Reynolds number formula will change slightly based upon the variable definitions set in this derivation.

$$\mathrm{Re} = \frac{\rho D |\mathbf{u}|}{\mu \phi} = \frac{\rho D |\mathbf{u}^*| \mathrm{L}}{\mu \phi \left(\mathrm{t}^\mathrm{r}\right)} = \frac{\rho D |\bar{\mathbf{u}}| \mathrm{L}}{\mu \left(\mathrm{t}^\mathrm{r}\right)} = \frac{\rho D |\bar{\mathbf{u}}| Q_i}{\mu \phi \ell_z \mathrm{L}} \tag{B.27}$$

we need to transform the resistance tensor term from equation (B.25) into a form like (B.26) such that the coefficients C_1 and C_2 can be specified.

$$\begin{aligned} R\bar{\mathbf{u}} \left[\frac{\ell_z \phi^2 \mathrm{L}^2}{\rho Q_i} \right] &= \left(A + B \frac{\mathrm{Re}}{\mathrm{Re} + \mathrm{Re}_0} \frac{\mathrm{Re}}{1-\phi} \right) \left(\frac{\mu \left(1-\phi\right)^2}{D^2 \phi^4} \right) \bar{\mathbf{u}} \left[\frac{\ell_z \phi^2 \mathrm{L}^2}{\rho Q_i} \right] \\ &= A\bar{\mathbf{u}} \left(\frac{\mu \left(1-\phi\right)^2 \ell_z \mathrm{L}^2}{\phi \rho D^2 Q_i} \right) + \frac{B \mathrm{Re}^2 \bar{\mathbf{u}}}{\left(\mathrm{Re} + \mathrm{Re}_0\right)} \left(\frac{\mu \left(1-\phi\right) \ell_z \mathrm{L}^2}{\phi \rho D^2 Q_i} \right) \end{aligned}$$

Let our coefficients be A^* and B^* as defined below.

$$\boxed{A^* = \frac{A\mu(1-\phi)^2\ell_z \mathrm{L}^2}{\phi\rho D^2 Q_i}} \tag{B.28}$$

$$\boxed{B^* = \frac{B\mu(1-\phi)\ell_z \mathrm{L}^2}{\phi\rho D^2 Q_i}} \tag{B.29}$$

From (B.20), we know that $Q_i^* = \frac{Q_i(\mathrm{t^r})}{\ell_z \mathrm{L}^2\phi}$, and since the residence time, $(\mathrm{t^r})$, has been defined to be $\frac{\phi\ell_z \mathrm{L}^2}{Q_i}$, the dimensionless pumping rate Q_i^* will always equal one.

Therefore, the dimensionless model simplifies to specifying three parameters, A^*, B^*, and

$$\boxed{C^* = \frac{g\ell_z^2\phi^2\mathrm{L}^3}{Q_i^2}}, \tag{B.30}$$

which leaves us with the following dimensionless system

$$\begin{cases} \nabla^* \cdot \bar{\mathbf{u}} = \sum_{i=1}^{NW} \delta^* \left(\mathbf{x} - \mathbf{x}_i\right) \\ \bar{\mathbf{u}} \cdot \nabla^* \bar{\mathbf{u}} + \bar{\mathbf{u}} \nabla^* \cdot \bar{\mathbf{u}} + C^* \nabla^* p^* - C^* \mathbf{e} = -A^* \bar{\mathbf{u}} - \frac{B^* \mathrm{Re}^2 \bar{\mathbf{u}}}{\mathrm{Re} + \mathrm{Re}_0} \end{cases}$$

The only parameter that is free to vary is the pumping rate Q_i.

Appendix C

GSLIB Input File

```
                  Parameters for SGSIM
                  ********************

START OF PARAMETERS:
../data/empty.dat                  \  file with data doesn't exist;
                                   \  sgsim will skip to debug level
1  2  0  3  5  0                   \  columns for X,Y,Z,vr,wt,sec.var.
-1.0       1.0e21                  \  trimming limits
0                                  \  transform the data (0=no, 1=yes)
sgsim.trn                          \  file for output trans table
0                                  \  consider ref. dist (0=no, 1=yes)
histsmth.out                       \  file with ref. dist distribution
1  2                               \  columns for vr and wt
0.0    15.0                        \  zmin,zmax(tail extrapolation)
1       0.0                        \  lower tail option, parameter
1      15.0                        \  upper tail option, parameter
1                                  \  debugging level: 0,1,2,3
file.dbg                           \  file for debugging output
file.out                           \  file for simulation output
1                                  \  number of realizations to generate
102   -5.0    10.0     \  nx,xmn,xsiz
102   -5.0    10.0    \  ny,ymn,ysiz
1     -5.0    10.0           \  nz,zmn,zsiz
69069                          \  random number seed
10    10                       \  unused ndmin and ndmax
12                            \  number of simulated nodes to use, ncnode
0                              \  unused sstrat
0     3                       \  multiple grid search (0=no, 1=yes),num
0                              \  maximum data per octant (0=not used)
100.0  100.0  100.0                \  a_hmax, a_hmin, a_vert
0.0   0.0   0.0                    \  angles for search ellipsoid
0     0.60   1.0                   \  ktype: 0=SK,1=OK,2=LVM,3=EXDR,4=COLC
../data/empty.dat                  \  file with LVM, EXDR, or COLC variable
```

```
4                               \  column for secondary variable
1    0                          \  nst, nugget effect
3    1.0  0.0   0.0   0.0       \  it,cc,ang1,ang2,ang3
100.0  100.0  100.0              \  a_hmax, a_hmin, a_vert
```